

โครงสร้างการละลายและพลวัตของไอออนโซเดียมในแอมโมเนียเหลว :
การจำลองพลวัตเชิงโมเลกุลบนพื้นฐานวิธีโอเนียม-เอ็กซ์เอส



วิทยานิพนธ์นี้เป็นส่วนหนึ่งของการศึกษาตามหลักสูตรปริญญาวิทยาศาสตรดุษฎีบัณฑิต
สาขาวิชาเคมี
มหาวิทยาลัยเทคโนโลยีสุรนารี
ปีการศึกษา 2557

**SOLVATION STRUCTURE AND DYNAMICS OF Na⁺ IN
LIQUID AMMONIA: AN ONIOM-XS MD
SIMULATIONS STUDY**

Jarukorn Sripradite



**A Thesis Submitted in Partial Fulfillment of the Requirements for the
Degree of Doctor of Philosophy in Chemistry
Suranaree University of Technology
Academic Year 2014**

**SOLVATION STRUCTURE AND DYNAMICS OF Na⁺ IN LIQUID
AMMONIA: AN ONIOM-XS MD SIMULATIONS STUDY**

Suranaree University of Technology has approved this thesis submitted in partial fulfillment of the requirements for the Degree of Doctor of Philosophy.

Thesis Examining Committee

(Assoc. Prof. Dr. Jatuporn Wittayakun)

Chairperson

(Assoc. Prof. Dr. Anan Tongraar)

Member (Thesis Advisor)

(Prof. Dr. Kritsana Sagarik)

Member

(Assoc. Prof. Dr. Albert Schulte)

Member

(Assoc. Prof. Dr. Chinapong Kritayakornupong)

Member

(Prof. Dr. Sukit Limpijumnong)

Vice Rector for Academic Affairs
and Innovation

(Assoc. Prof. Dr. Prapun Manyum)

Dean of Institute of Science

จารุกร ศรีประดิษฐ์: โครงสร้างการละลายและพลวัตของไอออนโซเดียมในแอมโมเนีย

เหลว : การจำลองพลวัตเชิงโมเลกุลบนพื้นฐานวิธีไอเนียม-เอ็กซ์เอส

(SOLVATION STRUCTURE AND DYNAMICS OF Na^+ IN LIQUID AMMONIA: AN ONIOM-XS MD SIMULATIONS STUDY) อาจารย์ที่ปรึกษา: รองศาสตราจารย์ ดร.

อนันต์ ทองระอา, 115 หน้า.

เทคนิคการจำลองพลวัตเชิงโมเลกุลที่ผสมผสานกลศาสตร์ควอนตัมและกลศาสตร์โมเลกุลบนพื้นฐานวิธีไอเนียม-เอ็กซ์เอส (เรียกโดยย่อว่า การจำลองพลวัตเชิงโมเลกุลบนพื้นฐานวิธีไอเนียม-เอ็กซ์เอส) ได้ถูกนำมาประยุกต์เพื่อศึกษาโครงสร้างการละลายและพลวัตของไอออนโซเดียมในแอมโมเนียเหลว บนพื้นฐานของเทคนิคการจำลองพลวัตเชิงโมเลกุลบนพื้นฐานวิธีไอเนียม-เอ็กซ์เอสนี้ ระบบที่ศึกษาจะถูกแบ่งออกเป็นสองส่วน ส่วนที่ให้ความสำคัญมากที่สุดจะเป็นส่วนเล็กๆ ในระบบ ได้แก่ ทรงกลมที่บรรจุไอออนโซเดียมเป็นศูนย์กลางและมีโมเลกุลแอมโมเนียล้อมรอบ ซึ่งอันตรกิริยาภายในทรงกลมนี้จะถูกอธิบายโดยกลศาสตร์ควอนตัม และส่วนที่เหลือของระบบจะถูกอธิบายบนพื้นฐานของกลศาสตร์โมเลกุล การศึกษาในครั้งนี้ การคำนวณกลศาสตร์ควอนตัมจะกระทำในระดับฮาร์ตรี-ฟ็อก (HF) โดยใช้เบสิสเซตชนิดดับเบิลเซตที่รวมการโพลาไรซ์ (DZP) สำหรับโมเลกุลแอมโมเนียและใช้เบสิสเซตชนิดคิกซ์ฟังก์ชันผลชื่อ LANL2DZ สำหรับไอออนโซเดียม ผลที่ได้จากการจำลองพลวัตเชิงโมเลกุลบนพื้นฐานวิธีไอเนียม-เอ็กซ์เอส ทำให้เข้าใจพฤติกรรมของไอออนโซเดียมที่เกี่ยวข้องกับความสามารถในการสร้างโครงสร้างการละลายในแอมโมเนียเหลว (โดยเฉพาะเมื่อเปรียบเทียบกับผลการจำลองพลวัตเชิงโมเลกุลที่ผสมผสานกลศาสตร์ควอนตัมและกลศาสตร์โมเลกุลแบบดั้งเดิม) ผลการจำลองพลวัตเชิงโมเลกุลบนพื้นฐานวิธีไอเนียม-เอ็กซ์เอสพบว่า ไอออนโซเดียมมีความสามารถในการสร้างโครงสร้างการละลายที่ค่อนข้างชัดเจน โดยสามารถเหนี่ยวนำโมเลกุลแอมโมเนียที่อยู่รอบๆ เพื่อสร้างชั้นการละลายที่หนึ่งและชั้นที่สองโดยมีแอมโมเนียบรรจุอยู่โดยเฉลี่ยจำนวน 5.1 และ 11.2 โมเลกุล ตามลำดับ โครงสร้างการละลายชั้นที่หนึ่งนั้นมีการจัดเรียงตัวที่ค่อนข้างชัดเจนในลักษณะโครงรูปพีระมิดฐานสี่เหลี่ยม ทั้งนี้ โครงสร้างการละลายชั้นที่หนึ่งที่ประกอบด้วยแอมโมเนียจำนวน 5 โมเลกุลดังกล่าว สามารถจะเปลี่ยนสลับไปมากับโครงสร้างการละลายอื่นที่ประกอบด้วยแอมโมเนียจำนวน 4 และ 6 โมเลกุลได้บ้าง โครงสร้างการละลายชั้นที่สองของไอออนโซเดียมที่ตรวจพบจากการจำลองพลวัตเชิงโมเลกุลบน

พื้นฐานวิธี โอนิยม-เอ็กซ์เอส แสดงให้เห็นอิทธิพลของ ไอออน โซเดียมที่มีต่อ โมเลกุลแอมโมเนียที่
อยู่ในชั้นการละลายที่สองด้วย



สาขาวิชาเคมี
ปีการศึกษา 2557

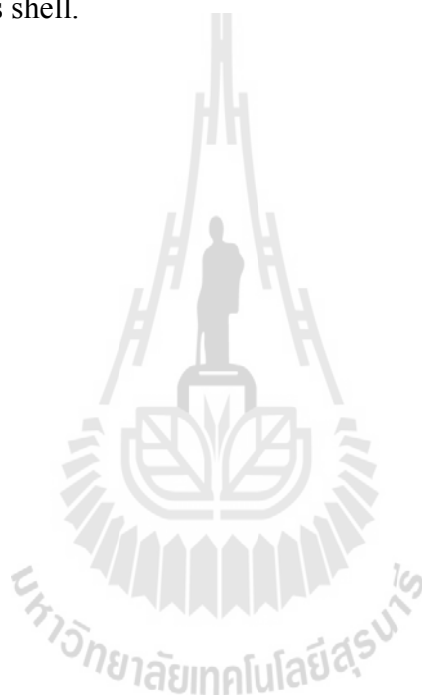
ลายมือชื่อนักศึกษา _____
ลายมือชื่ออาจารย์ที่ปรึกษา _____

JARUKORN SRIPRADITE : SOLVATION STRUCTURE AND
DYNAMICS OF Na⁺ IN LIQUID AMMONIA: AN ONIOM-XS MD
SIMULATIONS STUDY. THESIS ADVISOR : ASSOC. PROF. ANAN
TONGRAAR, Ph.D. 115 PP.

SODIUM ION/ LIQUID AMMONIA/ ONIOM-XS MD

A combined quantum mechanics/molecular mechanics (QM/MM) molecular dynamics (MD) technique based on the ONIOM-XS (Own N-layered Integrated molecular Orbital and molecular Mechanics – eXtension to Solvation) method, called briefly ONIOM-XS MD, has been applied to investigate the solvation structure and dynamics of Na⁺ in liquid ammonia (NH₃). Based on the ONIOM-XS MD technique, the system is composed of a “high-level” QM region, *i.e.*, a sphere which contains the Na⁺ ion and its surrounding NH₃ molecules, and the remaining “low-level” MM region. Inside the QM region, all interactions were treated at the Hartree-Fock (HF) level of accuracy using double- ζ plus polarization and LANL2DZ basis sets for NH₃ and Na⁺, respectively, whereas the interactions within the MM and between the QM and MM regions were described by MM potentials. The ONIOM-XS MD results provided more insights into the behaviors of Na⁺ with respect to its “structure-making” ability in liquid NH₃, especially when compared to the results obtained by the conventional QM/MM MD scheme. With regard to the detailed analyses on the ONIOM-XS MD’s trajectories, Na⁺ clearly acts as a “structure-maker” in this media, *i.e.*, this ion can order its surrounding NH₃ molecules to form specific first and second solvation shells

with the average coordination numbers of 5.1 and 11.2, respectively. In this respect, the first solvation shell of Na^+ is rather well-defined, forming a preferred 5-fold coordinated complex with a distorted square pyramidal geometry. Interestingly, it is observed that the most preferential $\text{Na}^+(\text{NH}_3)_5$ species could convert back and forth to the lower probability $\text{Na}^+(\text{NH}_3)_6$ and $\text{Na}^+(\text{NH}_3)_4$ configurations. The second solvation shell of Na^+ is also detectable, indicating a recognizable influence of Na^+ in ordering NH_3 molecules in this shell.



School of Chemistry

Academic Year 2014

Student's Signature _____

Advisor's Signature _____

ACKNOWLEDGEMENTS

I wish to express my deep gratitude to all people who gave me the possibility to complete this thesis. First of all, most of the credit in this thesis should justifiably go to my advisor, Assoc. Prof. Dr. Anan Tongraar, for his guidance, valuable suggestions, kindness, encouragement and immense knowledge throughout the course of my graduate. I would like to thank Prof. Dr. Kritsana Sagarik and all lecturers at School of Chemistry, Institute of Science, Suranaree University of Technology (SUT), for their encouragements and help. I would like to thank all committee members for their time and useful comments and suggestions. I am thankful to Prof. Dr. Debbie C. Crans for her kindness and sincere suggestions for my research work and life when I visited her research group at Colorado State University, United States of America. I would also like to thank my colleagues in the Crans group for their helpfulness and giving me the wonderful experiences.

I was supported by the Office of the Higher Education Commission (CHE-PhD-THA), Thailand. Special thanks should go to School of Chemistry, Institute of Science, Suranaree University of Technology (SUT), for powerful research facilities. Thank you very much to my friends for their friendship.

Finally, I would like to express my deepest gratitude to my parents, brother, and sister for their unconditional love, deep understanding, wonderful encouragement and all supports.

Jarukorn Sripradite

CONTENTS

	Page
ABSTRACT IN THAI	I
ABSTRACT IN ENGLISH	III
ACKNOWLEDGEMENTS.....	V
CONTENTS	VI
LIST OF TABLES	IX
LIST OF FIGURES.....	X
LIST OF ABBREVIATIONS.....	XII
CHAPTER	
I INTRODUCTION.....	1
1.1 Literature reviews	1
1.2 Research objectives.....	6
1.3 Scope and limitation of the study	7
1.4 References	8
II QUANTUM CHEMISTRY.....	15
2.1 Introduction to quantum mechanics.....	15
2.2 Schrödinger equation	15
2.3 The variation theory.....	17
2.4 Born-Oppenheimer approximation.....	19
2.5 Molecular orbital theory.....	20
2.6 The LCAO-MO approach and basis sets	23

CONTENTS (Continued)

	Page
2.7 Basis Set Superposition Error (BSSE)	29
2.8 Hartree-Fock method	30
2.9 Electron correlation.....	35
2.10 References	36
III MOLECULAR DYNAMICS SIMULATIONS	39
3.1 Introduction to molecular dynamics (MD) simulations.....	39
3.2 Time average and ensemble average	42
3.3 Intermolecular potentials.....	44
3.4 Time integration algorithms	47
3.4.1 Verlet algorithm	48
3.4.2 Predictor-corrector algorithm	51
3.5 Periodic boundary conditions	52
3.6 Cut-off and minimum image convention	53
3.7 Non-bonded neighbor lists	58
3.8 Long-range interactions	59
3.9 ONIOM-XS MD technique	61
3.10 Research procedures	64
3.10.1 Construction of pair potential functions.....	64
3.10.2 Simulation details.....	66
3.11 Determination of system's properties.....	67
3.11.1 Structural properties	67

CONTENTS (Continued)

	Page
3.11.2 Dynamical properties.....	68
3.12 References	69
IV RESULTS AND DISCUSSION	74
4.1 Structural properties.....	74
4.2 Dynamical properties	85
4.3 References	94
V CONCLUSION	97
APPENDICES	99
APPENDIX A THEORETICAL OBSERVATIONS OF Na ⁺ IN LIQUID NH ₃	100
APPENDIX B LIST OF PRESENTATIONS.....	101
APPENDIX C MANUSCRIPT.....	103
CURRICULUM VITAE	115

LIST OF TABLES

Table	Page
3.1 Optimized parameters of the analytical pair potential for the interaction of ammonia with Na ⁺ (interaction energies in kcal mol ⁻¹ and distances in Å).....	65
4.1 Two possible geometries of penta-coordinated ion-ligand complexes	81
4.2 Number of ligand exchange events (N_{ex}) and mean residence times (MRTs) of solvent molecules in the bulk and in the vicinity of Na ⁺ , as obtained by the ONIOM-XS MD simulations	94



LIST OF FIGURES

Figure	Page
2.1 The Slater-type and Gaussian-type for 1s orbital	26
2.2 The STO-3G basis set representing the desired STO.....	27
3.1 The scheme of molecular dynamics simulation.....	41
3.2 The Lennard-Jones potential.....	46
3.3 The periodic boundary conditions in two dimensions	53
3.4 The spherical cut-off and the minimum image convention.....	55
3.5 The discontinuity of cut-off.....	56
3.6 The effect of a switching function applied to the Lennard-Jones potential.....	58
3.7 The non-bonded neighbor list.....	59
3.8 Schematic diagram of the ONIOM-XS MD technique.....	62
4.1 a) Na-N and b) Na-H radial distribution functions (RDFs) and their corresponding integration numbers. The insertion refers to the corresponding RDFs obtained from the QM/MM MD simulation.....	76
4.2 Distributions of the coordination numbers, calculated within the first and second solvation shells of Na ⁺	78
4.3 Distributions of the N---Na---N angle, calculated within the first minimum of the Na-N RDF	79

LIST OF FIGURES (Continued)

Figure	Page
4.4 Probability distributions of θ angle in the first and second solvation shells of Na^+ , calculated within the first and second minima of the Na-N RDF	80
4.5 a) N-N, b) N-H, c) H-N and d) H-H radial distribution functions and their corresponding integration numbers, as obtained by the QM/MM and ONIOM-XS MD simulations.	84
4.6 Probability distributions of the coordination numbers, calculated up to first minimum of the N-N RDFs, as obtained by the QM/MM and ONIOM-XS MD simulations.....	85
4.7 Time dependence of a) Na^+ ---N distance and b) number of first-shell ammonia molecules, as obtained by the ONIOM-XS MD simulation. In Figure 4.7a), the dash line parallel to the x-axis indicates the first minimum of the Na-N RDF	87
4.8 Center-of-mass VACFs for NH_3 molecules in the first and second solvation shells of Na^+ and in the bulk.....	89
4.9 Fourier transforms of the translational motions of NH_3 in the first and second solvation shells of Na^+ and in the bulk.	90
4.10 Fourier transforms of the librational motions of NH_3 in the first and second solvation shells of Na^+ and in the bulk (the dash lines refer to z axis and the solid lines refer to x axis).	92

LIST OF ABBREVIATIONS

Å	=	Ångström
ADF	=	Angular distribution function
Au	=	Atomic unit
Aug-cc-pVDZ	=	Additional diffuse basis function and correlation consistent polarized valence double zeta
B3LYP	=	Becke three-parameter hybrid functional combined with Lee-Yang-Parr correlation function
BLYP	=	Becke hybrid functional combined with Lee-Yang-Parr correlation function
BO	=	Born-Oppenheimer
BOMD	=	Born-Oppenheimer molecular dynamics
BSSE	=	Basis set superposition error
Ca ²⁺	=	Calcium ion
CCSD	=	Coupled cluster calculations using both single and double substitutions from Hartree-Fock determinant
CF2	=	Central force model version 2
cm ⁻¹	=	Wavenumber
CN	=	Coordination number
CND	=	Coordination number distribution

LIST OF ABBREVIATIONS (Continued)

CP-MD	=	Car-Parrinello molecular dynamics
CPU	=	Central processing unit
D	=	Self-diffusion coefficient
DFT	=	Density functional theory
DZP	=	Double zeta polarization
e	=	Electron charge
E_{tot}	=	Total interaction energy
E_{MM}	=	Interaction within MM region
E_{QM-MM}	=	Interaction between QM and MM regions
$E^{ONIOM-XS}$	=	The potential energy of the entire system for ONIOM-XS
ECP	=	Effective core potential
F_i	=	Force acting on each particle
F_{MM}	=	MM force
F_{QM}	=	QM force
fs	=	Femtosecond
GGA	=	Generalized gradient approximation
GTO	=	Gaussian-type orbital
\hat{H}	=	Hamiltonian operator
HF	=	Hartree-Fock

LIST OF ABBREVIATIONS (Continued)

K	=	Kelvin
LANL2DZ	=	Los Alamos ECP plus DZ
LCAO-MO	=	Linear combination of atomic orbitals to molecular orbitals
l	=	Number of particles in the switching layer
M	=	Molarity
MC	=	Monte Carlo
MD	=	Molecular dynamics
MM	=	Molecular mechanics
MO	=	Molecular orbital
MP2	=	Second-order Møller-Plesset
MRT	=	Mean residence times
m	=	Mass
m_e	=	Mass of electron
m_k	=	Mass of nucleus
n_1	=	Number of particle in the QM sphere
ND	=	Neutron diffraction
NVE	=	Microcanonical ensemble
NVT	=	Canonical ensemble
n_2	=	Number of particle in the MM region

LIST OF ABBREVIATIONS (Continued)

N_{ex}	=	Number of exchange events
ONIOM	=	Own N-layered Integrated molecular Orbital and molecular Mechanics
ONIOM-XS	=	An extension of the ONIOM method for molecular simulation in condensed phase
PP	=	Pseudopotential
ps	=	Picosecond
QM	=	Quantum mechanics
QM/MM	=	Combined Quantum mechanics/molecular mechanics
RDF	=	Radial distribution function
RHF	=	Restricted Hartree-Fock
r_0	=	Distance characterizing the start of QM region
r_1	=	Distance characterizing the end of QM region
r_{min}	=	First minimum of RDF peak
r_{max}	=	First maximum of RDF peak
SCF	=	Self-consistent field
STO	=	Slater-type orbital
$S_m(r)$	=	Smoothing function
VACF	=	Velocity autocorrelation functions
XRD	=	X-ray diffraction

LIST OF ABBREVIATIONS (Continued)

μ	=	Chemical potential
Φ	=	Trial function
h	=	Planck's constant
$^{\circ}$	=	Degree
τ_{NH_3}	=	MRT of ammonia molecules
λ	=	Wavelength
t^*	=	Time for observing the number of exchange ammonia
t_{sim}	=	Simulation time
$\chi(x)$	=	Spin orbital
∇^2	=	Laplacian operator
Ψ	=	Wavefunction
$(\Psi_{QM} \hat{H} \Psi_{QM})$	=	Interaction within QM region

CHAPTER I

INTRODUCTION

1.1 Literature review

It is known that the basic machinery of human body is proteins, and one-third of them are metalloproteins containing at least one metal ion. In this respect, the metal ions are needed for the proteins to have some structural and functional roles. To understand the properties of metalloproteins, fundamental knowledge with respect to the structure and dynamics of ion coordination in simple solvents, such as water (H₂O) or ammonia (NH₃), is essential. The elucidation on the structure and dynamics of ions solvated in aqueous electrolyte solutions has long been an interesting subject for both experimental and theoretical studies (Impey, Madden and McDonald, 1983; Karplus and McCammon, 1983; Marcus, 1988; Morokuma, 2003; Roux and Karplus, 1994; Woolf and Roux, 1994). In addition to the study of aqueous ionic solutions, behavior of ions, in particular of metal ions, solvated in liquid NH₃ have also been a topic of scientific interest since these data can provide valuable insights into the coordinating environment of more complex ligands, *e.g.*, DNA, RNA and proteins. Regarding the metal-ammonia solution, most of the available information has been reported in the Colloque Weyl Symposia (D, 1965; Das, 2007; Johnson and Meyer, 1931; Salter and Ellis, 2007).

In general, experimental techniques, such as X-ray diffraction (XRD) and neutron diffraction (ND), are the useful tools for determining the static structure factors of ligands (*i.e.*, solvent molecules, such as H₂O or NH₃) solvating a given ion (Ansell, Barnes, Mason, Neilson and Ramos, 2006; Ohtaki and Radnai, 1993; Narten, 1976). However, most of experimental measurements often yield an incomplete description of ionic solvation, due to, *e.g.* the lack of suitable isotope substitutions in ND experiments, or difficulties in separating the atomic correlations or different species in diffraction data (Chowdhuri and Chandra, 2003; Koneshan, Rasaiah, Lynden-Bell and Lee, 1998; Zhou, Lu, Wang and Shi, 2002). In conjunction with experiments, computer simulations, *i.e.*, by means of Monte Carlo (MC) and molecular dynamics (MD), have become an alternative approach to provide microscopic details of such systems. For the system of ions in liquid NH₃, several MC and MD simulations have been carried out, providing detailed information on the structure and dynamics of the solvated ions (Kerdcharoen and Rode, 2000; Hannongbua, 1991; Marchi, Sprik and Klein, 1990; Hannongbua, 1997; Tongraar, Liedl and Rode, 1998; Lee and Rasaiah, 1994). However, most of the earlier studies had relied on simplified potentials (Beu and Buck, 2001; Gao, Xia and George, 1993; Hannongbua, Kerdcharoen and Rode, 1992; Kincaid and Scheraga, 1982) or on direct *ab initio* pair interactions (Hannongbua, 2000). In this respect, it has been demonstrated that the quality of the simulation results depend crucially on the quality of the potentials employed for describing the system's interactions, *i.e.* most of which are based on pairwise additive approximations. In particular, it has been shown that the simulations based on pair potentials with and without three-body correction revealed different results regarding the coordination numbers and the ion-ligand

distances (Hannongbua, 1997; Hannongbua, 1998; Hannongbua, Kerdcharoen and Rode, 1992; Kerdcharoen and Hannongbua, 1999; Pranowo, Mudasir, Kusumawardani and Purtadi, 2006; Pranowo and Rode, 1999). To obtain more reliable results, it has been demonstrated that the “quantum effects” are essential and that the inclusion of these effects in the simulations is mandatory (Rode, Schwenk and Tongraar, 2004).

By means of *ab initio* (AI) MD techniques, Car-Parrinello (CP-MD) and Born-Oppenheimer (BO-MD) are well-known. Undoubtedly, the main advantage of the AI-MD techniques is that the whole system is treated quantum mechanically, most of which are based on density functional theory (DFT). However, some limitations of the AI-MD techniques come from the use of simple generalized gradient approximation (GGA) functionals such as BLYP and PBE and of the relatively small system size. Consequently, this results in too strong ion-ligand interactions, and thus more rigidity of the structure of ion-ligand complexes. In addition, it has been demonstrated that the use of small system size may lead to problem of ion-ion interactions (Lyubartsev, Laaonen and Laaksonen, 2001). With regard to this point, an alternative approach is to apply a so-called combined quantum mechanics/molecular mechanics (QM/MM) MD technique (Armunanto, Schwenk, Randolph and Rode, 2004; Armunanto, Schwenk and Rode, 2004; Field, Bash and Karplus, 1990; Kerdcharoen, Liedl and Rode, 1996; Kerdcharoen and Rode, 2000; Schwenk and Rode, 2004; Tongraar, Kerdcharoen and Hannongbua, 2006). By the QM/MM MD technique, the most interesting part of the system (*i.e.* a sphere which includes the ion and its surrounding solvent molecules) is treated quantum mechanically, while the rest of the system is handled by simple MM force fields. During the past decades, the QM/MM MD technique has been

successfully applied for studying many condensed-phase systems (Gao, 2007; Kerdcharoen, Liedl and Rode, 1996; Rode, Schwenk and Tongraar, 2004; Sripa, Tongraar and Kerdcharoen, 2013; Thaomola, Tongraar and Kerdcharoen, 2012; Wanprakhon, Tongraar and Kerdcharoen, 2011; Singh and Kollman, 1986; Warshel and Levitt, 1976).

According to the QM/MM MD technique, however, there are some limitations that undermine its applicability. In particular, it has been well-demonstrated that only the exchanging particles are treated by a smoothing function when they are crossing the QM/MM boundary. This is not realistic since immediate addition or deletion of a particle in the QM region due to the exchange of solvent molecules also affects the forces acting on the remaining QM particles. As a consequence, such QM/MM MD simulations suffered from numerical instability whenever there are solvent exchanges between the QM and MM region. In addition, the QM/MM MD scheme cannot clearly define the appropriate energy expression during the solvent exchange process (Kerdcharoen and Morokuma, 2003). To overcome these problems, an alternative approach is to apply a more sophisticated QM/MM MD technique based on the ONIOM-XS method (which will be abbreviated throughout this work as “ONIOM-XS MD”). The ONIOM-XS MD technique (Kerdcharoen and Morokuma, 2002) avoids the above problems by smoothing the total potential energy of the entire system, and thus, allowing the forces on every QM particle to be smoothed. The ONIOM-XS MD technique has been successfully applied for studying various condensed-phase systems, such as Li^+ and Ca^{2+} in liquid NH_3 (Kerdcharoen and Morokuma, 2002; Kerdcharoen and Morokuma, 2003), Li^+ , Na^+ , K^+ and Ca^{2+} in aqueous solution (Sripa, Tongraar and Kerdcharoen, 2013; Wanprakhon, Tongraar and Kerdcharoen, 2011) as

well as liquid water (Thaomola, Tongraar and Kerdcharoen, 2012). In several cases, it has been proven that the ONIOM-XS MD technique can provide more insights into the properties of such systems, especially when compared to the results derived by the conventional QM/MM MD scheme. Interestingly, it has been demonstrated that the ONIOM-XS MD technique becomes more effective for the situation where the number of ligands that are crossing the QM/MM boundary is large, *i.e.*, a system in which the ion-ligand interactions are weak and ligand molecules surrounding the ion are labile (Wanprakhon, Tongraar and Kerdcharoen, 2011). For the study of ions in liquid NH_3 , such as for the case of $\text{Ca}^{2+}/\text{NH}_3$ solution, the ONIOM-XS MD simulation (Kerdcharoen and Morokuma, 2003) has predicted a lower coordination number of 6 for Ca^{2+} , compared to the values of 9 and 8.2 predicted by classical MD simulations using pair potentials with and without 3-body corrections (Sidhisoradej, Hannongbua and Ruffolo, 1998). This observed difference clearly confirms the importance of the QM treatment for obtaining more reliable simulation results.

In this work, the ONIOM-XS MD technique will be applied for studying the solvation structure and dynamics of Na^+ in liquid NH_3 . The Na^+ ion is abundant in nature and is known as one of the essential elements that play a vital role for all known life. In particular, the contrasting behavior of Na^+ , *i.e.*, compared to K^+ , is of special interest concerning the process of ionic pumps across the cell membrane. Recently, the ONIOM-XS MD simulations of Na^+ and K^+ in aqueous solution (Wanprakhon, Tongraar and Kerdcharoen, 2011) have provided more insights into the relationship of these two ions with respect to their “structure-making” and “structure-breaking” abilities. For the system of Na^+ in liquid NH_3 , some selected structural parameters for the Na^+ solvation, as obtained from different MC and MD simulations,

are summarized in Table A1 (See Appendix A). For example, the MD simulations using pair potentials based on primitive Gaussian basis sets for Na⁺/ammonia solution at 235 and 266 K have reported the coordination numbers of 8.0 and 7.0, with the average Na⁺-N distances of 2.49 and 2.42 Å, respectively (Hannongbua, 1991). Later, the MC simulations of Na⁺/ammonia solution at 277 K using pair potentials and pair plus three-body correction functions based on DZP basis sets have yielded the average coordination numbers of 9.0 and 8.1, respectively, with the similar Na⁺-N distance of 2.68 Å (Hannongbua, 1997). Another MC simulation using empirical potentials gave a rather small coordination number of 5, with the relatively shorter Na⁺-N distance of 2.25 Å (Marchi, Sprik and Klein, 1990). Interestingly, the results obtained by the conventional QM/MM MD simulation have revealed a lower coordination number of 5 (Kerdcharoen and Rode, 2000), compared to the corresponding values of 9 and 8 predicted by classical MD simulations using pair potentials (Hannongbua, 1991; Hannongbua, 1997; Kerdcharoen and Rode, 2000) or pair potentials plus three-body corrections (Hannongbua, 1997). In this context, the results obtained by the more sophisticated ONIOM-XS MD simulations are expected to provide more reliable descriptions on the structure and dynamics of this solvated ion, especially when compared to the conventional QM/MM MD results.

1.2 Research objectives

1. To apply the more accurate ONIOM-XS MD technique for studying the solvation structure and dynamics of Na⁺ in liquid NH₃.

2. To emphasize the importance of the treatment with the ONIOM-XS MD technique for obtaining detailed knowledge of such condensed-phase system.

1.3 Scope and limitation of the study

In this work, two ONIOM-XS MD simulations were performed. The first ONIOM-XS MD simulation refers to the system of Na^+ in liquid NH_3 and the second one refers to the system of pure liquid NH_3 . In this respect, the ONIOM-XS MD results for the system of pure liquid NH_3 will be used as reference (bulk) when discussing the effects of the ion on the local structure and dynamics of the solvent molecules. According to the computational expense for QM force calculations, the selection of QM method, as well as the QM size and basis sets, must be considered carefully, compromising between the quality of the simulation results and the requirement of CPU time (Xenides, Randolph and Rode, 2005). In this study, all interactions within the QM region were evaluated by performing *ab initio* calculations at the Hartree-Fock (HF) level of accuracy using double- ζ plus polarization (DZP) basis set (Dunning and Hay, 1977) for NH_3 and LANL2DZ basis set (Boys and Bernardi, 1970; Check, Faust, Bailey, Wright, Gilbert and Sunderlin, 2001; Hay and Wadt, 1985) for Na^+ . For the QM size, the QM radii of 4.4 Å and 5.2 Å were chosen for the cases of Na^+ in liquid NH_3 and of pure liquid NH_3 , respectively. These QM sizes are considered to be large enough to include most of the non-additive contributions and the polarization effects, *i.e.*, at least within the whole first solvation shell and some parts of the second solvation layer of Na^+ (or in the case of pure liquid NH_3 , within the whole first solvation shell of the reference NH_3 molecule located at

the center of the QM region). The structural properties of the Na^+ solvation will be analyzed by means of atom-atom radial distribution functions (RDFs) and their corresponding integration numbers, together with the angular distribution functions (ADFs) and dipole-oriented arrangements of NH_3 molecules surrounding the ion. The dynamics properties will be interpreted through ligand exchange processes and mean residence times (MRTs) of NH_3 molecules at the Na^+ ion. The observed differences between the ONIOM-XS MD results and those obtained from experimental data and theoretical investigations will be compared and discussed.

1.4 References

- Ansell, S., Barnes, A. C., Mason, P. E., Neilson, G. W. and Ramos, S. (2006). X-ray and neutron scattering studies of the hydration structure of alkali ions in concentrated aqueous solutions. **Biophysical Chemistry**. 124: 171-179.
- Armunanto, R., Schwenk, C. F., Randolph, B. R. and Rode, B. M. (2004). Structure and dynamics of Co^{2+} in liquid ammonia: *Ab initio* QM/MM molecular dynamics simulation. **Chemical Physics**. 305: 135-140.
- Armunanto, R., Schwenk, C. F. and Rode, B. M. (2004). Gold (I) in liquid ammonia: *Ab initio* QM/MM molecular dynamics simulation. **Journal of the American Chemical Society**. 126: 9934-9935.
- Beu, T. A. and Buck, U. (2001). Structure of ammonia clusters from $n=3$ to 18. **Journal of Chemical Physics**. 114: 7848-7852.
- Boys, S. F. and Bernardi, F. (1970). The calculation of small molecular interactions by the differences of separate total energies. Some procedures with reduced errors. **Molecular Physics**. 19: 553-566.

- Check, C. E., Faust, T. O., Bailey, J. M., Wright, B. J., Gilbert, T. M. and Sunderlin, L. S. (2001). Addition of polarization and diffuse functions to the LANL2DZ basis set for p-block elements. **The Journal of Physical Chemistry A**. 105: 8111-8116.
- Chowdhuri, S. and Chandra, A. (2003). Hydration structure and diffusion of ions in supercooled water: Ion size effects. **The Journal of Chemical Physics**. 118: 9719-9725.
- D, J. V. (1965). Metal ammonia solutions: Physicochemical properties (Lepoutre, G.; Sienko, M. J.; eds.). **Journal of Chemical Education**. 42: A236.
- Das, T. P. (2007). Structure and properties of metal-ammonia solutions **Advances in Chemical Physics**: John Wiley & Sons, Inc.
- Dunning, T. H. and Hay, P. J. (1977). Methods of electronic structure theory. **Modern Theoretical Chemistry**. III, Plenum, New York.
- Field, M. J., Bash, P. A. and Karplus, M. (1990). A combined quantum mechanical and molecular mechanical potential for molecular dynamics simulations. **Journal of Computational Chemistry**. 11: 700-733.
- Gao, J., Xia, X. and George, T. F. (1993). Importance of bimolecular interactions in developing empirical potential functions for liquid ammonia. **The Journal of Physical Chemistry**. 97: 9241-9247.
- Gao, J. (2007). Methods and applications of combined quantum mechanical and molecular mechanical potentials. **Reviews in Computational Chemistry**. 119-185.
- Hannongbua, S. (1991). A molecular dynamics simulation of the structure of sodium ion in liquid ammonia. **Australian Journal of Chemistry**. 44: 447-456.

- Hannongbua, S. (1997). The role of nonadditive effects in the first solvation shell of Na^+ and Mg^{2+} in liquid ammonia: Monte Carlo studies including three-body corrections. **Journal of Chemical Physics**. 106: 6076-6081.
- Hannongbua, S. (1998). On the solvation of lithium ions in liquid ammonia: Monte Carlo simulations with a three-body potential. **Chemical Physics Letters**. 288: 663-668.
- Hannongbua, S. (2000). The best structural data of liquid ammonia based on the pair approximation: First-principles Monte Carlo simulation. **Journal of Chemical Physics**. 113: 4707-4712.
- Hannongbua, S., Kerdcharoen, T. and Rode, B. M. (1992). Zinc (II) in liquid ammonia: Intermolecular potential including three-body terms and Monte Carlo simulation. **The Journal of Chemical Physics**. 96: 6945-6949.
- Hay, P. J. and Wadt, W. R. (1985). *Ab initio* effective core potentials for molecular calculations. Potentials for the transition metal atoms Sc to Hg. **The Journal of Chemical Physics**. 82: 270-283.
- Impey, R. W., Madden, P. A. and McDonald, I. R. (1983). Hydration and mobility of ions in solution. **The Journal of Physical Chemistry**. 87: 5071-5083.
- Johnson, W. C. and Meyer, A. W. (1931). The properties of solutions of metals in liquid ammonia. **Chemical Reviews**. 8: 273-301.
- Karplus, M. and McCammon, J. A. (1983). Dynamics of proteins: Elements and function. **Annual Review of Biochemistry**. 52: 263-300.
- Kerdcharoen, T. and Hannongbua, S. (1999). *Ab initio* study of ion-ammonia complexes: Geometry and many-body interactions. **Chemical Physics Letters**. 310: 333-341.

- Kerdcharoen, T., Liedl, K. R. and Rode, B. M. (1996). A QM/MM simulation method applied to the solution of Li^+ in liquid ammonia. **Chemical Physics**. 211: 313-323.
- Kerdcharoen, T. and Morokuma, K. (2002). ONIOM-XS: An extension of the ONIOM method for molecular simulation in condensed phase. **Chemical Physics Letters**. 355: 257-262.
- Kerdcharoen, T. and Morokuma, K. (2003). Combined quantum mechanics and molecular mechanics simulation of Ca^{2+} /ammonia solution based on the ONIOM-XS method: Octahedral coordination and implication to biology. **Journal of Chemical Physics**. 118: 8856-8862.
- Kerdcharoen, T. and Rode, B. M. (2000). What is the solvation number of Na^+ in ammonia? An *ab initio* QM/MM molecular dynamics study. **Journal of Physical Chemistry A**. 104: 7073-7078.
- Kincaid, R. H. and Scheraga, H. A. (1982). Revised empirical potential for conformational, intermolecular, and solvation studies. 6. Testing of parameters by application to liquid ammonia. **Journal of Physical Chemistry**. 86: 833-838.
- Koneshan, S., Rasaiah, J. C., Lynden-Bell, R. M. and Lee, S. H. (1998). Solvent structure, dynamics, and ion mobility in aqueous solutions at 25 °C. **The Journal of Physical Chemistry B**. 102: 4193-4204.
- Lee, S. H. and Rasaiah, J. C. (1994). Molecular dynamics simulation of ionic mobility. I. Alkali metal cations in water at 25 °C. **The Journal of Chemical Physics**. 101: 6964-6974.

- Lyubartsev, A. P., Laasonen, K. and Laaksonen, A. (2001). Hydration of Li^+ ion. An *ab initio* molecular dynamics simulation. **The Journal of Chemical Physics**. 114: 3120-3126.
- Marchi, M., Sprik, M. and Klein, M. L. (1990). Solvation and ionization of alkali metals in liquid ammonia : A path integral Monte Carlo study. **Journal of Physics**. 2: 5833-5848.
- Marcus, Y. (1988). Ionic radii in aqueous solutions. **Chemical Reviews**. 88: 1475-1498.
- Morokuma, K. (2003). ONIOM and its applications to material chemistry and catalyses. **Bulletin of the Korean Chemical Society**. 24: 797-801.
- Narten, A. H. (1976). Liquid ammonia: Molecular correlation functions from x-ray diffraction. **The Journal of Chemical Physics**. 66: 3117-3120.
- Ohtaki, H. and Radnai, T. (1993). Structure and dynamics of hydrated ions. **Chemical Reviews**. 93: 1157-1204.
- Pranowo, H. D., Mudasir, Kusumawardani, C. and Purtadi, S. (2006). The structure of Co^{2+} in liquid ammonia: Monte Carlo simulation including three-body correction. **Chemical Physics**. 324: 573-578.
- Pranowo, H. D. and Rode, B. M. (1999). Solvation of Cu^{2+} in liquid ammonia: Monte Carlo simulation including three-body corrections. **The Journal of Physical Chemistry A**. 103: 4298-4302.
- Rode, B. M., Schwenk, C. F. and Tongraar, A. (2004). Structure and dynamics of hydrated ions-new insights through quantum mechanical simulations. **Journal of Molecular Liquids**. 110: 105-122.

- Roux, B. and Karplus, M. (1994). Molecular dynamics simulations of the gramicidin channel. **Annual Review of Biophysics and Biomolecular Structure**. 23: 731-761.
- Salter, T. E. and Ellis, A. M. (2007). Microsolvation of lithium in ammonia: Dissociation energies and spectroscopic parameters of small $\text{Li}(\text{NH}_3)_n$ clusters ($n = 1$ and 2) and their cations. **Chemical Physics**. 332: 132-138.
- Schwenk, C. F. and Rode, B. M. (2004). Cu (II) in liquid ammonia: An approach by hybrid quantum-mechanical/molecular-mechanical molecular dynamics simulation. **ChemPhysChem**. 5: 342-348.
- Sidhisoradej, W., Hannongbua, S. and Ruffolo, D. (1998). Three-body effects in calcium(II)-ammonia solutions: Molecular dynamics simulations. **Zeitschrift fur Naturforschung - Section A Journal of Physical Sciences**. 53: 208-216.
- Singh, U. C. and Kollman, P. A. (1986). A combined *ab initio* quantum mechanical and molecular mechanical method for carrying out simulations on complex molecular systems: Applications to the $\text{CH}_3\text{Cl} + \text{Cl}^-$ exchange reaction and gas phase protonation of polyethers. **Journal of Computational Chemistry**. 7: 718-730.
- Sripa, P., Tongraar, A. and Kerdcharoen, T. (2013). "Structure-making" ability of Na^+ in dilute aqueous solution: An ONIOM-XS MD simulation study. **The Journal of Physical Chemistry A**. 117: 1826-1833.
- Thaomola, S., Tongraar, A. and Kerdcharoen, T. (2012). Insights into the structure and dynamics of liquid water: A comparative study of conventional QM/MM and ONIOM-XS MD simulations. **Journal of Molecular Liquids**. 174: 26-33.

- Tongraar, A., Kerdcharoen, T. and Hannongbua, S. (2006). Simulations of liquid ammonia based on the combined quantum mechanical/molecular mechanical (QM/MM) approach. **The Journal of Physical Chemistry A**. 110: 4924-4929.
- Tongraar, A., Liedl, K. R. and Rode, B. M. (1998). Born-Oppenheimer *ab initio* QM/MM dynamics simulations of Na⁺ and K⁺ in water : From structure making to structure breaking effects. **Journal of Physical Chemistry A**. 102: 10340-10347.
- Wanprakhon, S., Tongraar, A. and Kerdcharoen, T. (2011). Hydration structure and dynamics of K⁺ and Ca²⁺ in aqueous solution: Comparison of conventional QM/MM and ONIOM-XS MD simulations. **Chemical Physics Letters**. 517: 171-175.
- Warshel, A. and Levitt, M. (1976). Theoretical studies of enzymic reactions: Dielectric, electrostatic and steric stabilization of the carbonium ion in the reaction of lysozyme. **Journal of Molecular Biology**. 103: 227-249.
- Woolf, T. B. and Roux, B. (1994). Molecular dynamics simulation of the gramicidin channel in a phospholipid bilayer. **Proceedings of the National Academy of Sciences of the United States of America**. 91: 11631-11635.
- Xenides, D., Randolph, B. R., and Rode, B. M. (2005). Structure and ultrafast dynamics of liquid water: A quantum mechanics/molecular mechanics molecular dynamics simulations study. **The Journal of Chemical Physics**. 122: 174506.
- Zhou, J., Lu, X., Wang, Y. and Shi, J. (2002). Molecular dynamics study on ionic hydration. **Fluid Phase Equilibria**. 194: 257-270.

CHAPTER II

QUANTUM CHEMISTRY

2.1 Introduction to quantum mechanics

Quantum mechanics is known as an essential tool applied for describing the fundamental behavior of matter at molecular scale, in particular the electron behavior. Quantum mechanics explicitly treat the electrons in a calculation, and thus, it is possible to derive properties that depend upon the electronic distributions and in particular to investigate chemical reactions in which bonds are broken or formed. In this respect, the energy and some properties of a molecule can be derived from a wavefunction, which can be obtained by solving the *Schrödinger equation* (Schrödinger, 1926).

2.2 Schrödinger equation

Quantum mechanics describe molecules in terms of interactions among nuclei and electrons, and molecular geometry in terms of minimum energy arrangements of nuclei. It is straightforward to generalize the Schrödinger equation to a multinuclear, multielectron system. Note that the objective of most *ab initio* electronic structure theories is the solution of the time-independent Schrödinger equation, which can be expressed in a time independent form as

$$\hat{H}\Psi = E\Psi , \quad (2.1)$$

where \hat{H} is the *Hamiltonian operator*, which corresponds to the kinetic energy, \hat{T} , and potential energy, \hat{V} , of the system. In general, the *Hamiltonian operator* can be written as

$$\hat{H} = \hat{T} + \hat{V} , \quad (2.2)$$

where

$$\hat{T} = -\frac{\hbar^2}{2m} \nabla^2 , \quad (2.3)$$

and thus,

$$\hat{H} = -\frac{\hbar^2}{2m} \nabla^2 + \hat{V} . \quad (2.4)$$

In situations where the potential is independent of time, this enables us to write the time-dependent Schrödinger equation in a more familiar time-dependent form as

$$\left\{ -\frac{\hbar^2}{2m} \nabla^2 + \hat{V} \right\} \Psi = E\Psi , \quad (2.5)$$

where ∇^2 is the *Laplacian operator*, written as

$$\nabla^2 = \frac{\partial^2}{\partial x^2} + \frac{\partial^2}{\partial y^2} + \frac{\partial^2}{\partial z^2}. \quad (2.6)$$

Here, \hbar is Planck's constant divided by 2π . Ψ is an eigenfunction which characterizes the particle's properties, and E is the eigenvalue of the particle with respect to the eigenfunction.

2.3 The variation theory

One of the useful methods for estimating the lowest energy is based on a so-called variation theory, which assessing and improving guesses about the forms of wavefunctions in systems. The theory starts with a trial function (Φ), which can be written in terms of a linear combination of the wavefunctions (ψ_i),

$$\Phi = \sum_i c_i \psi_i, \quad (2.7)$$

where the individual ψ_i and coefficients c_i are unknown. Then, the normality of Φ imposes a constraint on the coefficients, deriving from

$$\begin{aligned} \int \Phi^2 dr = 1 &= \int \sum_i c_i \psi_i \sum_j c_j \psi_j dr \\ &= \sum_{ij} c_i c_j \int \psi_i \psi_j dr \\ &= \sum_{ij} c_i c_j \delta_{ij} \\ &= \sum_i c_i^2. \end{aligned} \quad (2.8)$$

Then, considering the energy associated with the wavefunction (Φ) as

$$\begin{aligned}
 \int \Phi H \Phi dr &= \int (\sum_i c_i \psi_i) H (\sum_j c_j \psi_j) dr \\
 &= \sum_{ij} c_i c_j \int \psi_i H \psi_j dr \\
 &= \sum_{ij} c_i c_j E_j \delta_{ij} \\
 &= \sum_i c_i^2 E_i.
 \end{aligned} \tag{2.9}$$

After that, combining the results from equations (2.8) and (2.9), give

$$\int \Phi H \Phi dr - E_0 \int \Phi^2 dr = \sum_i c_i^2 (E_i - E_0). \tag{2.10}$$

In general, the coefficients are assumed to be real numbers, thus, c_i^2 and the result of $(E_i - E_0)$ must be greater than or equal to zero. Therefore,

$$\int \Phi H \Phi dr - E_0 \int \Phi^2 dr \geq 0 \tag{2.11}$$

or

$$\frac{\int \Phi H \Phi dr}{\int \Phi^2 dr} \geq E_0. \tag{2.12}$$

According to equation (2.12), the quality of wavefunctions for describing the ground state of a system can be defined by their associated energies as the better wavefunction can be constructed in any manner, which determined the quality by the integral in equation (2.12).

2.4 Born-Oppenheimer approximation

It is known that the Schrödinger equation cannot be solved exactly for any molecular systems. On the other hand, it is possible to solve the equation exactly for the simplest molecular species when the motion of the electrons is decoupled from the motion of the nuclei in accordance with the *Born-Oppenheimer approximation* (Born and Oppenheimer, 1927). In fact, since the nuclei are heavier than electrons, the nuclei are moving slowly than the electrons (Szabo and Ostlund, 1989). According to this property, the approximation has been made by separating the nuclei and electrons motions, called the Born-Oppenheimer approximation.

For N particle system, the *Hamiltonian operator* (\hat{H}) takes into account five contributions to the total energy of a system, namely the kinetic energies of the electrons (\hat{T}_e) and nuclei (\hat{T}_n), the attraction of the electrons to the nuclei (\hat{V}_{en}), and the inter-electronic (\hat{V}_{ee}) and inter-nuclear (\hat{V}_{nn}) repulsions, as shown in equations (2.13) and (2.14),

$$\hat{H} = \hat{T}_e + \hat{T}_n + \hat{V}_{en} + \hat{V}_{ee} + \hat{V}_{nn}, \quad (2.13)$$

$$\hat{H} = -\sum_{i=1}^N \frac{1}{2} \nabla_i^2 - \sum_{A=1}^M \frac{1}{2M_A} \nabla_A^2 - \sum_{i=1}^N \sum_{A=1}^M \frac{Z_A}{r_{ij}} + \sum_{i=1}^N \sum_{j>i}^N \frac{1}{r_{ij}} + \sum_{A=1}^M \sum_{B>A}^M \frac{Z_A Z_B}{R_{AB}}, \quad (2.14)$$

where i and j represent electrons, A and B represent nuclei, M is the mass of nucleus, Z is the atomic number, r and R are the distances between particles.

Based on the Born-Oppenheimer approximation, the electronic energies are computed by fixing nuclear position. Consequently, the nuclear kinetic energy term is

independent, and thus, can be neglected and the last term in equation (2.14), the repulsion of nuclei, can be considered as a constant. The remaining terms in equation (2.14) are called the electronic Hamiltonian or Hamiltonian describing the motion of N electrons in the field of M point charges,

$$\hat{H}_{elec} = -\sum_{i=1}^N \frac{1}{2} \nabla_i^2 - \sum_{i=1}^N \sum_{A=1}^M \frac{Z_A}{r_{ij}} + \sum_{i=1}^N \sum_{j>i}^N \frac{1}{r_{ij}} + \sum_{A=1}^M \sum_{B>A}^M \frac{Z_A Z_B}{R_{AB}}. \quad (2.15)$$

2.5 Molecular orbital theory

The molecular orbital theory is a method for determining molecular structure. A molecular orbital is a region in which an electron can be found in a molecule. In general, the molecular orbital can be described by wavefunction of the electron in a molecule, in particular a spatial distribution $(|\psi_i(r)|^2)$ of an electron and energy of up to two electrons within it. A complete wavefunction for an electron consists of a molecular orbital and a spin function (α and β), which can be defined as a *spin orbital* ($\chi(x)$) where x indicates both space and spin coordinates. Therefore, a spatial orbital can be formed into two different spin orbitals as

$$\chi(x) = \begin{cases} \psi(r)\alpha(\varpi) \\ \psi(r)\beta(\varpi). \end{cases} \quad (2.16)$$

To simplify the treatment further, the next step is to assume that the electrons are non-interacting in which the appropriate functional form of the wavefunction for N electrons can be expressed as

$$H = \sum_{i=1}^N h(i), \quad (2.17)$$

where $h(i)$ is the operator that describes the kinetic and potential energies of electron i . Then, the set of spin orbitals ($\chi_j(x)$) have been added to the operator,

$$h(i)\chi_j(x_i) = \varepsilon_j\chi_j(x_i). \quad (2.18)$$

In this respect, the wavefunction is a simple product of spin orbital wavefunction for each electron as

$$\Psi^{HP}(x_1, x_2, \dots, x_N) = \chi_i(x_1)\chi_j(x_2)\dots\chi_k(x_N). \quad (2.19)$$

The above equation can be written as

$$H\Psi^{HP} = E\Psi^{HP}, \quad (2.20)$$

where E is the sum of the spin orbital energies of each spin orbitals in Ψ^{HP} ,

$$E = \varepsilon_i + \varepsilon_j + \dots + \varepsilon_k. \quad (2.21)$$

Accordingly, a N -electron wavefunction is termed a *Hartree product*, where the electron-one has been described by the spin orbital (χ_i), electron-two has been

described by the spin orbital (χ_j), *etc.* However, this wavefunction does not allow the antisymmetry principle.

To ensure the antisymmetric, considering a two-electron case in order to put electron-one in χ_i and electron-two in χ_j as

$$\Psi_{12}^{HP}(x_1, x_2) = \chi_i(x_1)\chi_j(x_2). \quad (2.22)$$

In the opposite way, putting electron-one in χ_j and electron-two in χ_i as

$$\Psi_{21}^{HP}(x_2, x_1) = \chi_i(x_2)\chi_j(x_1). \quad (2.23)$$

After that, taking the appropriate linear combination of these two Hartree products,

$$\Psi(x_1, x_2) = 2^{-1/2}(\chi_i(x_1)\chi_j(x_2)) - (\chi_i(x_2)\chi_j(x_1)), \quad (2.24)$$

where the factor $2^{-1/2}$ is a normalization factor and the minus sign insures that $\Psi(x_1, x_2)$ is antisymmetric with respect to the interchange of the coordinates of electrons one and two. From equation (2.24), the wavefunction will be disappeared if both electrons occupy the same spin orbital, *i.e.*, following the *Pauli exclusion principle*. Moreover, the antisymmetric wavefunction can be rewritten in terms of a determinant,

$$\Psi(x_1, x_2) = 2^{-1/2} \begin{vmatrix} \chi_i(x_1) & \chi_j(x_1) \\ \chi_i(x_2) & \chi_j(x_2) \end{vmatrix}, \quad (2.25)$$

which is called a *Slater determinant* (Slater, 1929). For an N -electron system, the generalization is

$$\Psi(x_1, x_2, \dots, x_N) = (N!)^{-1/2} \begin{vmatrix} \chi_i(x_1) & \chi_j(x_1) & \cdots & \chi_k(x_1) \\ \chi_i(x_2) & \chi_j(x_2) & \cdots & \chi_k(x_2) \\ \vdots & \vdots & \ddots & \vdots \\ \chi_i(x_N) & \chi_j(x_N) & \cdots & \chi_k(x_N) \end{vmatrix}, \quad (2.26)$$

Here, the factor $(N!)^{-1/2}$ ensures that the wave function is normalized. The short-hand notation for a normalized Slater determinant only shows the diagonal elements of determinant,

$$\Psi(x_1, x_2, \dots, x_N) = |\chi_i(x_1)\chi_j(x_2)\cdots\chi_k(x_N)\rangle. \quad (2.27)$$

2.6 The LCAO-MO approach and basis sets

In most of quantum mechanical calculations, the molecular orbitals can be built from the atomic orbitals by using *linear combination of atomic orbitals to molecular orbitals* (LCAO-MO) method. The molecular orbitals, ψ_i , can be composed of a set of atomic orbitals, known as basis functions. Thus, each molecular orbital can be written as a summation of the following form:

$$\psi_i = \sum_{\mu=1}^N c_{\mu i} \phi_{\mu}, \quad (2.28)$$

where $c_{\mu i}$ are the molecular orbital expansion coefficients, and N is the number of atomic basis function. Here, a set of N function ϕ_{μ} is called *basis set*. The $c_{\mu i}$ can be calculated using various approaches, most of which are based on the linear variation methods.

Two common types of basis function used in the electronic structure calculations are Slater Type Orbitals (STOs) (Slater, 1930) and Gaussian Type Orbitals (GTOs) (Boys, 1950).

The formalism of the STOs can be expressed as

$$\psi(n, l, m_l; r, \theta, \phi) = N r^{n_{eff}-1} e^{-Z_{eff} r / n_{eff}} Y_{lm_l}(\theta, \phi), \quad (2.29)$$

where n , l , and m_l are the quantum numbers referring to principal, angular momentum and magnetic, respectively, N is the normalization constant and Y_{lm_l} is a spherical harmonic. The STOs screening constants are calculated for small model molecules using rigorous self-consistent field methods, and then being generated for use with actual molecules of interest. The accuracy of STOs can be improved by combining two or more STOs into a single one-electron wavefunction (double ζ basis set). Z_{eff} is the effective nuclear charge, while the effective principal quantum number (n_{eff}) is related to the true principal quantum (n) by the mapping of

$$n \rightarrow n_{eff} : 1 \rightarrow 1 \quad 2 \rightarrow 2 \quad 3 \rightarrow 3 \quad 4 \rightarrow 3.7 \quad 5 \rightarrow 4.0 \quad 6 \rightarrow 4.2,$$

in which the value of ρ equal r/a_0 , where a_0 is *Bohr radius*.

The STOs are usually applied for atomic and diatomic system, which high accuracy, such as in semi-empirical methods where all three- and four-center integrals are neglected and in density functional methods that do not include exact exchange and that the coulomb energy is calculated by fitting the density into a set of auxiliary functions. However, the STOs do not satisfy in the case of two-electron integral problem. With regard to this point, the feasible basis function is *Gaussian type orbitals* (GTOs), which are function of the form

$$\theta_{ijk}(r_1 - r_c) = (x_1 - x_c)^i (y_1 - y_c)^j (z_1 - z_c)^k e^{-\alpha|r_1 - r_c|^2}, \quad (2.30)$$

where (x_c, y_c, z_c) are the Cartesian coordinates of the center of the Gaussian function at r_c , (x_1, y_1, z_1) are the Cartesian coordinates of an electron at r_1 , i , j and k are nonnegative integers and α is a positive exponent. The advantage of GTOs is that the product of two Gaussians at different centers is equivalent to a single Gaussian function centered at a point between the two centers. Therefore, the two-electron integral problem on three and four or more different atomic centers can be reduced to integrals over two different centers. However, it is known that the GTO gives an inferior representation of the orbitals at the atomic nuclei, which can be considered at 1s-orbital. Note that the 1s-orbital of STO has a *cusp* at the atomic nucleus while a GTO does not, as can be seen in Figure 2.1. In this respect, the larger basis must be used to achieve the accuracy comparable to that obtained from STOs.

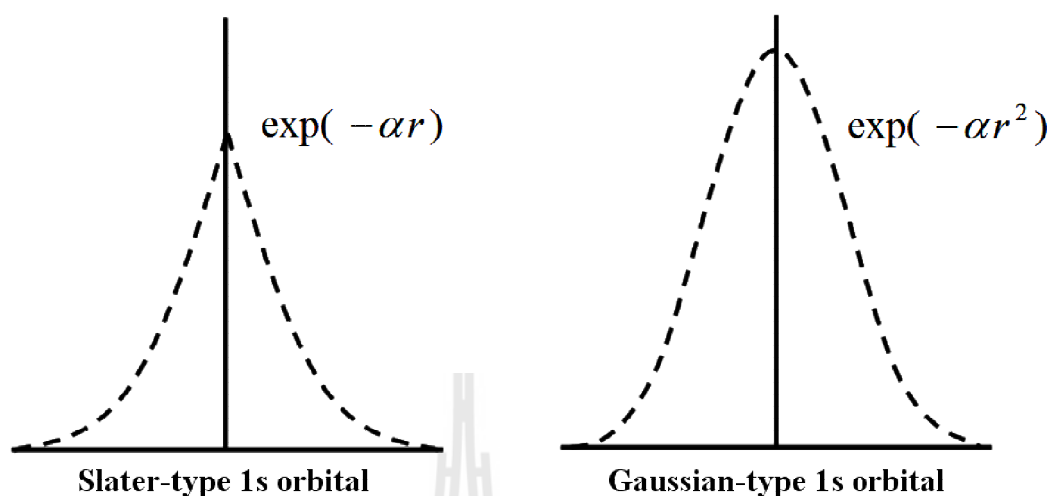


Figure 2.1 The Slater-type and Gaussian-type for 1s orbital.

The most important factor for creating the molecular orbital is a set of parameters applied to the basis function, called *basis set*. The smallest number of function possible for constructing the molecular orbital is called a *minimum basis set*. The improvement of the basis set can be made by replacing two basis functions into each basis function in the minimal basis set, called *double zeta* (DZ). The larger basis set is a *triple zeta* (TZ), where three basis functions are used to represent each of the minimal basis set. The compromise between the DZ and TZ basis sets is called a *split valence* (SV) basis set, in which each valence atomic orbital is represented by two basis functions while each core orbital is represented by a single basis function.

In 1969, Pople and coworkers (Hehre, Stewart, and Pople, 1969) designed the basis set by expanding the STO in terms of n primitive Gaussians, called STO-nG basis set. The primitive Gaussian has been derived for $n = 2-6$. However, the STO-3G basis set is a widely used minimal basis set, as shown in Figure 2.2. The STO-3G

basis set partially represents the *cusp* of s-type orbital, which is quite reasonable for representing the orbital at the atomic nuclei.

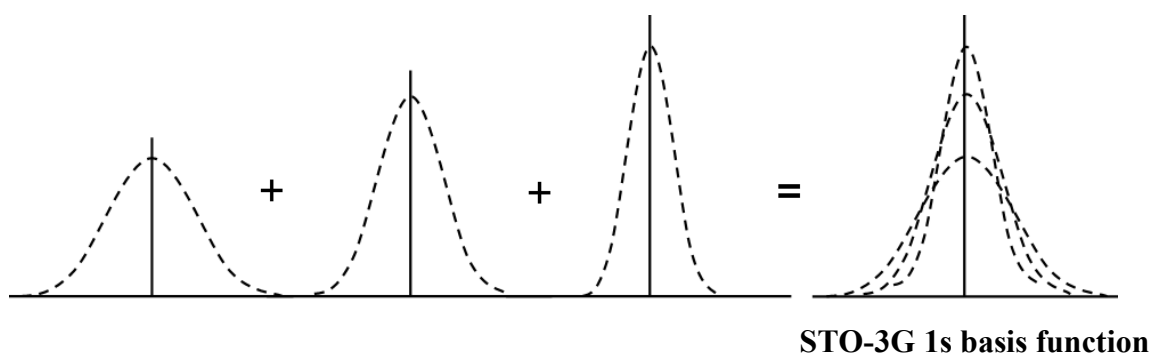


Figure 2.2 The STO-3G basis set representing the desired STO.

In addition, Pople and coworkers have applied the split valence to obtain flexibility in the basis set, which can be designed as k - nlm G basis set. The first parameter (k) indicates the number of primitives used in the contracted core, while the two values (nl) refer to a split valence, and three values (nlm) refer to a triple split valence, such as 6-311G. For the triple split valence basis, the core orbitals are a contraction of six primitives and the valence splits into three functions, represented by three, one and one primitive GTOs, respectively. The Pople's style basis sets may include diffuse and/or polarization functions. The diffuse function can be denoted as + or ++ before the G, in which the first + indicates one set of diffuse s- and p-function adding on heavy atoms and the second + refer to the inclusion of diffuse s-function for hydrogen atom. The polarization function can be put after the G, which separates designation for heavy and hydrogen atoms. For example, 6-31+G(d) basis set refers to a split valence with additional diffuse sp-functions and a single d-type polarization

function only on heavy atoms. The largest standard Pople style basis set is 6-311++G(3df,3pd). In addition, the polarization function can be replaced with * notation, for example, the 6-311G* basis set is identical to 6-311G(d) and 6-311G** basis set is identical to 6-311G(d,p).

Since several GTOs are often grouped together, the *contracted Gaussian function* has been applied to *Dunning-Huzinaga* (DZ) basis set (Dunning, 1970; Dunning 1971; Huzinaga, 1965). The DZ basis set can be made by a contraction such as the (9s5p) primitive GTOs to [4s,2p]. The contraction scheme is 6,1,1,1 for s-functions and 4,1 for the p-functions. In addition, the development of basis set by Dunning and coworkers for recovering the correlation energy of the valence electrons is known as the *correlation consistent* (cc) basis sets. The general formulation can be written as cc-pVnZ, where $n = D$ for double zeta, T for triple zeta, Q for quadruple zeta, 5 for quintuple zeta or 6 for sextuple zeta. The diffuse functions can be augmented into the correlation consistent basis set by adding the prefix aug-, such as aug-cc-pVnZ. The correlation consistent basis set provides accurate description of anions and weak interactions, in particular for systems involving van der Waals forces and hydrogen bonding.

For the systems having large number of core electron elements, it is necessary to use a large number of basis functions for describing them. However, since the deep core electrons are not much important in a chemical sense, this leads to an approximation by replacing the core electrons with analytical functions, called an *Effective Core Potential* (ECP) (Collins, Schleyer, Binkley, and Pople, 1976) or *pseudopotential* (PP) (Aqvist and Warshel, 1993), which would reasonably

accurately, and much more efficiently, representing the combined nuclear-electronic core to the remaining electrons.

2.7 Basis Set Superposition Error (BSSE)

In the calculations of molecular energies using atomic basis sets, especially for weak interactions, an error occurs due to the use of basis functions on adjacent molecules (Davidson and Chakravorty, 1994). The results are regarded as “*Basis Set Superposition Error* (BSSE)” (Boys and Bernardi, 1970). The BSSE causes overestimation of the attractive contribution to the interaction energy and consequently provides an illegitimate increase of binding energy in a molecule. As a consequence, this may lead to less accurate results regarding to molecular geometry optimization and molecular charge distribution. The BSSE can be calculated with the help of *ghost* atoms. In this respect, the amount of BSSE can be estimated using *Counterpoise Procedure* (CP) (Boys and Bernardi, 1970). The counterpoise correction is the energy lowering of single monomer in the presence of *ghost* basis functions located at the position of the atomic centers of that monomer, but without additional nuclear charges or electrons. The correction for BSSE in the molecular calculations with medium and small basis sets can result in values of interaction energies which are fairly close to those obtained by using more expensive and large basis sets. However, it should be realized that the counterpoise method will not provide effective improvement of the results if the atomic basis sets are very poor. The counterpoise procedure has been used as a standard tool of theoretical chemistry although some researchers have raised serious doubts on the usefulness of this procedure (Schwenke and Truhlar, 1986). The counterpoise correction can be very reasonable for the

estimation of weak electronic interaction energies with small basis sets at Hartree-Fock level of accuracy. However, this approach has failed for the estimation of strong electronic interaction energies even if with up to date basis sets, as demonstrated by a study of cyclic hydrogen fluoride trimer (Liedl, 1998).

2.8 Hartree-Fock method

The important factor in the electronic structure calculations is the electron-electron repulsions, which must be included in any accurate electronic structure treatment. The *Hartree-Fock* (HF) method treats the electron-electron repulsions in an average way. The Hamiltonian operator considers that each electron individually move in the average field of all other electrons in the molecule. This is the basis of the self-consistent field (SCF) procedure. For closed-shell systems (all electrons spin-paired, two per occupied orbital), the formalism is well known as restricted Hartree-Fock (RHF). The Hamiltonian operator for one-electron is called Fock operator, \hat{F} , which can be defined as

$$\hat{F}(1) = \hat{H}_{(1)}^{core} + \sum_{a=1}^{N/2} (2\hat{J}_a(1) - \hat{K}_a(1)), \quad (2.31)$$

where $\hat{H}_{(1)}^{core}$ is the core Hamiltonian operator,

$$\hat{H}_{(1)}^{core} = -\frac{1}{2}\nabla_1^2 - \sum_{a=1}^{N/2} \frac{Z_a}{r_{1a}}, \quad (2.32)$$

where \hat{J}_a is Coulomb operator representing the classical repulsion between two electron distributions (*i.e.*, interaction potential of electron a with all of the other electrons), which can be defined as

$$\hat{J}_a(1)\phi_a(\chi_1) = \left\{ \int \phi_a^*(\chi_2) \frac{1}{r_{12}} \phi_a(\chi_2) dx_2 \right\} \phi_a(\chi_1), \quad (2.33)$$

and \hat{K}_a is exchange operator representing the exchange function according to the fact that the two electrons exchange their positions corresponds to Pauli's principle. The exchange of electrons in two-spin orbitals can be defined as

$$\hat{K}_a(1)\phi_a(\chi_1) = \left\{ \int \phi_a(\chi_2) \frac{1}{r_{12}} \phi_a^*(\chi_2) dx_2 \right\} \phi_a(\chi_1). \quad (2.34)$$

The Fock operator and the exact Hamiltonian are different, *i.e.*, the coulomb operator has been replaced by an operator describing the interaction of each electron with the average field of all other electrons. In this respect, the expansion of the wavefunction in terms of basis functions from the application of LCAO-MO method lead to a limitation of the accuracy of the *ab initio* HF approach since there is limited number of basis functions available. The greater the number of basis functions, the better the wavefunction and the lower the energy. The limit of an infinite basis set is known as the *Hartree-Fock limit*. Moreover, the HF equation for atom can be solved by numerical integration. Nevertheless, complication arises when molecules are

considered because there is more than one center. Thus, the HF equation can be written independently using *Roothaan-Hall equations*,

$$\sum_{v=1}^N (F_{\mu v} - \varepsilon_i S_{\mu v}) c_{vi} = 0, \quad \mu = 1, 2, 3, \dots, N \quad (2.35)$$

with the normalization conditions,

$$\sum_{\mu=1}^N \sum_{v=1}^N c_{\mu i}^* S_{\mu v} c_{vi} = 1, \quad (2.36)$$

where ε_i is the one-electron energy of molecular orbital ψ_i and $S_{\mu v}$ is the element of an $N \times N$ matrix termed the overlap matrix.

$$S_{\mu v} = \int \phi_{\mu}^*(1) \phi_v(1) dx_1 dy_1 dz_1, \quad (2.37)$$

and $F_{\mu v}$ is the element of another $N \times N$ matrix, called the *Fock matrix*,

$$F_{\mu v} = H_{\mu v}^{core} + \sum_{\lambda=1}^N \sum_{\sigma=1}^N P_{\lambda\sigma} \left[(\mu\nu|\lambda\sigma) - \frac{1}{2}(\mu\lambda|\nu\sigma) \right]. \quad (2.38)$$

In this expression, $H_{\mu\nu}^{core}$ is a matrix representing the energy of a single electron in a field of “bare” nuclei. Its elements are

$$H_{\mu\nu}^{core} = \int \phi_{\mu}^*(1) \hat{H}^{core}(1) \phi_{\nu}(1) dx_1 dy_1 dz_1, \quad (2.39)$$

in which

$$\hat{H}^{core}(1) = -\frac{1}{2} \left(\frac{\partial^2}{\partial x_1^2} + \frac{\partial^2}{\partial y_1^2} + \frac{\partial^2}{\partial z_1^2} \right) - \sum_{A=1}^M \frac{Z_A}{r_{1A}}, \quad (2.40)$$

where Z_A and is the atomic number of atom A , and summation is carried out over all atoms. The quantities $(\mu\nu|\lambda\sigma)$ and $(\mu\lambda|\nu\sigma)$ appearing in (2.38) are two-electron integrals,

$$(\mu\nu|\lambda\sigma) = \iint \phi_\mu^*(1)\phi_\nu(1) \left(\frac{1}{r_{12}} \right) \phi_\lambda^*(2)\phi_\sigma(2) dx_1 dy_1 dz_1 dx_2 dy_2 dz_2, \quad (2.41)$$

$$(\mu\lambda|\nu\sigma) = \iint \phi_\mu^*(1)\phi_\lambda(1) \left(\frac{1}{r_{12}} \right) \phi_\nu^*(2)\phi_\sigma(2) dx_1 dy_1 dz_1 dx_2 dy_2 dz_2, \quad (2.42)$$

which are multiplied by the elements of the one-electron density matrix, $P_{\lambda\sigma}$,

$$P_{\lambda\sigma} = 2 \sum_{i=1}^{occ} c_{\lambda i}^* c_{\sigma i}. \quad (2.43)$$

The significance of the density matrix is that it describes the electron density of the molecules. Thus, the criterion for judging convergence of the self-consistent, called as self-consistent field (SCF), which refers to the density as well as to the energy because both have to be stationary at self-consistence. In equation (2.43), the summation refers to occupied molecular orbitals only. The factor of two indicates that two electrons

occupy each molecular orbital, and the asterisk represents complex conjugation (required if the molecular orbitals are not the real functions). The electronic energy, E^{elec} , is now given by

$$E^{elec} = \frac{1}{2} \sum_{\mu=1}^N \sum_{\nu=1}^N P_{\mu\nu} (F_{\mu\nu} + H_{\mu\nu}^{core}), \quad (2.44)$$

and when adding the internuclear repulsion,

$$E^{elec} = \sum_A^N \sum_{B>A}^N \frac{Z_A Z_B}{R_{AB}}, \quad (2.45)$$

yields an expression for the total energy.

With regard to the two-electron integrals, the amount of atomic basis functions give rise to a major practical problem in the application of the *ab initio* HF method due to the computational requirement which is approximated to $N^4/8$ for N basis functions. In fact, not only time consuming of the integral calculation, but also their storage on disk is practically impossible for large molecular systems. Consequently, the *Direct SCF methods* have become available, which reduce these problems significantly. By these approaches, the two-electron integrals are not stored but recalculated as required. This makes sense because the CPU of modern computers is very fast, while I/O operation takes quite long time. Secondly, only those integrals that are expected to have a significant value are actually calculated. With these tricks built into modern programs, the direct algorithms are actually faster than the conventional one for systems of more than about 100 basis functions (depending on the particular

computer). On small workstations, direct SCF methods are only practical option, even for small systems.

Since *ab initio* quantum chemical methods are limited in their practical applicability (*i.e.*, because of their heavy demands of CPU time and storage space on disk or in computer memory), evaluation of the two-electron integrals for molecules with large number of electrons becomes computationally impractical. The *Semiempirical* HF methods have been developed to simplify these integrals that compensate for neglecting some of that time consuming mathematical terms. In general, the parameters used by semiempirical methods can be derived from experimental measurement or by performing *ab initio* calculations on model systems.

2.9 Electron correlation

It is known that motions of electrons are correlated and they tend to repel each other to give a lower energy. According to the HF method, each electron moves in the static electric field created by all of the other electrons in the system. On the other hand, the electron cannot see other electrons during the HF calculation. Thus, the significant deficiency of the HF method is that it fails to adequately treat the correlation between motions of electrons. The effects of electron correlation are usually neglected in the Hamiltonian in the previous section. This leads to limitation of the HF energy calculations. The difference between HF and exact (non-relativistic) energies is the correlation energy,

$$E_{exact} = E_{HF} + E_{correlation} . \quad (2.46)$$

Since the HF energy is always above the exact energy, the correlation energy is always negative,

$$E_{corr} < 0. \quad (2.47)$$

In several cases, the neglect of electron correlation effects can lead to some anomaly of qualitative information. As a consequence, the Ψ and E cannot be used to correctly predict atomic properties without somewhere accounting for electron correlation.

The electron correlation methods calculate the coefficient in front of the other determinants in different way, such as *configuration interaction* (CI) (Sherrill and Schaefer Iii, 1999), *many-body perturbation* (MP) (Møller and Plesset, 1934), *coupled cluster* (CC) (Bartlett, 1989) and *density functional theory* (DFT).

2.10 References

- Aqvist, J. and Warshel, A. (1993). Simulation of enzyme reactions using valence bond force fields and other hybrid quantum/classical approaches. **Chemical Reviews**. 93: 2523-2544.
- Bartlett, R. J. (1989). Coupled-cluster approach to molecular structure and spectra: A step toward predictive quantum chemistry. **The Journal of Physical Chemistry**. 93: 1697-1708.
- Born, M. and Oppenheimer, J. R. (1927). On the quantum theory of molecule. **Annalen der Physik**. 84: 457.

- Boys, S. F. (1950). Electronic wavefunctions. I. A general method of calculation for the stationary states of any molecular system. **Proceedings of the Royal Society of London. Series A. Mathematical and Physical Sciences.** 200: 542-554.
- Boys, S. F. and Bernardi, F. (1970). The calculation of small molecular interactions by the differences of separate total energies. Some procedures with reduced errors. **Molecular Physics.** 19: 553-566.
- Collins, J. B., Schleyer, P. V. R., Binkley, J. S. and Pople, J. A. (1976). Self-consistent molecular orbital methods. XVII. Geometries and binding energies of second-row molecules. A comparison of three basis sets. **The Journal of Chemical Physics.** 64: 5142-5151.
- Davidson, E. R. and Chakravorty, S. J. (1994). A possible definition of basis set superposition error. **Chemical Physics Letters.** 217: 48-54.
- Dunning, T. H. J. (1970). Gaussian basis functions for use in molecular calculations. I. Contraction of (9s5p) atomic basis sets for the first-row atoms. **The Journal of Chemical Physics.** 53: 2823-2833.
- Dunning, T. H. J. (1971). Gaussian basis functions for use in molecular calculations. III. Contraction of (10s6p) atomic basis sets for the first-row atoms. **The Journal of Chemical Physics.** 55: 716-723.
- Hehre, W. J., Stewart, R. F. and Pople, J. A. (1969). Self-consistent molecular-orbital methods. I. Use of gaussian expansions of Slater-type atomic orbitals. **The Journal of Chemical Physics.** 51: 2657-2664.
- Huzinaga, S. (1965). Gaussian-type functions for polyatomic systems. I. **The Journal of Chemical Physics.** 42: 1293-1302.

- Liedl, K. R. (1998). Dangers of counterpoise corrected hypersurfaces. Advantages of basis set superposition improvement. **The Journal of Chemical Physics**. 108: 3199-3204.
- Møller, C. and Plesset, M. S. (1934). Note on an approximation treatment for many electron systems. **Physical Review**. 46: 618-622.
- Schrödinger, E. (1926). Quantisierung als eigenwertproblem. **Annalen der Physik**. 385: 437-490.
- Schwenke, D. W. and Truhlar, D. G. (1986). Erratum: Systematic study of basis set superposition errors in the calculated interaction energy of two HF molecules. **The Journal of Chemical Physics**. 84: 4113-4113.
- Sherrill, C. D. and Schaefer Iii, H. F. (1999). The configuration interaction method: Advances in highly correlated approaches. **Advances in Quantum Chemistry**. 34: 143-269.
- Slater, J. C. (1929). The theory of complex spectra. **Physical Review**. 34: 1293-1322.
- Slater, J. C. (1930). Atomic shielding constants. **Physical Review**. 36: 57-64.
- Szabo, A. and Ostlund, N. S. (1989). **Modern quantum chemistry: Introduction to advanced electronic structure theory**. New York: McGraw-Hill.

CHAPTER III

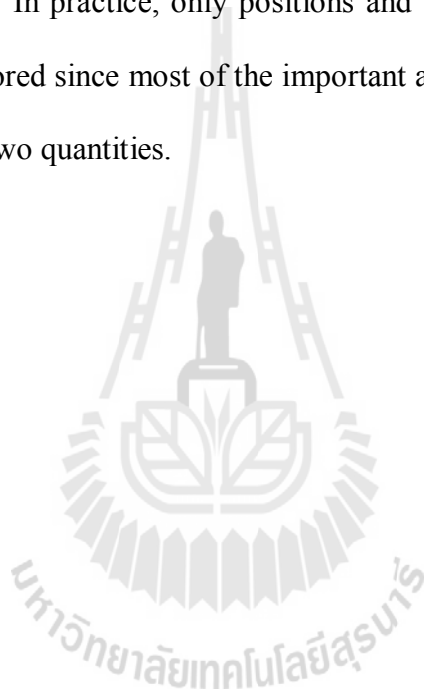
MOLECULAR DYNAMICS SIMULATIONS

3.1 Introduction to molecular dynamics (MD) simulations

With regard to computer simulations, two well-known techniques are Monte Carlo (MC) and molecular dynamics (MD). In terms of MC, each particle moves randomly based on system's energy criteria, and mostly, the structural details are of specific interest. For the MD technique, all particles in the system will be moved by time-dependent forces of neighbor particles, and thus, allowing time-dependent properties to be calculated. In this sense, the main advantage of the MD over the MC technique is that it can provide not only the structural properties, but also the dynamics details.

The common scheme of the MD technique is depicted in Figure 3.1. By the MD technique, the Newton's equation of motion is employed, in which each particle in the system can be moved with respect to force from neighboring particles. The MD simulation starts with reading in the starting configuration, velocities, accelerations and forces. The starting configuration can be obtained either from experimental data such as from X-ray or random configuration. According to the Newton's equation of motion, $F = ma$, since there is no time-dependent force that shall act in the system, the *time integration algorithms* will be employed to obtain detailed knowledge with respect to positions, velocities and accelerations of two successive time steps. The

energy of the system can be obtained from either molecular mechanics (MM) or quantum mechanics (QM) calculations. Next, the forces on each atom in the system can be derived from the energy with respect to the change in the atom's position. These new forces will be used to obtain new configuration and the steps will be repeated until the system reaches equilibrium. Then, the coordinates, velocities, accelerations, forces and so on are collected for further structural and dynamical property calculations. In practice, only positions and velocities of all particles in the system are usually stored since most of the important and interesting properties can be obtained from these two quantities.



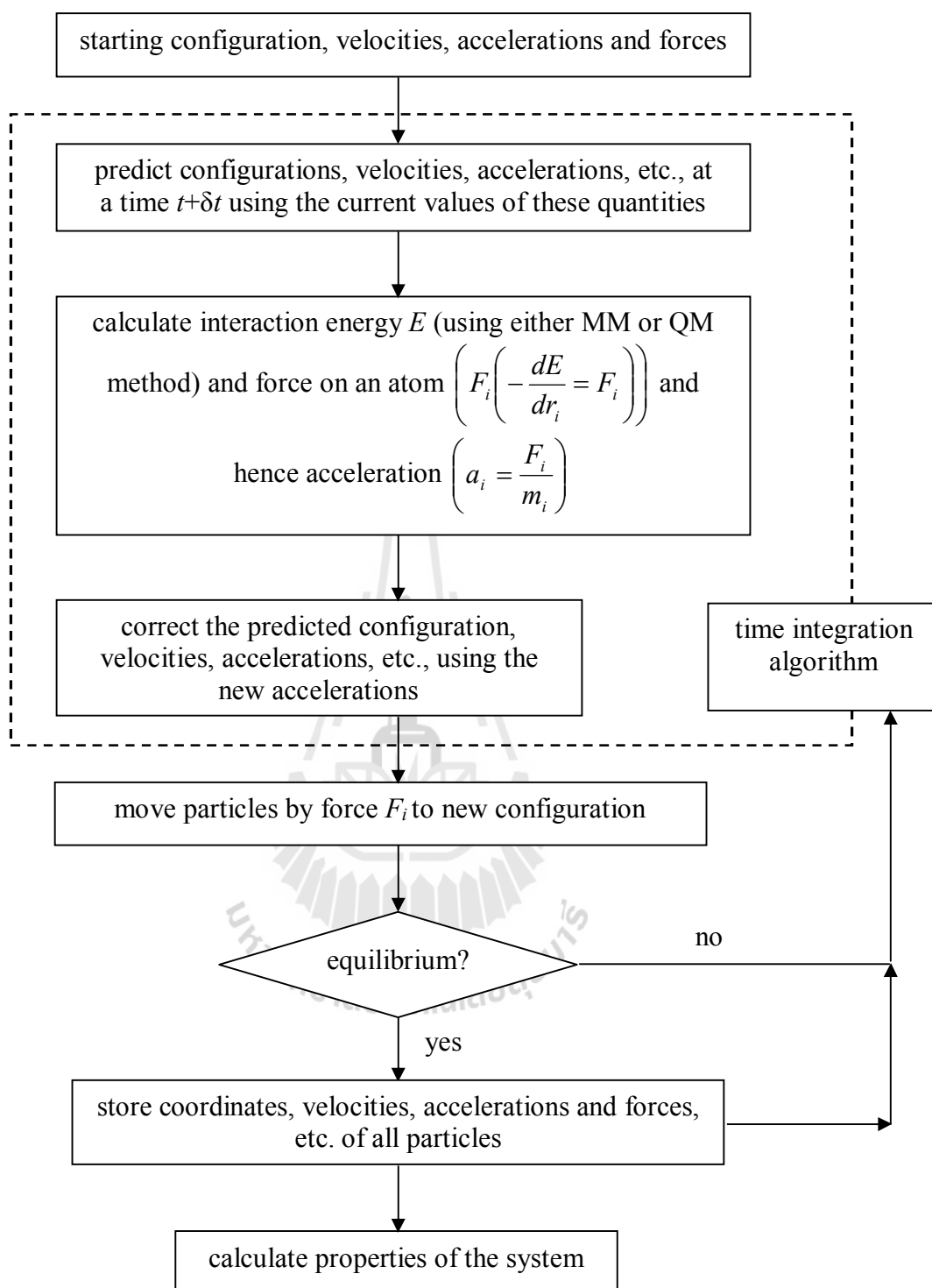


Figure 3.1 The scheme of molecular dynamics simulation.

3.2 Time average and ensemble average

Since the properties of a system will depend upon the positions and the momenta of N particles that comprise the system, the value of the property A can be written as

$$A(p^N(t), r^N(t)), \quad (3.1)$$

where $p^N(t)$ and $r^N(t)$ represent the N momenta and positions, respectively. The value of property A is the average of the A over the time of the measurement, known as a *time average*. In principle, if the time measurement reaches infinity, the value of the property A is then the *true value*.

$$A_{ave} = \lim_{\tau \rightarrow \infty} \frac{1}{\tau} \int_{t=0}^{\tau} A(p^N(t), r^N(t)) dt. \quad (3.2)$$

Note that the time average is directly related to real experiments. By means of theoretical investigations, however, the treatment of a real system which contains a large number of atoms or molecules is not feasible. On the other hand, it is rather impossible even to determine an initial configuration of a real system, since one cannot prepare an infinite number of identical system in a real situation. With regard to this point, Boltzmann and Gibbs have developed statistical mechanics, known as ensemble. The ensemble is a single system evolving in time that contains a large number of mental copies of a system, considered all at once, each of which represents

a possible state of the real system. The time average is then replaced by an ensemble average as

$$\langle A \rangle_{ensemble} = \iint dp^N dr^N A(p^N, r^N) \rho(p^N, r^N), \quad (3.3)$$

where $A(p^N, r^N)$ is the observable of interest and it is expressed as a function of the momenta, p , and the position, r , of the system. The angle bracket ($\langle \rangle$) indicates an ensemble generated by the simulation. It is postulated that theoretical predictions based on ensemble averaging are equivalent to experimental measurements, the time averaging, when a so-called *ergodic ensemble* is achieved. In this respect, the estimation of time average can be obtained over an enormous number of replicas of the system considered simultaneously,

$$\langle A \rangle_{time} = \langle A \rangle_{ensemble?} \quad (3.4)$$

To make the simulation becomes feasible, the ensemble must be generated under some constraints, such as constant number of particles (N), volume (V), energy (E), temperature (T), chemical potential (μ), pressure (P) and so on. Note that different macroscopic environmental constraints lead to different types of ensemble. For example, a simple ensemble is the *microcanonical ensemble (NVE)*, which is a thermodynamically isolated system, where the N , V and E are fixed throughout the simulation. The equilibrium states of the *NVE* ensemble are characterized by the entropy. The development of the *NVE* ensemble is the *canonical ensemble (NVT)*, in which the N and V are fixed and the ensemble has a well-defined temperature given by

the temperature of the heat bath. The thermodynamic property of the system derived from the NVT ensemble is Helmholtz free energy. Other ensembles include the *grand canonical ensemble* (μVT), *i.e.*, the extension of the NVT ensemble which allows the energy exchange, but fixes the μ , V and T .

3.3 Intermolecular potentials

According to classical MD simulations, the forces on each particle in the system are usually derived from potential energy function, V . The potential energy function is the total intermolecular interaction energy comprising all of pair, three-body, four-body, and so on up to N -body interactions,

$$V_{total} = \sum V(i, j) + \sum V(i, j, k) + \dots + \sum V(i, j, k, \dots, N). \quad (3.5)$$

In equation (3.5), the upper terms are usually assumed to converge rather slowly and the terms tend to have alternating signs (Kistenmacher, Popkie, and Clementi, 1974). In this respect, the total interactions of the system are assumed to be the summation of only pair interactions, known as *pairwise additive approximations*.

In general, the pair potential functions can be constructed by using a set of experimental data. However, the popular way in obtaining the pair potential functions is to construct with respect to *ab initio* calculations. The interaction potential might contain explicitly both an angular and a radial dependency,

$$V = \sum_{j>i} V_{ij}(r_{ij}, \Omega_{ij}), \quad (3.6)$$

where r_{ij} and Ω_{ij} specify intermolecular separation and orientation, most of which are relied on radial function and compromise between two conflicting requirements. For accuracy and flexibility, one might use a fairly long series of terms. However, it should be realized that the longer the series, the larger the number of associated fitting parameters, and thus the larger the number of machine cycles required to compute interaction energies in the MD simulation. The most commonly used interaction model is the *Lennard-Jones pair potential*,

$$\phi_{LJ}(r) = 4\varepsilon \left[\left(\frac{\sigma}{r} \right)^{12} - \left(\frac{\sigma}{r} \right)^6 \right], \quad (3.7)$$

where the parameters ε and σ are chosen to fit the physical properties of the function. This potential function has an attractive tail at long distances r , *i.e.*, it reaches a minimum around 1.122σ , and it is strongly repulsive at shorter distance, passing through 0 at $r = \sigma$, and increasing steeply as r is decreased further. The term $\frac{1}{r^{12}}$ dominates at short distance and models the repulsion between particles when they are close to each other, *i.e.*, its physical origin is related to the *Pauli principle*; when the electronic clouds surrounding the atoms start to overlap, the energy of the system increased abruptly. Sometimes, the exponential behavior is more appropriate to replace this repulsive term. The term $\frac{1}{r^6}$ dominates at large distances, constituting the attractive part. This term is originated by van der Waals dispersion forces and by dipole-dipole interactions according to fluctuating dipoles. These are rather weak interactions which, however, dominate the bonding character of closed-shell systems,

such as Ar or Kr. When the Lennard-Jones potential is applied, the Coulombic terms are needed to sufficiently represent the long-range and charge-charge interactions, as depicted in Figure 3.2.

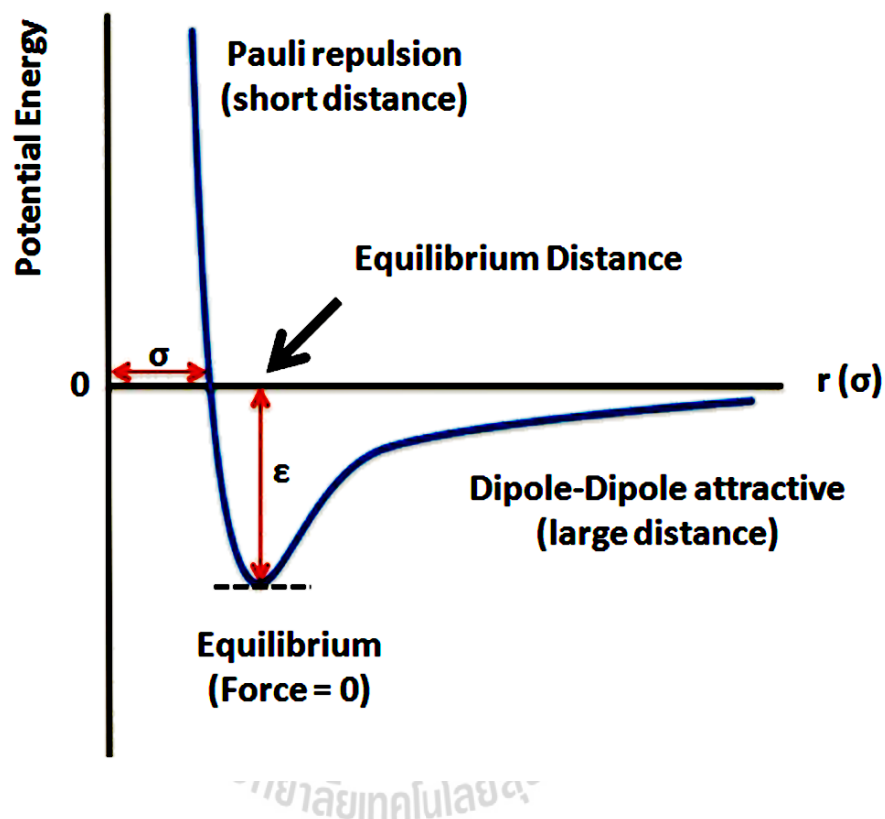


Figure 3.2 The Lennard-Jones potential.

In general, a Lennard-Jones potential is not at all adequate, especially for the treatment of an open shell system where strong localized bonds may form (as in covalent systems), or where there is delocalized “electron sea”. In this respect, the two-body interactions scheme itself fails very badly. However, regardless of how well they are able to model actual materials, the Lennard-Jones 12-6 potential constitutes

nowadays an extremely important model system. During the past decades, there are a vast number of scientists who have investigated the behavior of atom interacting via Lennard-Jones by a variety of different geometries (solids, liquids, surfaces, clusters, *etc.*). On the other hand, one could say that the Lennard-Jones is the standard potential to use for all investigations where the focus is on fundamental issues, rather than studying the properties of a specific material. In addition, it should be noted that many-body effects in the system's interaction always play a significant role and in all cases, more accurate potentials have been developed.

3.4 Time integration algorithms

The important engine of the MD simulation technique is the time integration algorithm. The time integration algorithms are based on *finite difference methods*, in which the MD trajectories can be generated with continuous potential models. The essential idea is that the integration is divided into many small steps, each of which is separated by a fixed time interval δt . The force on each particle at a time t can be calculated from the summation of interactions from other particles. Once the force is known, the accelerations of the particles can be determined, which are then combined with the positions and velocities at a time t to calculate the positions and velocities at a time $t + \delta t$.

There are many algorithms for integrating the equations of motion using finite difference methods, most of which assume that the positions and dynamics properties (positions, velocities, accelerations, *etc.*) can be expressed through the *Taylor series expansions*,

$$r(t + \delta t) = r(t) + v(t)\delta t + \frac{1}{2}a(t)\delta t^2 + \frac{1}{6}b(t)\delta t^3 + \frac{1}{24}c(t)\delta t^4 + \dots \quad (3.8)$$

$$v(t + \delta t) = v(t) + a(t)\delta t + \frac{1}{2}b(t)\delta t^2 + \frac{1}{6}c(t)\delta t^3 + \dots \quad (3.9)$$

$$a(t + \delta t) = a(t) + b(t)\delta t + \frac{1}{2}c(t)\delta t^2 + \dots \quad (3.10)$$

$$b(t + \delta t) = b(t) + c(t)\delta t + \dots, \quad (3.11)$$

where r is the position, v is the velocity (the first derivative of the position with respect to time), a is the acceleration (the second derivative), b is the third derivative, and so on.

Many integration algorithms have been developed for integrating the equations of motion. Two popular integration methods for MD simulations are *Verlet algorithm* (Verlet, 1967) and *predictor-corrector algorithm* (Gear, 1971).

3.4.1 Verlet algorithm

The Verlet algorithm is the most broadly used method for integrating the trajectories of motion in MD simulations. This algorithm uses the positions and accelerations at time t and the positions from the previous step, $r(t - \delta t)$, to calculate the new positions at time $t + \delta t$. We can write down the following equations between these quantities and the velocities at a time t ,

$$r(t + \delta t) = r(t) + v(t)\delta t + \frac{1}{2}a(t)\delta t^2 \quad (3.12)$$

$$r(t - \delta t) = r(t) - v(t)\delta t + \frac{1}{2}a(t)\delta t^2. \quad (3.13)$$

The summation of these two equations gives

$$r(t + \delta t) = 2r(t) - r(t - \delta t) + a(t)\delta t^2. \quad (3.14)$$

Note that the velocities do not explicitly appear in the Verlet integration algorithm. However, the velocities can be calculated by dividing the difference in positions at time $t + \delta t$ and $t - \delta t$ by $2\delta t$ as

$$v(t) = [r(t + \delta t) - r(t - \delta t)] / 2\delta t. \quad (3.15)$$

The weakness of the Verlet algorithm is that the calculation of the velocities cannot be obtained until the positions at the next step are known. Thus, it is not a *self-starting algorithm*. With regard to this point, some variants of the Verlet algorithm have been developed. For example, the *leap-frog* algorithm (Hockney, 1970), which uses the following expansions,

$$r(t + \delta t) = r(t) + v(t + \frac{1}{2}\delta t)\delta t \quad (3.16)$$

$$v(t + \frac{1}{2}\delta t) = v(t - \frac{1}{2}\delta t) + a(t)\delta t. \quad (3.17)$$

By this scheme, the velocities $v(t + \frac{1}{2}\delta t)$ are firstly calculated from the velocities at time $(t - \frac{1}{2}\delta t)$, and the accelerations at time t . The positions at time $t + \delta t$ are then deduced from the velocities just calculated together with the positions at time t using equation (3.16). The velocities at time t can be calculated from

$$v(t) = \frac{1}{2} \left[v(t + \frac{1}{2}\delta t) + v(t - \frac{1}{2}\delta t) \right]. \quad (3.18)$$

The advantage of this algorithm is that the velocities are explicitly calculated. However, some disadvantages exist, such as they are not calculated at the same time as the positions. An even better implementation of the similar basic algorithm is the *velocity Verlet algorithm* (Swope, Andersen, Berens, and Wilson, 1982), which gives positions, velocities and accelerations at the same time and does not compromise precision,

$$r(t + \delta t) = r(t) + v(t)\delta t + \frac{1}{2}a(t)\delta t^2 \quad (3.19)$$

$$v(t + \delta t) = v(t) + \frac{1}{2}[a(t) + a(t + \delta t)]\delta t. \quad (3.20)$$

Another integration method is Beeman's algorithm (Beeman, 1976), which is related to the Verlet method, and can be expressed as

$$r(t + \delta t) = r(t) + v(t)\delta t + \frac{2}{3}a(t)\delta t^2 - \frac{1}{6}a(t - \delta t)\delta t^2 \quad (3.21)$$

$$v(t + \delta t) = v(t) + \frac{1}{3} a(t) \delta t + \frac{5}{6} a(t) \delta t - \frac{1}{6} a(t - \delta t) \delta t. \quad (3.22)$$

The Beeman's algorithm makes use of a more accurate expression for the velocities and gives the better energy conservation, since the kinetic energy is calculated directly from the velocities. However, this method is more complicate than the Verlet algorithm, as well as it is more time-consuming.

3.4.2 Predictor-corrector algorithm

The performance of the predictor-corrector algorithm contains three basic steps. First, the new positions, velocities, accelerations and the higher-order terms are predicted according to the Taylor expansion, as shown in equations (3.8)-(3.11). Second, the forces are then evaluated at the new positions to give the accelerations, $a(t + \delta t)$. These accelerations are compared with the accelerations predicted from the Taylor series expansion ($a^c(t + \delta t)$). In this respect, the difference between the predicted and the calculated accelerations is an *error signal*,

$$\Delta a(t + \delta t) = a^c(t + \delta t) - a^p(t + \delta t). \quad (3.23)$$

Then, the error signal is used to correct positions and their derivatives. All the corrections are proportional to the error signal, the coefficient of proportionality being a magic number determined to maximize the stability of the algorithm,

$$r^c(t + \delta t) = r^p(t + \delta t) + c_0 \Delta a(t + \delta t) \quad (3.24)$$

$$v^c(t + \delta t) = v^p(t + \delta t) + c_1 \Delta a(t + \delta t) \quad (3.25)$$

$$a^c(t + \delta t) = a^p(t + \delta t) + c_2 \Delta a(t + \delta t) \quad (3.26)$$

$$b^c(t + \delta t) = b^p(t + \delta t) + c_3 \Delta a(t + \delta t), \quad (3.27)$$

where the superscript p represents as predicted values, r and v stand for the complete set of positions and velocities, respectively, a represents the accelerations and b denotes all the third order derivatives of r .

3.5 Periodic boundary conditions

According to Figure 3.3, the periodic boundary (PB) condition is employed to solve the effects of interactions at surface, especially for the simulation of small system size where the interactions between particles and the wall could reflect in wrong system's properties. The cubic box is replicated throughout the space, being thought as interacting not only with other particles in the same box, but also with their images in nearby boxes. By this scheme, when a particle leaves a unit cells, its image particle enters from the opposite side at the same time with the same velocity to conserve overall mass and momentum in the simulation box. This is a very useful technique possible to keep track of particles in only one cell, rather than to follow the specific particles of all replicated cells.

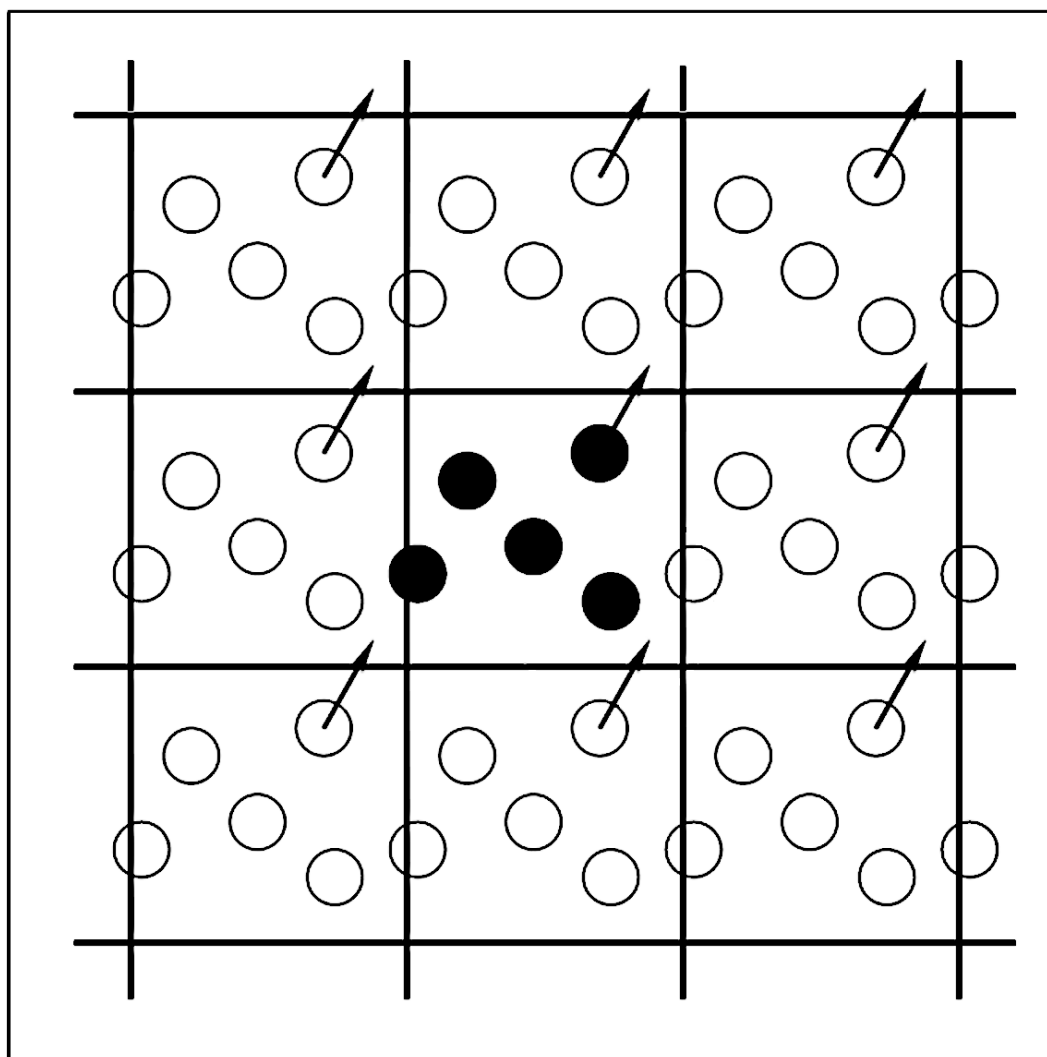
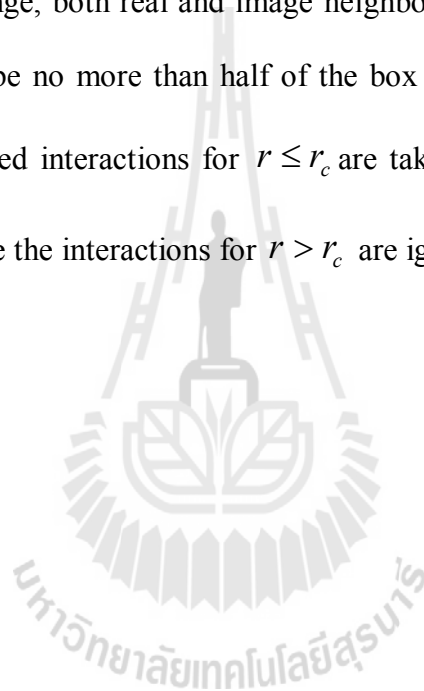


Figure 3.3 The periodic boundary conditions in two dimensions.

3.6 Cut-off and minimum image convention

In classical MD simulations, the non-bonded interactions are of the most time-consuming part of the energy and force calculations. For N atom system, the number of non-bonded interactions are $N*(N-1)/2$. According to the use of PB conditions, since particles in the systems will be duplicated infinitely, the calculations of non-bond energies and forces of all particles become impractical. To solve this problem,

the *minimum image criterion* is introduced in which only the nearest images of distinguishable particles are taken into account, *i.e.*, considering that most short range interactions usually fall off rapidly and can be neglected beyond the distance called the *cut-off limit*. According to Figure 3.4, the energies and forces are computed with respect to only the closest atoms or image, thus, reducing the number of non-bonded interactions that will be calculated in each MD step. In calculating particle interactions within the cut-off range, both real and image neighbors are included. In practice, the cut-off limit should be no more than half of the box length ($r_c \leq L/2$). On the other hand, only non-bonded interactions for $r \leq r_c$ are taken into account for calculating energy or force, while the interactions for $r > r_c$ are ignored.



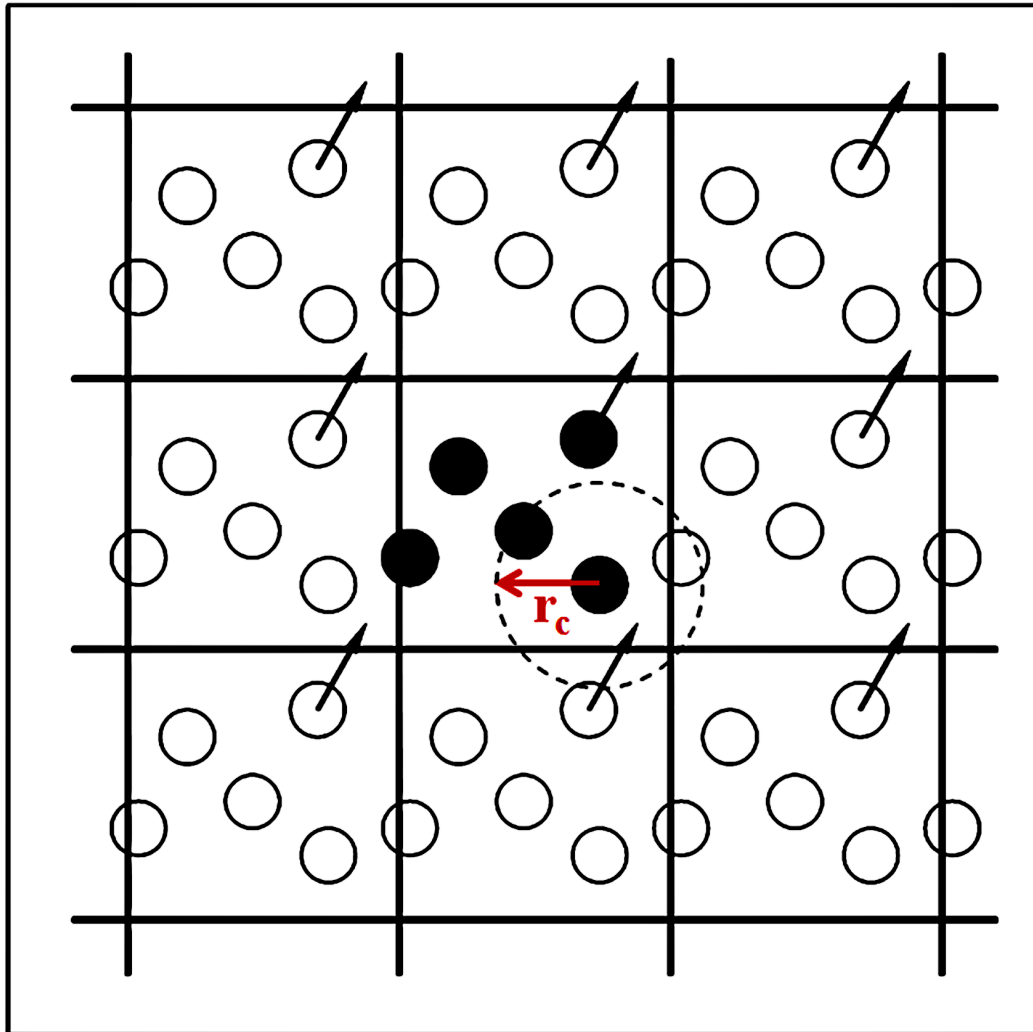


Figure 3.4 The spherical cut-off and the minimum image convention.

By using the cut-off, the interactions between all pairs of atoms that are further apart from the cut-off value are set to zero. In this regard, the cut-off distance should not be greater than half of the length of their image. However, the use of cut-off leads to a serious problem in the simulation, as can be seen in Figure 3.5

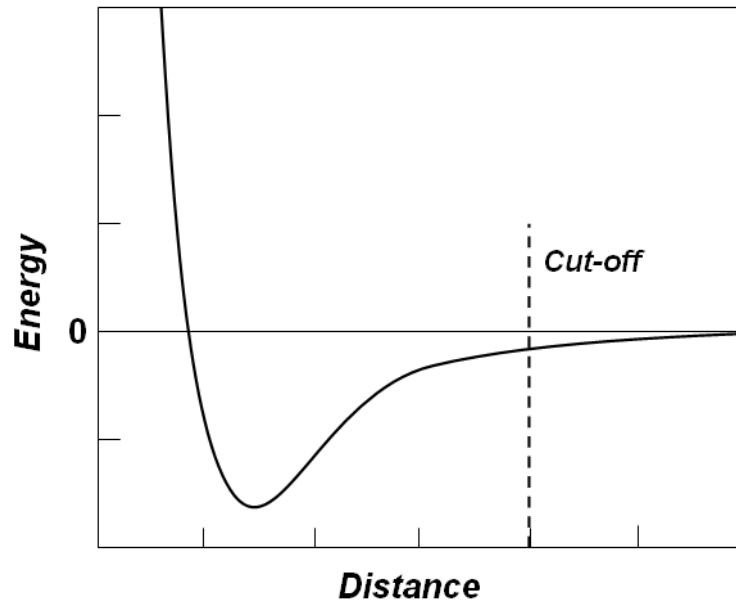


Figure 3.5 The discontinuity of cut-off.

As can be seen in Figure 3.5, the use of cut-off limit reflects in the discontinuity of both the potential energy and the force after the cut-off value. This problem can be solved by *shifting the potential function* by an amount V_c ,

$$V'(r) = \begin{cases} V(r) - V_c & \text{if } r \leq r_c \\ 0 & \text{if } r > r_c \end{cases}, \quad (3.28)$$

where r_c is the cut-off distance and V_c corresponds to the value of the potential at the cut-off distance. Although the energy conservation can be improved by the shifted potential, however, the discontinuity in the force with the shifted potential still exists.

At the cut-off distance, since the force will have a finite value, a suitable shifted potential would be of the form

$$V'(r) = \begin{cases} V(r) - V_c - \left(\frac{dV(r)}{dr} \right)_{r=r_c} (r - r_c) & \text{if } r \leq r_c \\ 0 & \text{if } r > r_c \end{cases} \quad (3.29)$$

In practice, it should be realized that the application of the shifted potential is not easy for inhomogeneous systems containing many different types of atom. An alternative approach is to eliminate the discontinuities in the energy and force by using a *switching function*. The switched potential ($V^{SF}(r)$) is related to the true potential ($V(r)$) as

$$V'(r) = V(r)S(r). \quad (3.30)$$

In several cases, the switching functions are applied to the entire range of the potential up to the cut-off point. In this respect, the switching function has a value of 1 at $r = 0$ and a value of 0 at $r = r_c$, while the switching function values between two cut-offs are varied. The example of a switching function applied to the Lennard-Jones potential is given in Figure 3.6.

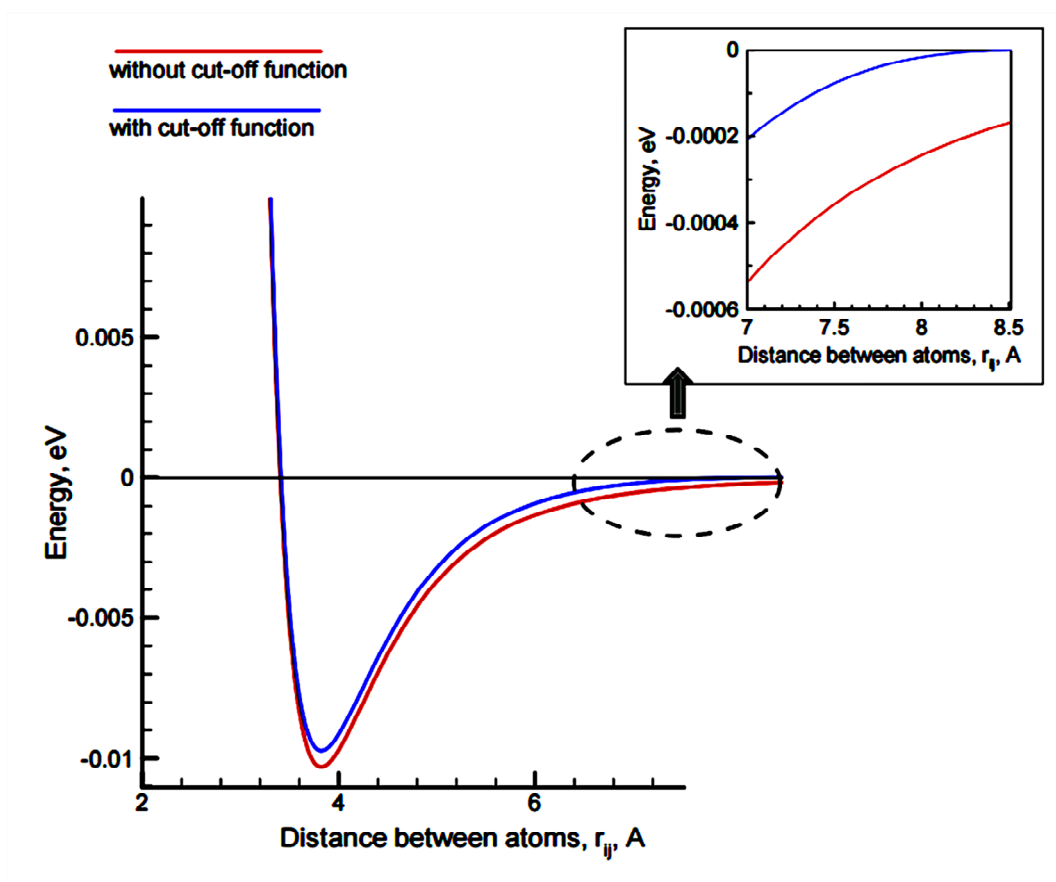


Figure 3.6 The effect of a switching function applied to the Lennard-Jones potential.

3.7 Non-bonded neighbor lists

In practice, the use of cut-off and minimum image convention is not actually reduce the time for calculating the non-bonded interactions, since the distance between every pair of atoms still have to be calculated in each simulation step. As a matter of fact that most of atoms move within a time step of less than 0.2 \AA , the local neighbors of a given atom remain almost the same for many time steps. In this regard, the *non-bonded neighbor list*, as shown in Figure 3.7, is employed. The first non-bonded neighbor list has been proposed by Verlet (Verlet, 1967). The Verlet neighbor list stores all atoms within the cut-off distance (the solid circle (r_c)) and atoms are

slightly further away than the cut-off distance (the dashed circle (r_m)). The neighbor list will frequently be updated throughout the simulation. With regard to this point, the distance used to calculate each atom's neighbors should be slightly larger than the actual cut-off distance in order to ensure that the atoms outside the cut-off will not move closer than the cut-off distance before the neighbor list is updated again.

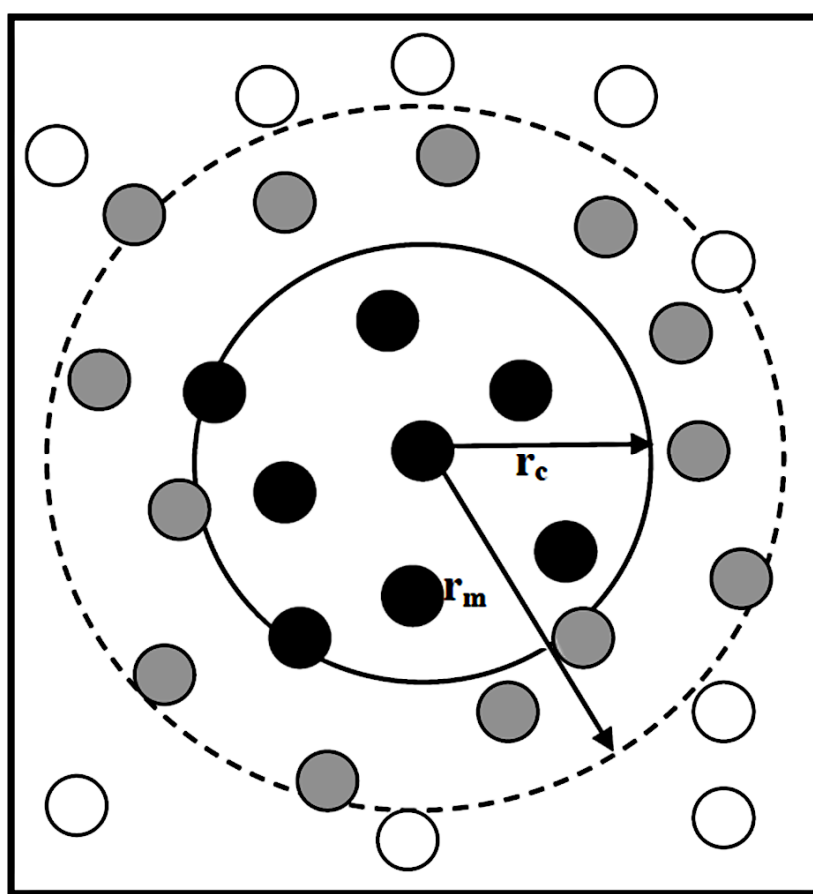


Figure 3.7 The non-bonded neighbor list.

3.8 Long-range interactions

The neglect of interactions beyond the cut-off distance, especially for the strong interacting systems, may results in an incorrect description of molecular

properties. One simple way to treat the long-range interactions is to use a large simulation cell, but this reflects in more time-consuming. There are many suitable methods for the treatment of long-range interactions. The first method is the *Ewald summation method*, which derived by Ewald in 1921 (Ewald, 1921). This method studies the energetic of ionic crystals, *i.e.*, a particle interacts with all the other particles in the simulation box and with all of their images in an infinite array of periodic cells. The charge-charge contribution to the potential energy of the Ewald summation method could be of the form

$$V = \frac{1}{2} \sum'_{|\mathbf{n}|=0} \sum_{i=1}^N \sum_{j=1}^N \frac{q_i q_j}{4\pi\epsilon_0 |r_{ij} + \mathbf{n}|}, \quad (3.31)$$

where the prime on the first summation indicates that the series does not include the interaction $i = j$ for $\mathbf{n} = 0$, q_i and q_j are charges and \mathbf{n} is a cubic lattice point. The Ewald summation method is the most correct way to accurately include all the effects of long-range forces in the computer simulation. However, this method is rather expensive to implement since the equation (3.31) converges extremely slowly.

Another method for the treatment of long-range interactions is the *reaction field method* (Foulkes and Haydock, 1989). This method constructs the sphere around the molecule with a radius equal to the cut-off distance. By this scheme, all interactions within the sphere are calculated explicitly, while those outside of the sphere are modeled as a homogeneous medium of dielectric constant (ϵ_s). The electrostatic field due to the surrounding dielectric is given by

$$E_i = \frac{2(\epsilon_s - 1)}{\epsilon_s + 1} \left(\frac{1}{r_c^3} \right) \sum_{j: r_{ij} \leq r_c} \mu_j, \quad (3.32)$$

where μ_j are the dipoles of the neighboring molecules that are located within the cut-off distance (r_c) of the molecules i . The interaction between molecule i and the reaction field equals to $E_i \cdot \mu_i$.

3.9 ONIOM-XS MD technique

The ONIOM (Own N-layered Integrated molecular Orbital and molecular Mechanics) method was originally proposed by Morokuma *et al.* (Svensson, Humbel, Froese, Matsubara, Sieber and Morokuma, 1996). The extension of the ONIOM method for the treatment of condensed-phase system was firstly applied by Kerdcharoen and co-worker, called ONIOM-XS (XS = eXtension to Solvation) (Kerdcharoen and Morokuma, 2002). According to the ONIOM-XS MD technique, the system is comprised of a “high-level” QM sphere, *i.e.*, a sphere which contains a central reference particle (atomic or molecular species) and its nearest-neighbors, and the remaining “low-level” MM bulk solvents. A thin switching shell located between the QM and MM regions is then introduced in order to smooth the transition of force due to the solvent exchange.

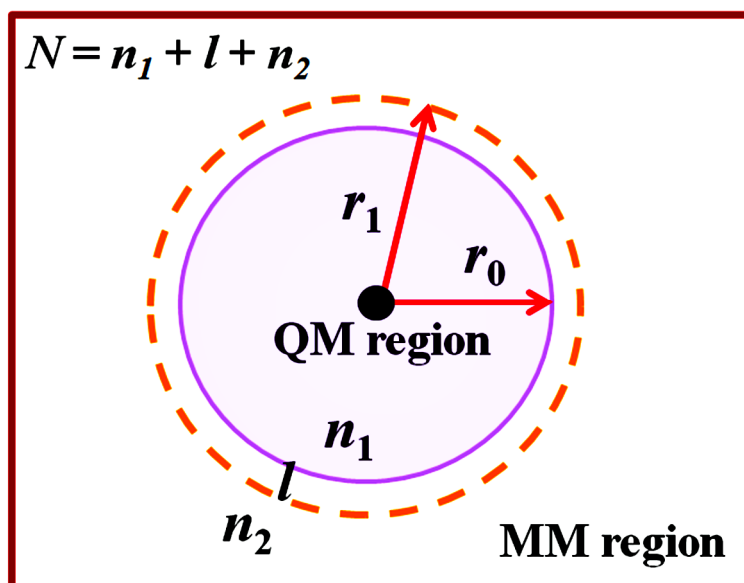


Figure 3.8 Schematic diagram of the ONIOM-XS MD technique (Kerdcharoen and Morokuma, 2002).

According to Figure 3.8, given n_1 , l and n_2 as number of particles in the QM sphere, the switching layer and the MM region, respectively, and $N(= n_1+l+n_2)$ as the total number of particles, the potential energy term can be written by equations (3.33) and (3.34) based on the ONIOM extrapolation scheme (Svensson, Humbel, Froese, Matsubara, Sieber and Morokuma, 1996). If the switching layer is included into the high-level (QM) calculation, the energy expression is written as

$$E^{ONIOM}(n_1 + l; N) = E^{QM}(n_1 + l) - E^{MM}(n_1 + l) + E^{MM}(N). \quad (3.33)$$

If the switching layer is considered as part of the low-level (MM) region, the energy expression is written as

$$E^{ONIOM}(n_1; N) = E^{QM}(n_1) - E^{MM}(n_1) + E^{MM}(N). \quad (3.34)$$

The potential energy of the entire system is taken as a hybrid between both energy terms (3.33) and (3.34),

$$E^{ONIOM-XS}(\{r_i\}) = (1 - \bar{s}(\{r_i\})) \cdot E^{ONIOM}(n_1 + l; N) + \bar{s}(\{r_i\}) \cdot E^{ONIOM}(n_1 + N), \quad (3.35)$$

where $\bar{s}(\{r_i\})$ is an average over a set of switching functions for individual exchanging particle in the switching layer $s_i(x_i)$ (Tasaki, McDonald and Brady, 1993),

$$\bar{s}(\{r_i\}) = \frac{1}{l} \sum_{i=1}^l s_i(x_i). \quad (3.36)$$

The switching function in equation (3.36) can have any form. In the present study, a polynomial form is employed,

$$s_i(x_i) = 6\left(x_i - \frac{1}{2}\right)^5 - 5\left(x_i - \frac{1}{2}\right)^3 + \frac{15}{8}\left(x_i - \frac{1}{2}\right) + \frac{1}{2}, \quad (3.37)$$

where $x_i = ((r_i - r_0)/(r_1 - r_0))$, r_0 and r_1 are the radius of inner and outer surfaces of the switching shell, respectively, and r_i is the distance between the center of mass of the exchanging particle and the center of QM sphere. In this respect, the whole solvent particles will be switched between QM and MM regions based on its center of mass.

The above polynomial form has an S-shape and converges to 0 and 1 at r_0 and r_1 , respectively. Finally, the gradient of the energy can be written as

$$\begin{aligned} \nabla_R E^{ONIOM-XS}(\{r_l\}) = & (1 - \bar{s}(\{r_l\})) \cdot \nabla_R E^{ONIOM}(n_l + l; N) + \bar{s}(\{r_l\}) \\ & \cdot \nabla_R E^{ONIOM}(n_1; N) + \frac{1}{(r_1 - r_0)} \nabla \bar{s}(\{r_l\}) \\ & \cdot (E^{ONIOM}(n_1; N) - E^{ONIOM}(n_l + l; N)) \end{aligned} \quad (3.38)$$

By the ONIOM-XS MD scheme, it is worth noting that forces on every particle in the QM region will be smoothed, in contrast to the conventional QM/MM scheme in which only the exchanging particles that will be treated by the switching function.

3.10 Research procedures

3.10.1 Construction of pair potential functions

For the interactions within the MM and between the QM and MM regions, a flexible model, which describes inter- and intra-molecular interactions (Hannongbua, 1991; Hannongbua, Ishida, Spohr and Heinzinger, 1988), was employed for NH₃. The use of a flexible model is favorable, ensuring compatibility and a smooth transition when ammonia molecules move from the QM region with their full flexibility to the MM region, and vice versa. The pair potential functions for describing Na⁺-NH₃ interactions were newly constructed. The 1819 HF interaction energy points for various Na⁺-NH₃ configurations obtained from Gaussian03 calculations (Frisch *et al.*, 2005), using DZP basis set (Dunning and Hay, 1977) for

NH₃ and LANL2DZ basis set (Check, Faust, Bailey, Wright, Gilbert and Sunderlin, 2001; Hay and Wadt, 1985) for Na⁺, were fitted to the analytical forms of

$$\Delta E_{Na^+-NH_3} = \sum_{i=1}^4 \left(\frac{A_{ic}}{r_{ic}^6} + \frac{B_{ic}}{r_{ic}^7} + C_{ic} \exp(-D_{ic} r_{ic}) + \frac{q_i q_c}{r_{ic}} \right), \quad (3.39)$$

where A , B , C and D are the fitting parameters (see Table 3.1), r_{ic} denotes the distances between the ions and the i -th atom of NH₃, and q_i and q_c are the atomic net charges. The charge values for Na⁺ was set to 1.0 and for N and H of NH₃ were set to -0.8022 and 0.2674, respectively.

Table 3.1 Optimized parameters of the analytical pair potential for the interactions of ammonia with Na⁺ (interaction energies in kcal mol⁻¹ and distances in Å).

Pair	A (kcal mol ⁻¹ Å ⁶)	B (kcal mol ⁻¹ Å ⁷)	C (kcal mol ⁻¹)	D (Å ⁻¹)
Na-N	-32461.57236	37734.03948	47752.17357	2.711467277
Na-H	-901.0111121	1323.287312	151.4842753	1.237012174

3.10.2 Simulation details

For the system of Na^+ in liquid NH_3 , a QM radius of 4.4 Å and a switching width of 0.2 Å were chosen, which correspond to the ONIOM-XS parameters r_0 and r_1 of 4.2 and 4.4 Å, respectively. This QM region is considered to be large enough to include the whole first solvation shell and some parts of the outer region. Inside the QM region, all interactions were treated at the Hartree-Fock (HF) level of accuracy using LANL2DZ (Boys and Bernardi, 1970; Check, Faust, Bailey, Wright, Gilbert and Sunderlin, 2001; Hay and Wadt, 1985) and DZP (Dunning and Hay, 1977) basis sets for Na^+ and NH_3 , respectively. For the system of liquid NH_3 , a QM radius of 5.2 Å and a switching width of 0.2 Å were chosen, which correspond to the ONIOM-XS parameters r_0 and r_1 of 5.0 and 5.2 Å, respectively. Note that, according to the previous QM/MM MD study (Tongraar, Kerdcharoen and Hannongbua, 2006), the first minimum of the N-N radial distribution function (RDF) is located between 4.8-5.0 Å. The selected QM region contains around 12-16 ammonia molecules, covering the first shell coordination numbers predicted by most of experimental and theoretical reports (Beu and Buck, 2001; Hannongbua, 2000; Impey and Klein, 1984; Kincaid and Scheraga, 1982; Kiselev, Kerdcharoen, Hannongbua and Heinzinger, 2000; Narten, 1976; Ricci, Nardone, Ricci, Andreani and Soper, 1995; Tongraar, Kerdcharoen and Hannongbua, 2006).

All ONIOM-XS MD simulations will be performed in a canonical ensemble (NVT) at 235 K with periodic boundary conditions. For the system of Na^+ in liquid NH_3 , a periodic box, with a box length of 21.80 Å, employed in the simulation contains one Na^+ and 255 ammonia molecules, assuming the experimental density of pure NH_3 (0.699 g cm^{-3}). For the system of liquid NH_3 , a similar periodic box is

employed, which contains 256 ammonia molecules (*i.e.*, the central Na^+ ion was replaced by an ammonia molecule), corresponding to the experimental density of pure liquid NH_3 (0.6988 g cm^{-3}). The Newtonian equations of motions were treated by a general predictor-corrector algorithm. The reaction-field method (Adams, Adams and Hills, 1979) was employed for the treatment of long-range interactions. The time step size was set to 0.2 fs, which allows for the explicit movement of the hydrogen atoms of ammonia molecules. For the system of Na^+ in liquid NH_3 , the starting configuration was obtained from the previous QM/MM MD study of liquid NH_3 (Tongraar, Kerdcharoen and Hannongbua, 2006), *i.e.*, simply by replacing Na^+ to one ammonia molecule. The ONIOM-XS MD simulation was performed with the system's re-equilibration for 30,000 time steps, followed by another 200,000 time steps to collect configurations every 10^{th} step. For the system of liquid NH_3 , the starting configuration was also obtained from the previous QM/MM MD study (Tongraar, Kerdcharoen and Hannongbua, 2006). The system was re-equilibrated by performing the ONIOM-XS MD simulation for 20,000 time steps, followed by another 150,000 time steps to collect configurations every 10^{th} step.

3.11 Determination of system's properties

3.11.1 Structural properties

The structural properties will be characterized through atom-atom RDFs and their corresponding integration numbers, together with detailed analyses on angular distribution functions (ADFs) and orientations of ammonia molecules, both in the solvation shell of Na^+ and in the bulk liquid NH_3 . The RDF, $g_{\alpha\beta}(r)$, is the set of

site-site pair correlation functions, which describes how (on average) the atoms in the system are radially packed around each other. The RDF can be expressed as

$$g_{\alpha\beta}(r) = N_{\alpha\beta}(r) / (4\pi r^2 \Delta r \rho_{\beta}), \quad (3.40)$$

where $N_{\alpha\beta}(r)$ is the average number of β sites located in the shell $(r, r+\Delta r)$ centered on site α , and $\rho_{\beta} = \frac{N_{\beta}}{V}$ is the average number density of β sites in the system.

The corresponding integration number of RDF is defined as

$$n_{\alpha\beta}(r) = 4\pi\rho_{\beta} \int_0^r g_{\alpha\beta}(r') r'^2 dr'. \quad (3.41)$$

3.11.2 Dynamical properties

The dynamical properties will be analyzed through mean residence times (MRTs) and self-diffusion coefficients (D). The mobility of ammonia molecules surrounding the ion or surrounding the central NH_3 molecule (*i.e.*, in the case of liquid NH_3) can be interpreted through the D value, which can be calculated from their center-of-mass velocity autocorrelation functions (VACFs) using the Green-Kubo relation (Spohr, Palinkas, Heinzinger, Bopp, and Probst, 1988),

$$D = \frac{1}{3} \lim_{t \rightarrow \infty} \int_0^t C_{vv}(t) dt. \quad (3.42)$$

The rates of ligand exchange processes at Na^+ or at the central NH_3 molecule (*i.e.*, in the case of liquid NH_3) were evaluated through MRTs of ammonia molecules in the solvation shell of Na^+ or in the solvation shell of the central NH_3 molecule (*i.e.*, in the case of liquid NH_3). In this work, the MRT data were calculated using the “direct” method (Hofer, Tran, Schwenk, and Rode, 2004), as the product of the average number of ammonia molecules in the solvation shell of ion or in the solvation shell of the central NH_3 molecule (*i.e.*, in the case of liquid NH_3) with the duration of the ONIOM-XS MD simulation, divided by the observed number of exchange events lasting a given time interval t^* ,

$$MRT(\tau) = \frac{CN \times t_{sim}}{N_{ex}}, \quad (3.43)$$

where CN is the average coordination number, t_{sim} is the duration of the simulation and N_{ex} equals the number of events. In general, a t^* value of 0.0 ps is recommended for the estimation of hydrogen bond lifetimes, while a t^* value of 0.5 ps is chosen as a good measure for ligand exchange processes.

3.12 References

- Adams, D. J., Adams, E. M. and Hills, G. J. (1979). The computer simulation of polar liquids. **Molecular Physics**. 38: 387-400.
- Beeman, D. (1976). Some multistep methods for use in molecular dynamics calculations. **Journal of Computational Physics**. 20: 130-139.

- Beu, T. A. and Buck, U. (2001). Structure of ammonia clusters from $n=3$ to 18. **Journal of Chemical Physics**. 114: 7848-7852.
- Boys, S. F. and Bernardi, F. (1970). The calculation of small molecular interactions by the differences of separate total energies. Some procedures with reduced errors. **Molecular Physics**. 19: 553-566.
- Check, C., Faust, T., Bailey, J., Wright, B., Gilbert, T. and Sunderlin, L. (2001). Addition of polarization and diffuse functions to the LANL2DZ basis set for P-Block elements. **The Journal of Physical Chemistry A**. 105: 8111-8116.
- Dunning, T. H. and Hay, P. J. (1977). **Methods of electronic structure theory**.
- Ewald, P. P. (1921). Die berechnung optischer and elektrostatischer gitterpotentiale. **Annalen der Physik**. 369: 253-287.
- Foulkes, W. M. C. and Haydock, R. (1989). Tight-binding models and density functional theory. **Physical Review B**. 39: 12520-12536.
- Frisch, M. J., Trucks, G. W., Schlegel, H. B., Scuseria, G. E., Robb, M. A., Cheeseman, J. R., Zakrzewski, V. G., Montgomery, J. A., Stratmann, R. E., Burant, J. C., Dapprich, S., Millam, J. M., Daniel, A. D., Kudin, K. N., Strain, M. C., Farkas, O., Tomasi, J., Barone, V., Mennucci, B., Pomelli, C., Adamo, C., Clifford, S., Ochterski, J., Petersson, G. A., P. Y. Ayala, Q. C., Morokuma, K., Salvador, P., Foresman, Cioslowski, J., Ortiz, J. V., Baboul, A. G., Stefanov, B. B., Liu, G., Liashenko, A., Piskorz, P., Komaromi, I., Gomperts, R., Martin, R. L., Fox, D. J., T. Keith, M. A. A. L., Peng, C. Y., Nanayakkara, A., Gill, B. J., Chen, W., Gonzalez, C. and Pople, J. A. (2005). Gaussian 03 (Revision D.1) [Computer Software]. Gaussian: Wallingford, CT, USA.

- Gear, C. W. (1971). **Numerical initial value problems in ordinary differential equations**. Englewood Cliffs, N.J.: Prentice-Hall.
- Hannongbua, S. (1991). A molecular dynamics simulation of the structure of sodium ion in liquid ammonia. **Australian Journal of Chemistry**. 44: 447-456.
- Hannongbua, S. (2000). The best structural data of liquid ammonia based on the pair approximation: First-principles Monte Carlo simulation. **Journal of Chemical Physics**. 113: 4707-4712.
- Hannongbua, S. V., Ishida, T., Spohr, E. and Heinzinger, K. (1988). Molecular-dynamics study of a lithium ion in ammonia. **Zeitschrift fuer Naturforschung, A: Physical Sciences**. 43: 572.
- Hay, P. J. and Wadt, W. R. (1985). *Ab initio* effective core potentials for molecular calculations. Potentials for the transition metal atoms Sc to Hg. **The Journal of Chemical Physics**. 82: 270-283.
- Hockney, R. W. (1970). The potential calculation and some applications. **Methods in Computational Physics**. 9: 136-211.
- Hofer, T. S., Tran, H. T., Schwenk, C. F. and Rode, B. M. (2004). Characterization of dynamics and reactivities of solvated ions by *ab initio* simulations. **Journal of Computational Chemistry**. 25: 211-217.
- Impey, R. W. and Klein, M. L. (1984). A simple intermolecular potential for liquid ammonia. **Chemical Physics Letters**. 104: 579-582.
- Kerdcharoen, T. and Morokuma, K. (2002). ONIOM-XS: An extension of the ONIOM method for molecular simulation in condensed phase. **Chemical Physics Letters**. 355: 257-262.

- Kincaid, R. H. and Scheraga, H. A. (1982). Revised empirical potential for conformational, intermolecular, and solvation studies. 6. Testing of parameters by application to liquid ammonia. **Journal of Physical Chemistry**. 86: 833-838.
- Kiselev, M., Kerdcharoen, T., Hannongbua, S. and Heinzinger, K. (2000). The structure of supercritical ammonia as studied by molecular dynamics simulations. **Chemical Physics Letters**. 327: 425-428.
- Kistenmacher, H., Popkie, H. and Clementi, E. (1974). Study of the structure of molecular complexes. VIII. Small clusters of water molecules surrounding Li^+ , Na^+ , K^+ , F^- , and Cl^- ions. **The Journal of Chemical Physics**. 61: 799-815.
- Narten, A. H. (1976). Liquid ammonia: Molecular correlation functions from x-ray diffraction. **The Journal of Chemical Physics**. 66: 3117-3120.
- Ricci, M. A., Nardone, M., Ricci, F. P., Andreani, C. and Soper, A. K. (1995). Microscopic structure of low temperature liquid ammonia: A neutron diffraction experiment. **The Journal of Chemical Physics**. 102: 7650-7655.
- Spohr, E., Palinkas, G., Heinzinger, K., Bopp, P. and Probst, M. M. (1988). Molecular dynamics study of an aqueous strontium chloride solution. **The Journal of Physical Chemistry**. 92: 6754-6761.
- Svensson, M., Humbel, S., Froese, R. D. J., Matsubara, T., Sieber, S. and Morokuma, K. (1996). ONIOM: A multilayered integrated MO + MM method for geometry optimizations and single point energy predictions. A test for Diels–Alder reactions and $\text{Pt}(\text{P}(\text{t-Bu})_3)_2 + \text{H}_2$ oxidative addition. **The Journal of Physical Chemistry**. 100: 19357-19363.

- Swope, W. C., Andersen, H. C., Berens, P. H. and Wilson, K. R. (1982). A computer simulation method for the calculation of equilibrium constants for the formation of physical clusters of molecules: Application to small water clusters. **The Journal of Chemical Physics**. 76: 637-649.
- Tasaki, K., McDonald, S. and Brady, J. W. (1993). Observations concerning the treatment of long-range interactions in molecular dynamics simulations. **Journal of Computational Chemistry**. 14: 278-284.
- Tongraar, A., Kerdcharoen, T. and Hannongbua, S. (2006). Simulations of liquid ammonia based on the combined quantum mechanical/molecular mechanical (QM/MM) approach. **The Journal of Physical Chemistry A**. 110: 4924-4929.
- Verlet, L. (1967). Computer “Experiments” on classical fluids. I. Thermodynamical properties of Lennard-Jones molecules. **Physical Review**. 159: 98-103.



CHAPTER IV

RESULTS AND DISCUSSION

4.1 Structural properties

The structural details of the Na^+ solvation can be illustrated through the Na-N and Na-H radial distribution functions (RDFs) and their corresponding integration numbers, as depicted in Figure 4.1. Note that the insertion given in Figure 4.1 refers to the corresponding RDFs obtained from the QM/MM MD simulation (Kerdcharoen and Rode, 2000). By means of the ONIOM-XS MD simulation, a pronounced first Na-N RDF is exhibited at 2.58 Å, together with a recognizable second Na-N peak centered at around 4.22 Å. As can be seen in Figure 4.1a, the smooth shape of the Na-N RDF between 4.2 and 4.4 Å (which correspond to the ONIOM-XS parameters r_0 and r_1) clearly confirms that the transition of NH_3 molecules between the QM and MM regions occurs smoothly, and that the ion-ligand and ligand-ligand interactions beyond the QM region could be well accounted for by the MM potentials. The shape and height of the first and second Na-N RDFs reveal a clear “structure-making” ability of Na^+ in liquid NH_3 , *i.e.*, a significant influence of the Na^+ ion in ordering its surrounding NH_3 ligands to form specific ion-ligand complexes. Note that, according to the recent ONIOM-XS MD simulation of Na^+ in aqueous solution (Sripa, Tongraar and Kerdcharoen, 2013), the Na^+ ion has been classified as a weak “structure-maker”.

In liquid NH_3 , the observed higher intensity of the Na-N RDF, *i.e.*, when compared to the Na-O RDF for the case of Na^+ in aqueous solution (Sripa, Tongraar and Kerdcharoen, 2013), clearly implies a stronger “structure-making” ability of Na^+ in this media. In addition, the pronounced second peak of the Na-N RDF clearly indicates the influence of Na^+ beyond the first solvation layer. With regard to the Na-N RDF in Figure 4.1a, the first solvation shell of Na^+ is rather well separated from the second one, suggesting that NH_3 molecules in the first solvation shell are strongly attached to the ion, and that ligand exchange processes between the first and the second solvation shells may not frequently occur during the ONIOM-XS MD simulation. Integrations up to first and second minimum of the Na-N RDF yield about 5.1 and 16.3 NH_3 molecules, respectively. Note that, since the second minimum of the Na-N RDF is broad, the structural parameters with respect to the second solvation shell are considered as rough estimates, *i.e.*, the position of the second Na-N minimum is assumed to be 5.25 Å throughout this work.



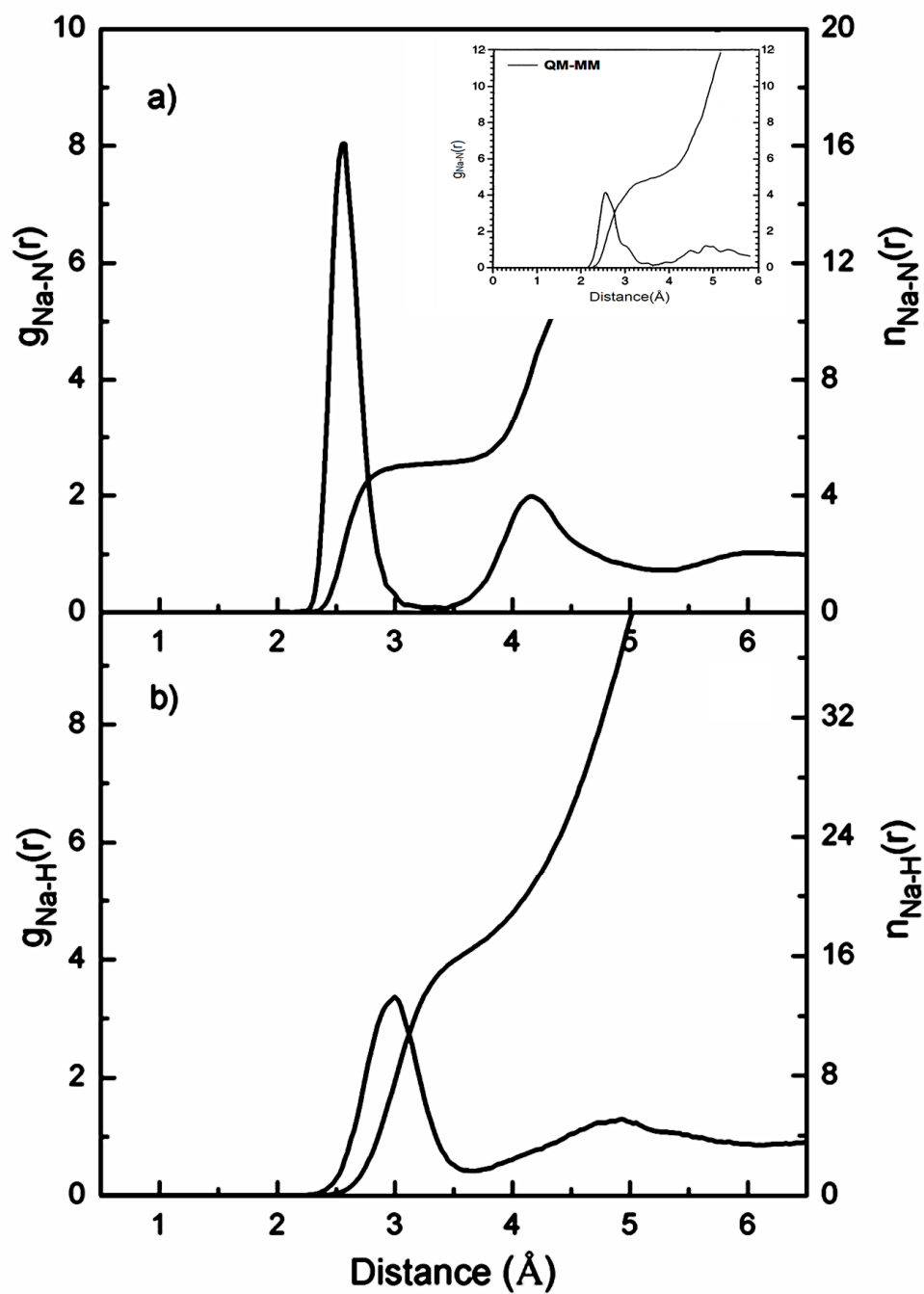


Figure 4.1 a) Na-N and b) Na-H radial distribution functions (RDFs) and their corresponding integration numbers. The insertion refers to the corresponding RDFs obtained from the QM/MM MD simulation (Kerdcharoen and Rode, 2000).

Some structural parameters for the first solvation shell of Na^+ , as obtained from various MC and MD simulations, are summarized in Table 4.1. As compared to the recent QM/MM MD study (Kerdcharoen and Rode, 2000), the ONIOM-XS MD simulation, although predicts a similar coordination number of about 5, reveals significant difference regarding the characteristics of the Na-N RDF (see insertion in Figure 4.1). In particular, the ONIOM-XS MD results clearly show relatively higher, sharper and more pronounced first and second peaks of the Na-N RDF, leading to better defined first and second solvation shells. This observed difference clearly confirms the important treatment of the ONIOM-XS MD technique for the study of such condensed-phase system. Regarding the observed discrepancies between the ONIOM-XS and QM/MM (Kerdcharoen and Rode, 2000) MD studies, it should be noticed that the latter one was performed with the use of different basis set, namely the ECP, as well as with the relatively shorter simulation period of 12 ps. According to the data in Table A1, it is obvious that most MC and MD simulations using pair potentials or pair plus three-body correction functions fail to predict the solvation structure of Na^+ in liquid NH_3 , *i.e.*, most of which predict sharper, narrower and better separated first Na-N peaks with relative higher coordination numbers.

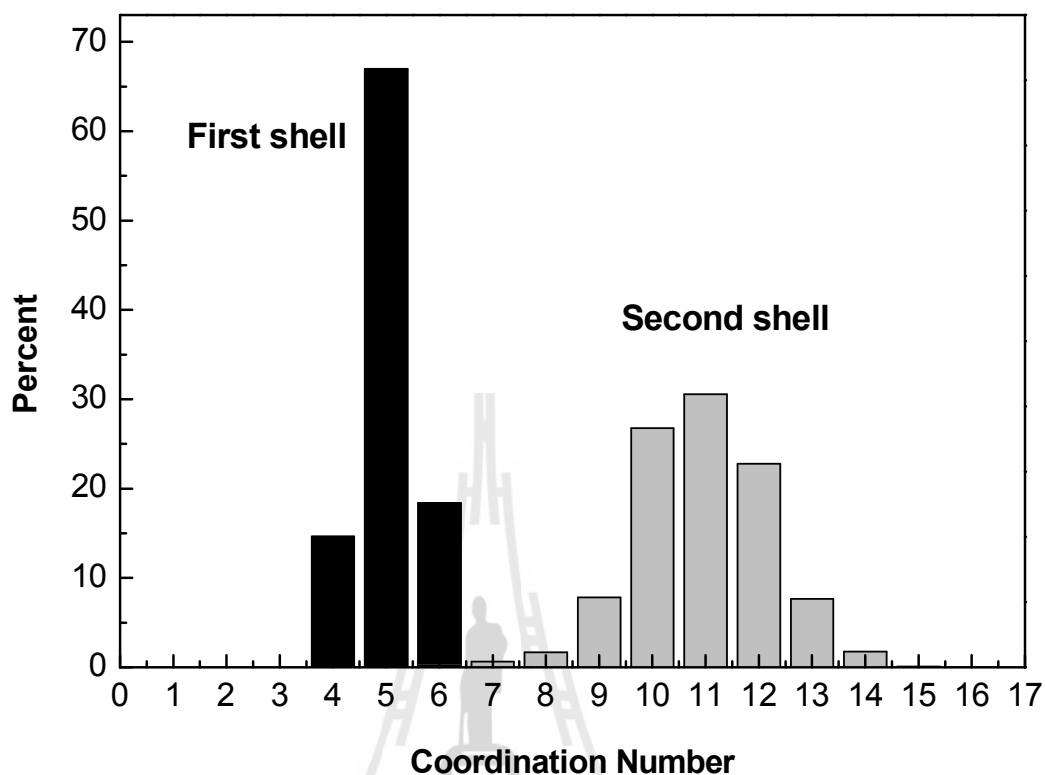


Figure 4.2 Distributions of the coordination numbers, calculated within the first and second solvation shells of Na^+ .

The probability distributions of the coordination numbers, calculated within the first and second solvation shells of Na^+ , are displayed in Figure 4.2. Within the first solvation shell of Na^+ , it is apparent that this ion prefers the coordination number of 5, followed by 6 and 4 in smaller amounts. In the second solvation layer, a number of NH_3 molecules, ranging from 7 to 14 with the most prevalent number of 11, are observed. The arrangement of NH_3 molecules in the first solvation shell of Na^+ can be analyzed from the distributions of $\text{N}---\text{Na}---\text{N}$ angle, as depicted in Figure 4.3. With regard to the coordination number of 5, one could assume two possible geometrical

arrangements, namely a trigonal bipyramidal and a square pyramidal structure (cf. Table 4.2). In general, the trigonal bipyramidal structure is characterized by the N---Na---N angles of 90, 120 and 180°, with the probability ratio of 6:3:1, while the square pyramidal structure corresponds to the N---Na---N angles of 90 and 180°, with the probability ratio of 8:2. According to the plot in Figure 4.3, it is apparent that NH₃ molecules in the first solvation shell of Na⁺ are somewhat flexible, forming the preferred 5-fold coordinated complexes with respect to the distorted square pyramidal geometry.

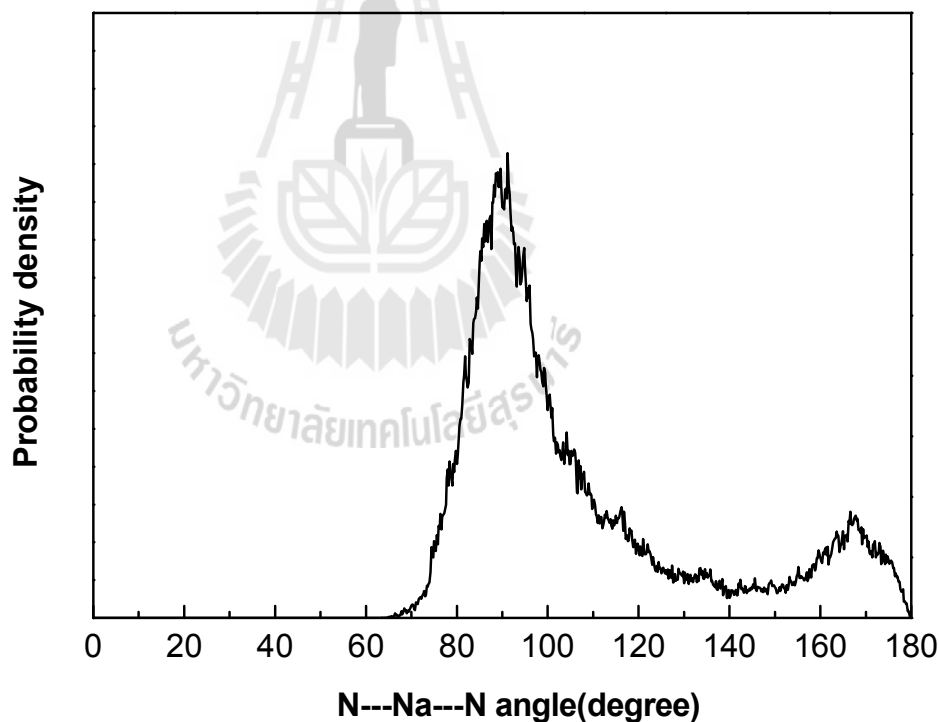


Figure 4.3 Distributions of the N---Na---N angle, calculated within the first minimum of the Na-N RDF.

Additional information regarding the orientation of NH_3 molecules in the vicinity of Na^+ is also given in Figure 4.4. In this context, the angle θ is defined by the $\text{Na}^+ \text{---} \text{N}$ axis and the dipole vector of the surrounding NH_3 molecules. As can be seen in Figure 4.4, the shape of the distribution peaks clearly indicates that NH_3 molecules in the first solvation shell of Na^+ stick quite rigidly to their dipole-oriented configurations, and that NH_3 molecules in the second solvation layer are also arranged with respect to a remarkable influence of Na^+ .

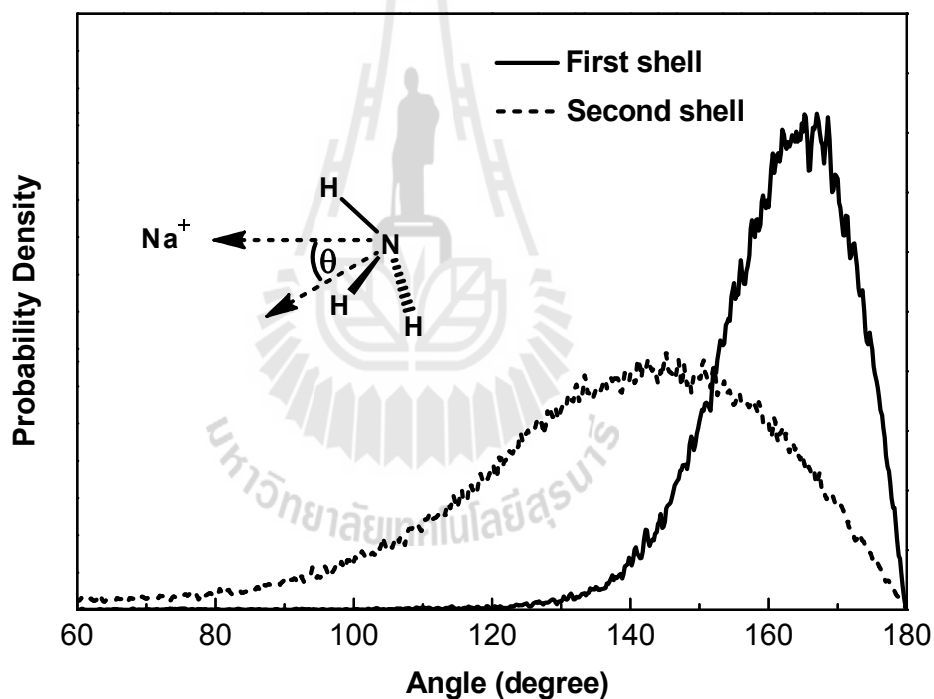
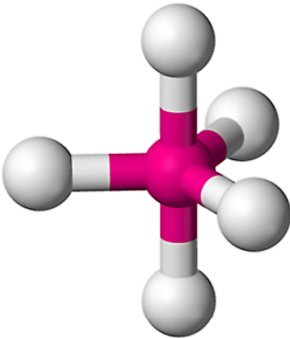
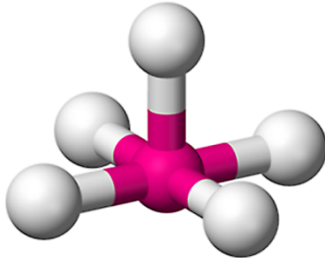


Figure 4.4 Probability distributions of θ angle in the first and second solvation shells of Na^+ , calculated within the first and second minima of the Na-N RDF.

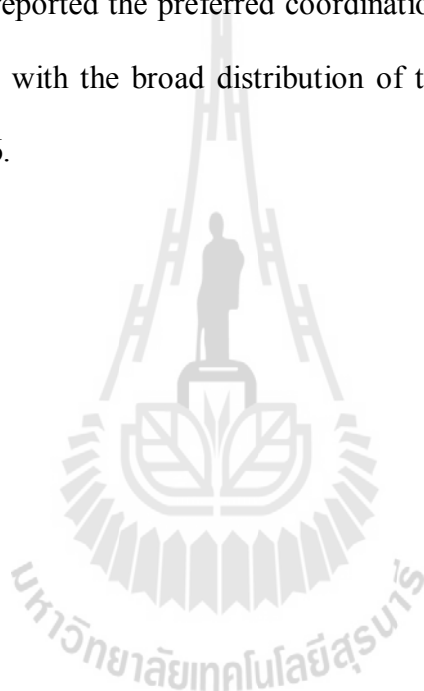
Table 4.1 Two possible geometries of penta-coordinated ion-ligand complexes.

Coordination number	Geometry	Bond angles	Probability ratio
5	 <p>Trigonal bipyramidal</p>	90°, 120°, 180°	6:3:1
5	 <p>Square pyramidal</p>	90°, 180°	8:2

With regard to the ONIOM-XS MD simulation of liquid NH₃, the structural details of this liquid are characterized through the N-N, N-H, H-N and H-H RDFs and their corresponding integration numbers, as shown in Figure 4.5, comparing the results to those obtained by the QM/MM MD simulation (Tongraar, Kerdcharoen and Hannongbua, 2006). In this context, the first atom in the RDFs refer to the atom of the central reference NH₃, and the latter represents the atom of other NH₃ molecules. As can be seen in Figure 4.5, the QM/MM and ONIOM-XS MD results are quite similar, implying that the deficiency of the QM/MM MD scheme is not affect much in describing the local structure of the liquid NH₃. According to the QM/MM MD study

of liquid NH_3 (Tongraar, Kerdcharoen and Hannongbua, 2006), it has been demonstrated that the hydrogen bonding in this peculiar liquid is weak, *i.e.*, the structure and dynamics of this liquid are suggested to be determined by the steric packing effects, rather than by the directional hydrogen bonding interactions. Based on the present ONIOM-XS MD simulation, the first N-N peak is exhibited at 3.62 Å in which the integration up to first N-N minima yields the average coordination number of 12.3. This value is in good accord with the experimental data for about 14 NH_3 molecules (Ricci, Nardene, Ricci, Andreani and Soper, 1995). The characteristics of hydrogen bonds in liquid NH_3 can be interpreted through the N-H, H-N and H-H RDFs (cf. Figures 4.5b-d). In experiment (Ricci, Nardene, Ricci, Andreani and Soper, 1995), the hydrogen-bond formation in the liquid NH_3 was interpreted from the feature of N-H RDF at ~ 2.25 Å. In the ONIOM-XS MD simulation, however, this feature is less evident, *i.e.*, only a slightly distinct peak is recognizable at N---H distances between 2.4 and 2.7 Å. Thus, it is more ambiguous to evaluate the average number of hydrogen bonds in the liquid NH_3 . According to the N-H RDF in Figure 4.5b, an integration up to a N---H (hydrogen-bond acceptor) distance of 2.7 Å yields about 1.2 hydrogen atoms being bonded to nitrogen atom of the central reference molecule. Likewise, according to the H-N RDF in Figure 4.5c, an integration up to a H---N (hydrogen-bond donor) distance of 2.7 Å gives about 1.1 nitrogen atoms being bonded to hydrogen atoms of the central NH_3 . These data suggest that each NH_3 molecule in the liquid phase has on the average close to one donor and one acceptor hydrogen bonds. With regard to the rather large nearest surrounding molecules (~ 12), it is apparent that the observed number of hydrogen bonds in the liquid phase are much smaller, especially when compared to those of liquid water. Figure 4.6 displays

the probability distributions of the number of NH_3 molecules surrounding the central reference molecule, calculated up to first minimum of the N-N RDFs. By means of the ONIOM-XS MD simulation, a favored coordination number of 12 is observed, followed by 11 and 13 in decreasing amounts. As can be seen in Figure 4.6, the broad distribution of the coordination number, varying from 8 to 15 coordinated molecules, clearly indicates the distorted close-packing structure of the liquid NH_3 . Note that the QM/MM MD study reported the preferred coordination numbers of 12, 13 and 14 in comparable amounts, with the broad distribution of the numbers of NH_3 molecules, ranging from 10 to 16.



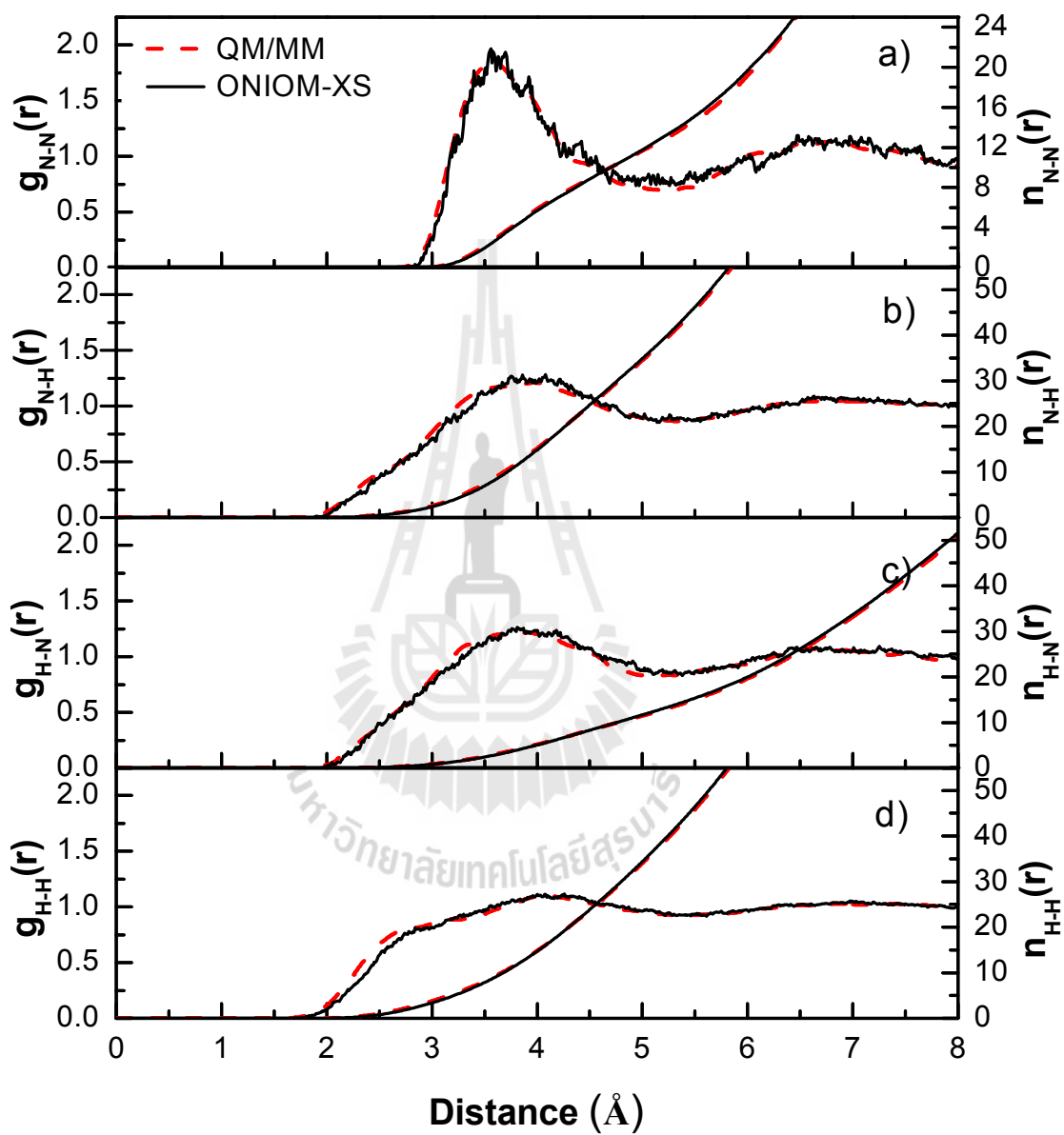


Figure 4.5 a) N-N, b) N-H, c) H-N and d) H-H radial distribution functions and their corresponding integration numbers, as obtained by the QM/MM (Tongraar, Kerdcharoen and Hannongbua, 2006) and ONIOM-XS MD simulations.

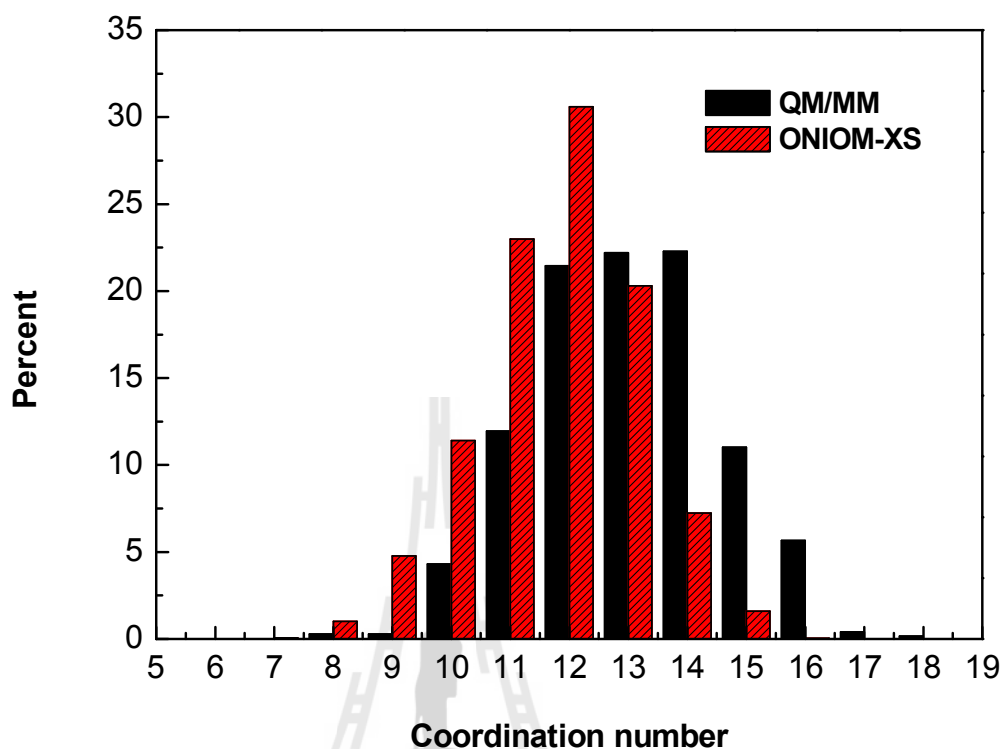


Figure 4.6 Probability distributions of the coordination numbers, calculated up to first minimum of the N-N RDFs, as obtained by the QM/MM (Tongraar, Kerdcharoen and Hannongbua, 2006) and ONIOM-XS MD simulations.

4.2 Dynamical properties

The dynamics properties of the ion-ligand complexes can be visualized from plots of time dependence of the Na-N distance and number of first-shell ligands, as shown in Figure 4.7. Within the 40 ps of the ONIOM-XS MD simulation, it is observed that the first solvation shell of Na^+ is arranged with respect to the preferred $\text{Na}^+(\text{NH}_3)_5$ configuration, *i.e.*, this penta-coordinated ion-ligand complex is found to dominate over the 6- and 4-fold coordinated complexes with the probability

distributions of about 67%, 18% and 15%, respectively (cf. Figure 4.2). In this respect, it is observed that the most favorable $\text{Na}^+(\text{NH}_3)_5$ species can convert back and forth to the lower probability $\text{Na}^+(\text{NH}_3)_6$ and $\text{Na}^+(\text{NH}_3)_4$ structures. For example, at the simulation time of 2.5 ps, an arrangement of $\text{Na}^+(\text{NH}_3)_4$ complex is formed, in which one NH_3 molecule in the favorable $\text{Na}^+(\text{NH}_3)_5$ complex is repelled. At the simulation time of 21 ps, one NH_3 molecule from the outer (second-shell) region come into the favorable $\text{Na}^+(\text{NH}_3)_5$ complex, forming an $\text{Na}^+(\text{NH}_3)_6$ intermediate.

According to Figure 4.1a, the non-zero first minimum of the Na-N RDF suggests that NH_3 molecules in the first solvation shell of Na^+ can possibly exchange with those in the outer region, in particular the second solvation layer. The lability of NH_3 molecules in the first and second solvation shells of Na^+ can be interpreted from the self-diffusion coefficient (D). In this study, the D values for NH_3 molecules surrounding the ion were calculated from their center-of-mass velocity autocorrelation functions (VACFs) using the Green-Kubo relation (McQuarrie, 1976),

$$D = \frac{1}{3} \lim_{t \rightarrow \infty} \int_0^t C_v(t) dt. \quad (4.1)$$

Based on the ONIOM-XS MD simulation, the D values for NH_3 molecules in the first and second solvation shells of Na^+ are estimated to be 1.98×10^{-5} and $3.82 \times 10^{-5} \text{ cm}^2 \text{ s}^{-1}$, respectively, which are significantly less than the value of $11.99 \times 10^{-5} \text{ cm}^2 \text{ s}^{-1}$ of liquid NH_3 derived by a compatible ONIOM-XS MD simulation (*i.e.*, an additional ONIOM-XS MD simulation in which the Na^+ ion was replaced by a

reference NH_3 molecule using the ONIOM-XS parameters r_0 and r_1 of 5.0 and 5.2 Å, respectively). With regard to the ONIOM-XS MD results, it is obvious that Na^+ can order its surrounding NH_3 molecules to form both the first and second solvation structures. In this context, it is worth noting that the correct degree of lability of NH_3 molecules in the solvation shells of Na^+ is crucial in accurately determining the reactivity of Na^+ in liquid NH_3 .

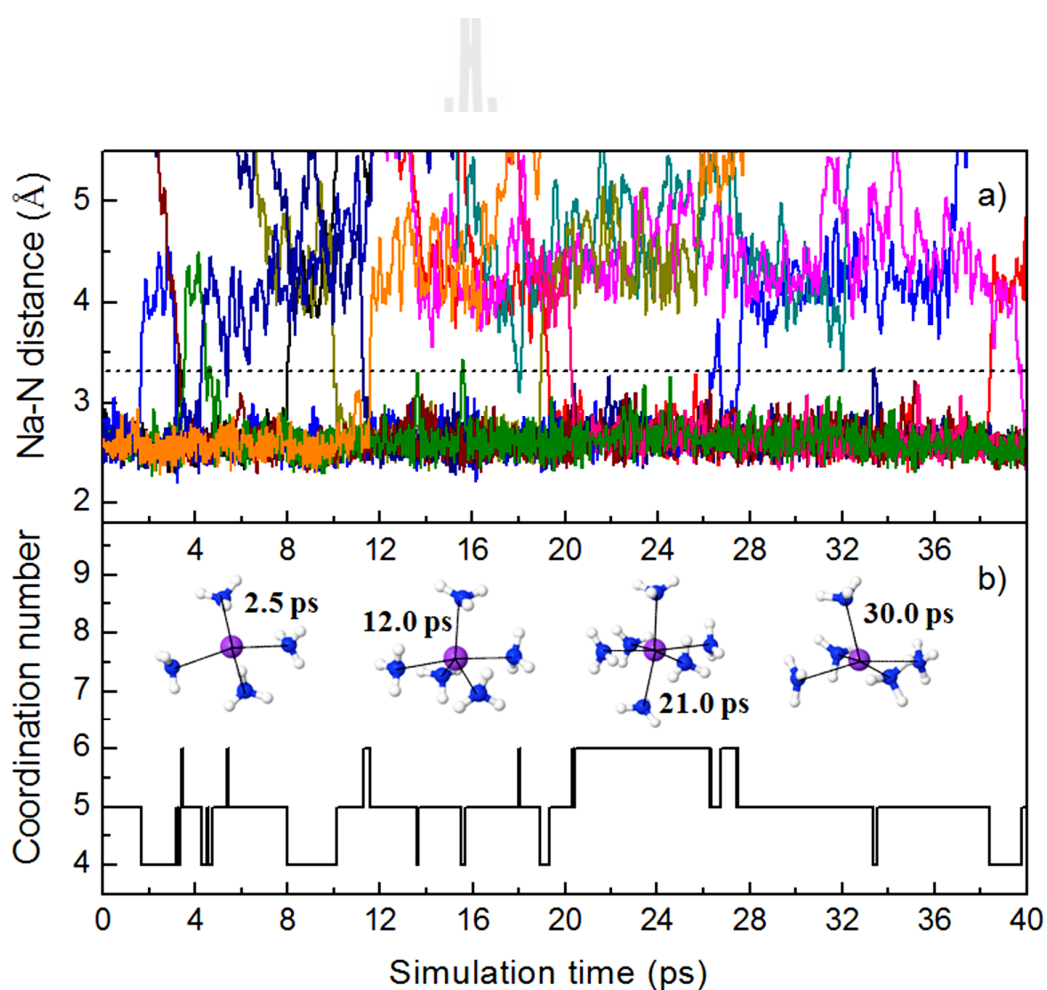
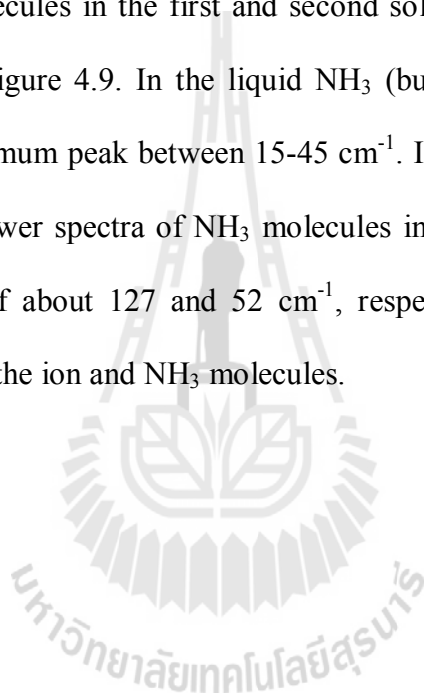


Figure 4.7 Time dependence of a) $\text{Na}^+\text{---N}$ distance and b) number of first-shell ammonia molecules, as obtained by the ONIOM-XS MD simulation. In Figure 4.7a), the dash line parallel to the x-axis indicates the first minimum of the Na-N RDF.

More details regarding the particle motions can be gained by computing the center-of-mass VACFs for NH_3 molecules in the first and second solvation shells of Na^+ and in the bulk, as shown in Figure 4.8. Obviously, the VACFs of NH_3 molecules surrounding the ion decay to zero faster than that of NH_3 molecules in the bulk, which corresponds to the strength of the Na^+ -ligand interactions, *i.e.*, when compared to the interactions among NH_3 molecules in the bulk. Fourier transforms of the translational motions of NH_3 molecules in the first and second solvation shells of Na^+ and in the bulk are shown in Figure 4.9. In the liquid NH_3 (bulk), the Fourier transformation reveals a broad maximum peak between $15\text{-}45\text{ cm}^{-1}$. In the first and second solvation shells of Na^+ , the power spectra of NH_3 molecules in these two shells are shifted to higher frequencies of about 127 and 52 cm^{-1} , respectively, *i.e.*, due to the strong interactions between the ion and NH_3 molecules.



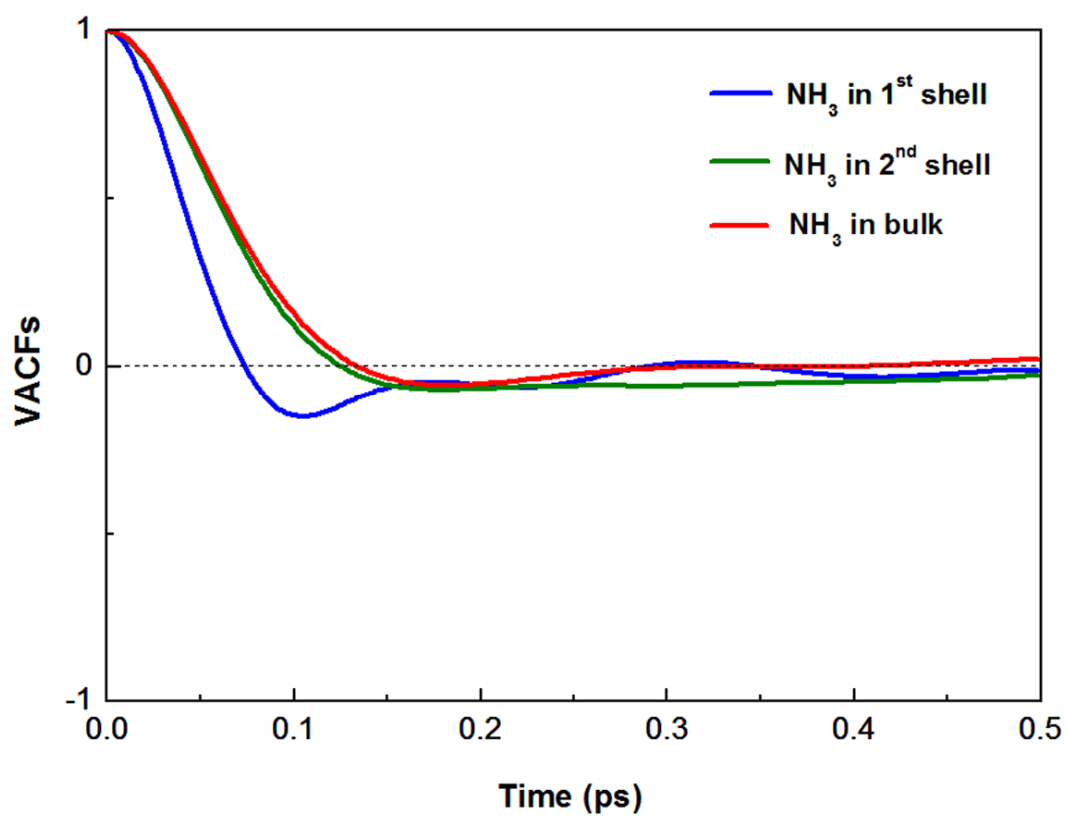


Figure 4.8 Center-of-mass VACFs for NH₃ molecules in the first and second solvation shells of Na⁺ and in the bulk.

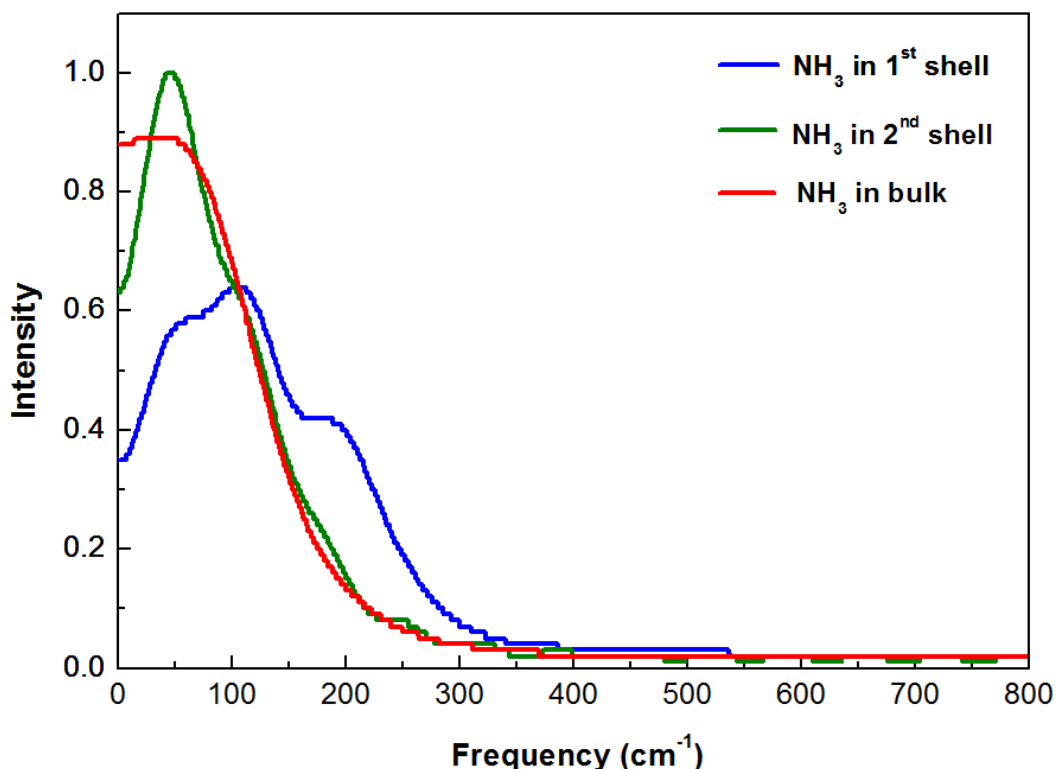


Figure 4.9 Fourier transforms of the translational motions of NH_3 in the first and second solvation shells of Na^+ and in the bulk.

In addition to the translational motions, the Fourier transforms of the librational motions of NH_3 molecules in the first and second solvation shells of Na^+ and in the bulk are also plotted in Figure 4.10. Note that, according to the normal-coordinate analyses (Bopp, 1986), the power spectra of the librational motions are calculated from the three components of the hydrogen's velocities of all NH_3 molecules found within the defined solvation layer. In the liquid NH_3 (bulk), the rotation about the dipole axis (z axis) exhibits a maximum at zero frequency, implying a rather free rotational motion around this axis, while the rotation around the x axis shows a maximum peak at 160 cm^{-1} . As compared to liquid water (Tongraar, Liedl

and Rode, 1997; Xenides, Randolf and Rode, 2005), it is apparent that the rotational motions of NH_3 molecules in the liquid phase are rather fast processes, which reflect in short-time dynamics of the hydrogen bonds in liquid NH_3 . With regard to the power spectra in Figure 4.10, the rotations of NH_3 molecules in the solvation shells of Na^+ are subject to the effects of the ion. In this respect, the effects of the ion cause the spectral densities shift to higher frequencies. Regarding the rotations about the x axis, as compared to the peak for bulk NH_3 , the power spectra of NH_3 molecules in the first and second solvation shells of Na^+ increase to 490 and 235 cm^{-1} , respectively. For the rotations about the z axis, the frequency for the first-shell NH_3 molecules is shifted from zero frequency (in the bulk) to 135 cm^{-1} , while that of the second-shell NH_3 molecules shows spectrum at 0 cm^{-1} , but with a tailing peak shifted to higher frequency.

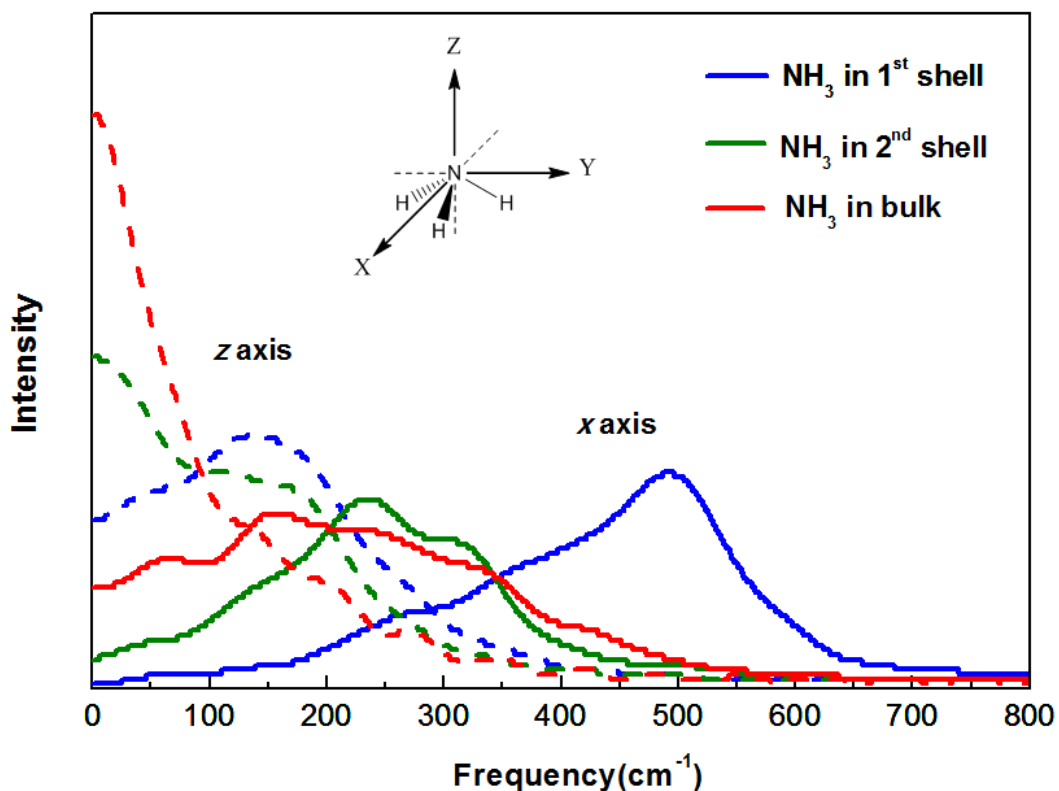


Figure 4.10 Fourier transforms of the librational motions of NH₃ in the first and second solvation shells of Na⁺ and in the bulk (the dash lines refer to *z* axis and the solid lines refer to *x* axis).

The rates of ligand exchange processes at Na⁺ were evaluated through mean residence times (MRTs) of NH₃ molecules in the first and second solvation shells of the ion. In this work, the MRT data were calculated using the “direct” method (Hofer, Tran, Schwenk and Rode, 2004), as the product of the average number of NH₃ molecules in the solvation shell of ion with the duration of the ONIOM-XS MD simulation, divided by the observed number of exchange events lasting a given time interval t^* . In general, a t^* value of 0.0 ps is recommended for the estimation of

hydrogen bond lifetimes, while a t^* value of 0.5 ps is chosen as a good measure for ligand exchange processes (Hofer, Tran, Schwenk and Rode, 2004). The calculated MRT data with respect to t^* values of 0.0 and 0.5 ps are summarized in Table 4.3. To provide useful discussion with respect to the “structure-making” ability of Na^+ , the MRT data for liquid NH_3 , as well as for the cases of Na^+ in aqueous solution (Sripa, Tongraar and Kerdcharoen, 2013) and pure water (Thaomola, Tongraar and Kerdcharoen, 2012), obtained by the compatible ONIOM-XS MD simulations are also given for comparison. As compared to the MRT value of bulk NH_3 , Na^+ clearly acts as a “structure-maker”, *i.e.*, the MRT values for NH_3 molecules in the first and second solvation shells of Na^+ are higher than the corresponding value observed in the liquid NH_3 . As can be seen in Table 4.3, the “structure-making” ability of Na^+ in liquid NH_3 is significantly stronger than in aqueous solution. In particular, it is obvious that the ability of Na^+ in ordering its surrounding NH_3 molecules to form specific ion-ligand complexes exists beyond the first solvation shell.



Table 4.2 Number of ligand exchange events (N_{ex}) and mean residence times (MRTs) of solvent molecules in the bulk and in the vicinity of Na^+ , as obtained by the ONIOM-XS MD simulations.

System	CN	t_{sim}	$t^* = 0.0$ ps		$t^* = 0.5$ ps	
			$N_{ex}^{0.0}$	$\tau_{NH_3}^{0.0}$	$N_{ex}^{0.5}$	$\tau_{NH_3}^{0.5}$
<i>Na⁺ in liquid NH₃</i>						
Na ⁺ (1 st shell)	5.1	40.0	42	4.86	16	12.75
Na ⁺ (2 nd shell)	11.2	40.0	734	0.61	157	2.85
<i>Na⁺ in liquid water</i>						
Na ⁺ (1 st shell) *	5.4	41.0	164	1.35	36	6.18
<i>Pure solvents</i>						
Liquid NH ₃	11.8	30.0	885	0.40	270	1.31
Pure H ₂ O **	4.7	30.0	607	0.23	65	2.17

* (Sripa, Tongraar and Kerdcharoen, 2013)

** (Thaomola, Tongraar and Kerdcharoen, 2012)

4.3 References

- Bopp, P. (1986). A study of the vibrational motions of water in an aqueous CaCl_2 solution. **Chemical Physics**. 106: 205-212.
- Hannongbua, S. (1991). A molecular dynamics simulation of the structure of sodium ion in liquid ammonia. **Australian Journal of Chemistry**. 44: 447-456.

- Hannongbua, S. (1997). The role of nonadditive effects in the first solvation shell of Na^+ and Mg^{2+} in liquid ammonia: Monte Carlo studies including three-body corrections. **Journal of Chemical Physics**. 106: 6076-6081.
- Hofer, T. S., Tran, H. T., Schwenk, C. F. and Rode, B. M. (2004). Characterization of dynamics and reactivities of solvated ions by *ab initio* simulations. **Journal of Computational Chemistry**. 25: 211-217.
- Kerdcharoen, T. and Rode, B. M. (2000). What is the solvation number of Na^+ in ammonia? An *ab initio* QM/MM molecular dynamics study. **Journal of Physical Chemistry A**. 104: 7073-7078.
- Marchi, M., Sprik, M. and Klein, M. L. (1990). Solvation and ionization of alkali metals in liquid ammonia : A path integral Monte Carlo study. **Journal of Physics**. 2: 5833-5848.
- McQuarrie, D. A. (1976). **Statistical Mechanics; Harper & Row: New York**.
- Ricci, M. A., Nardene, M., Ricci, F. P., Andreani, C. and Soper, A. K. (1995). Microscopic structure of low temperature liquid ammonia: A neutron diffraction experiment. **Journal of Chemical Physics**. 102: 7650-7655.
- Sripa, P., Tongraar, A. and Kerdcharoen, T. (2013). "Structure-making" ability of Na^+ in dilute aqueous solution: An ONIOM-XS MD simulation study. **The Journal of Physical Chemistry A**. 117: 1826-1833.
- Thaomola, S., Tongraar, A. and Kerdcharoen, T. (2012). Insights into the structure and dynamics of liquid water: A comparative study of conventional QM/MM and ONIOM-XS MD simulations. **Journal of Molecular Liquids**. 174: 26-33.

Tongraar, A., Liedl, K. R. and Rode, B. M. (1997). Solvation of Ca^{2+} in water studied by Born-Oppenheimer *ab initio* QM/MM dynamics. **Journal of Physical Chemistry A**. 101: 6299-6309.

Xenides, D., Randolph, B. R. and Rode, B. M. (2005). Structure and ultrafast dynamics of liquid water: A quantum mechanics/molecular mechanics molecular dynamics simulations study. **Journal of Chemical Physics**. 122: 174506-174510.

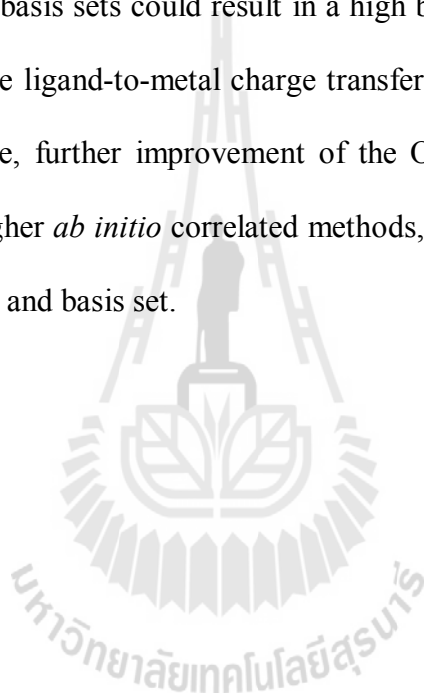


CHAPTER V

CONCLUSION

In this work, a high-level ONIOM-XS MD technique has been applied for studying the solvation structure and dynamics of Na^+ in liquid NH_3 . Two ONIOM-XS MD simulations have been separately performed, namely for the systems of Na^+ in liquid NH_3 and of the pure liquid NH_3 . In the case of pure liquid NH_3 , the ONIOM-XS MD results were used as reference (bulk) when discussing the effects of the ion on the local structure and dynamics of the solvent molecules. With regard to the detailed analyzes on the ONIOM-XS MD's trajectories, Na^+ clearly acts as a “structure-maker” in this media, *i.e.*, this ion can order its surrounding NH_3 molecules to form specific first and second solvation shells with the average coordination numbers of 5.1 and 11.2, respectively. In this respect, the first solvation shell of Na^+ is rather well-defined, forming a preferred 5-fold coordinated complex with a distorted square pyramidal geometry. Interestingly, it is observed that the most preferential $\text{Na}^+(\text{NH}_3)_5$ species could convert back and forth to the lower probability $\text{Na}^+(\text{NH}_3)_6$ and $\text{Na}^+(\text{NH}_3)_4$ configurations. The second solvation shell of Na^+ is also detectable, indicating a recognizable influence of Na^+ in ordering NH_3 molecules in this shell. The ONIOM-XS MD results are significantly different from those derived by the QM/MM MD scheme, implying the important treatment of the ONIOM-XS MD technique for obtaining more reliable descriptions of such condensed-phase system.

With regard to the ONIOM-XS MD results, it is worth noting that the HF method and the DZP and LANL2DZ basis sets employed in this work were considered to be good enough to provide reliable data, compromising between the quality of the simulation results and the requirement of the CPU time. In this respect, it should be realized that the instantaneous electron correlation and the charge transfer effects may not be typically well-described by the HF theory, and that the use of the DZP and LANL2DZ basis sets could result in a high basis set superposition error and an exaggeration of the ligand-to-metal charge transfer. When computational facilities become more feasible, further improvement of the ONIOM-XS MD results can be achieved by using higher *ab initio* correlated methods, such as MP2, together with the use of larger QM size and basis set.





APPENDICES

APPENDIX A

THEORETICAL OBSERVATIONS OF Na⁺ IN LIQUID

NH₃

Table A1 Theoretical observations for the system of Na⁺ in liquid NH₃.

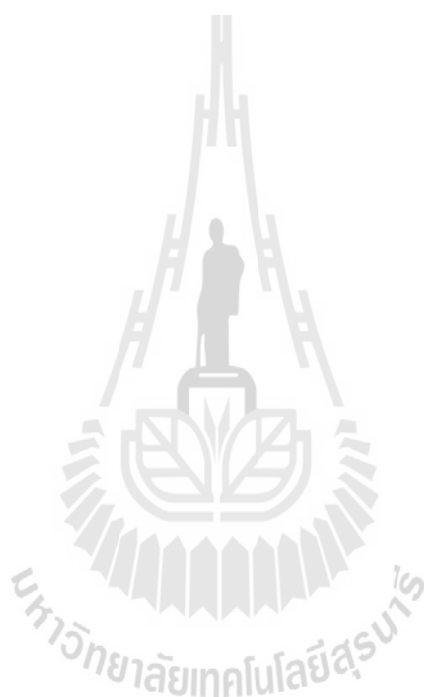
Method	ion/ solvent	Temp (K)	r_{\max} (Å)	RDF (r_{\max})	CN	Year	Ref.
ONIOM-XS MD	1/215	235	2.58	8.0	5.1	2014	This work
QM/MM MD	1/215	235	2.55	4.4	5.0	2000	Kerdcharoen
MM MD (2-body)	1/215	235	2.55	14.8	8.0	2000	Kerdcharoen
MM MC (2-body)	1/201	277	2.68	11.6	9.0	1997	Hannongbua
MM MC (2+3-body)	1/201	277	2.68	10.0	8.0	1997	Hannongbua
MM MD (2-body)	1/215	235	2.49	16.6	8.0	1991	Hannongbua
MM MD (2-body)	1/215	266	2.42	14.6	7.0	1991	Hannongbua
MC (empirical)	1/250	260	2.25	9.5	5.0	1990	Marchi <i>et al.</i>

APPENDIX B

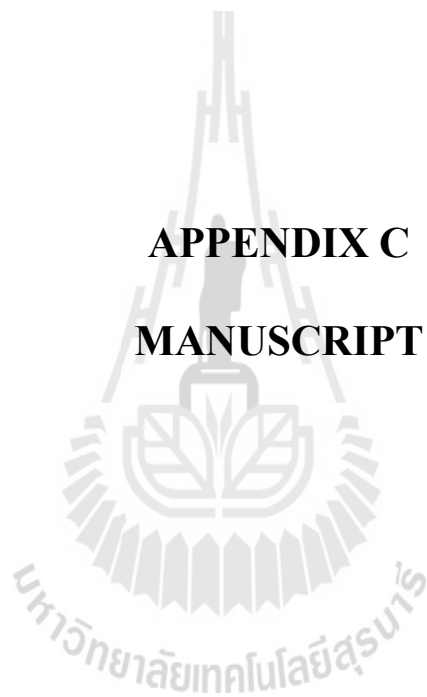
LIST OF PRESENTATIONS

1. Jarukorn Sripradite and Anan Tongraar. (March 27-29, 2013). Solvation structure and dynamics of Na^+ in liquid NH_3 : An *ab initio* QM/MM MD simulation based on ONIOM-XS method. **International Annual Symposium on Computational Science and Engineering (ANSCSE) 17th**, Khon Kaen University, Thailand.
2. Jarukorn Sripradite and Anan Tongraar. (July 23-28, 2013). Characteristics of Na^+ in liquid ammonia: Insights through an ONIOM-XS MD simulation. **The 7th Conference of the Asian Consortium on Computational Materials Science (ACCMS-7)**, Suranaree University of Technology, Nakhon Ratchasima, Thailand.
3. Jarukorn Sripradite and Anan Tongraar. (January 8-10, 2014). On the Solvation of Na^+ in liquid ammonia: An ONIOM-XS MD simulations study. **Pure and Applied Chemistry International Conference 2014 (PACCON2014)**, Centara Hotel and Convention Centre, Khon Kaen, Thailand.

4. Jarukorn Sripradite and Anan Tongraar. (March 16-20, 2014). Solvation structure and dynamics of Na^+ in weak H-bond liquid ammonia studied by ONIOM-XS MD simulations. **247th American Chemical Society (247th-ACS) National Meeting and Exposition**, Dallas Convention Center, Dallas, Texas, USA.



APPENDIX C
MANUSCRIPT



Solvation structure and dynamics of Na⁺ in liquid NH₃: An ONIOM-XS MD simulations study

Jarukom Sripadit,¹ Anan Tongraat^{*} and Teerakiat Kerdcharoen²

¹ School of Chemistry, Institute of Science, Suranaree University of Technology and NANOTEC-SUT Center of Excellence on Advanced Functional Nanomaterials,

Nakhon Ratchasima 30000, Thailand

² Department of Physics and NANOTEC Center of Excellence, Faculty of Science,

Mahidol University, Bangkok 10400, Thailand

Abstract

Molecular dynamics (MD) technique based on the ONIOM-XS method, known as the ONIOM-XS MD, has been employed to investigate the solvation structure and dynamics of Na⁺ in liquid ammonia. With regard to the ONIOM-XS MD results, Na⁺ acts as a clear "structure-maker" in this media, *i.e.*, this ion can order the surrounding ammonia molecules to form its specific first and second solvation shells with the average coordination numbers of 5.1 and 11.2, respectively. The first solvation shell of Na⁺ is rather well-defined, forming the preferred 5-fold coordinated complexes with respect to the distorted square pyramidal geometry. In this respect, the most preferential Na⁺(NH₃)₅ species could convert back and forth to the lower probability Na⁺(NH₃)₆ and Na⁺(NH₃)₄ complexes. The second solvation shell of Na⁺ is also detectable, revealing a recognizable influence of Na⁺ in ordering the solvent molecules in this shell.

^{*} Corresponding author. E-mail: anan_tongraat@yahoo.com, fax: 0066-44-224017.

1. Introduction

It is known that the basic machinery of human body is proteins and that one-third of them is metalloproteins, *i.e.*, the proteins that contain at least one metal ion. In this respect, the metal ions are needed for the proteins to have their specific structural and/or functional roles. To understand the properties of such metalloproteins, detailed knowledge with respect to the structure and dynamics of ion coordination in simple solvents, such as water (H₂O) and ammonia (NH₃), is essential since these data can provide some insights into the coordinating environment of more complex ligands, *e.g.*, DNA, RNA and proteins. In this study, the topic of our interest is to investigate the solvation structure and dynamics of sodium ion (Na⁺) in liquid NH₃. In terms of theoretical investigations, prior molecular dynamics (MD) [1] and Monte Carlo (MC) [2,3] simulations have reported some microscopic properties of this ion under the environments of NH₃ molecules. However, those MC and MD simulations had relied on simplified potential energy models, leading to different results regarding the coordination numbers and the ion-ammonia distances. For example, the MD simulations using pair potentials based on primitive Gaussian basis sets for Na⁺/ammonia solution at 235 and 266 K have reported the coordination numbers of 8.0 and 7.0, with the average Na⁺-N distances of 2.49 and 2.42 Å, respectively [1]. Later, the MC simulations of Na⁺/ammonia solution at 277 K using pair potentials and pair plus three-body correction functions based on DZP basis sets have yielded the average coordination numbers of 9.0 and 8.1, respectively, with the similar Na⁺-N distance of 2.68 Å [2]. Another MC simulation using empirical potentials gave a rather small coordination number of 5, with the relatively shorter Na⁺-N distance of 2.25 Å [3].

To obtain more reliable results, an *ab initio* MD simulation based on a so-called combined quantum mechanics/molecular mechanics (QM/MM) approach [4-7] has been performed for Na⁺ in liquid NH₃ [8]. By the QM/MM MD technique, the system is partitioned into a small part, *i.e.*, a sphere which contains the Na⁺ ion and its surrounding NH₃ molecules, described by quantum mechanics and another part treated by means of MM potentials. With this approach, the complicated many-body interactions as well as the polarization effects, *i.e.*, at least within the defined QM region, can be reliably included. According to the QM/MM MD simulation [8], the coordination number of 5 was observed, which is in contrast to the corresponding

value of 8 derived by the analogous MD simulation using pair potentials. In addition, the QM/MM MD simulation has reported the Na⁺-N distance of 2.55 Å, which is also different to those obtained from the earlier MM-based MC and MD simulations [1-3]. With regard to the QM/MM MD simulation, since the exchange of NH₃ molecules between the QM and MM regions can occur frequently, a smoothing function [9] is employed to ensure a smooth change of forces at the transition between the QM and MM regions. In practice, however, the smoothing function is applied only for the exchanging NH₃ molecules that are crossing the QM/MM boundary. This is not satisfactory since an interchange of NH₃ molecules between the QM and MM regions will also affect the forces acting on the remaining QM particles. In addition, the QM/MM MD framework cannot clearly define the system's energy expression during the solvent exchange process [10, 11].

To solve these methodical problems, a more sophisticated QM/MM MD technique based on the ONIOM-XS (Own N-layered Integrated molecular Orbital and molecular Mechanics – eXtension to Solvation) method, called briefly the ONIOM-XS MD, has been proposed [10, 11]. By the ONIOM-XS MD technique, the forces on all QM particles will be smoothed during the particle exchanges and, thus, it better defines the system's energy expression. Furthermore, this technique allows both the energies and forces to be smoothed, in contrast to the QM/MM MD scheme in which only the forces were taken into account. The ONIOM-XS MD technique has been successfully applied for condensed-phase systems [10-17], revealing its capability in providing more reliable results which are in better agreement with experiments. Interestingly, according to a recent ONIOM-XS MD simulation of Na⁺ in aqueous solution [13], it has shown that the hydrated Na⁺ complexes are rather flexible, in which the most stable Na⁺(H₂O)₅ species can convert back and forth to the lower probability Na⁺(H₂O)₆ complexes. This leads to frequent structural re-arrangements of the Na⁺(H₂O)₅ and Na⁺(H₂O)₆ complexes as well as numerous attempts of inner-shell water molecules to interchange with water molecules in the outer region, *i.e.*, revealing a weak “structure-making” ability of Na⁺ in aqueous solution. In this study, therefore, the results obtained by the ONIOM-XS MD simulation could be expected to provide more insights into the structure and dynamics of Na⁺ in liquid NH₃ as well.

2. Methods

Based on the ONIOM-XS MD technique [10-17], the system is divided into a “high-level” QM region, *i.e.*, a small subsystem which contains the central Na⁺ and its surrounding ammonia molecules, and the remaining “low-level” MM region. A thin switching layer located between the QM and MM regions is employed in order to detect the exchanging particles, as well as to help in smoothing the energy and forces of the combined system. In this respect, three parameters, namely n_1 , l and n_2 , are defined as the number of particles involved in the QM region, the switching layer and the MM region, respectively, and N is set as the total number of particles (*i.e.*, $N = n_1 + l + n_2$). Regarding the ONIOM extrapolation scheme [18], the potential energy of the system can be written in two ways. First, if the switching layer is included into the “high-level” QM region, the energy expression is written as

$$E^{ONIOM}(n_1 + l; N) = E^{QM}(n_1 + l) - E^{MM}(n_1 + l) + E^{MM}(N). \quad (1)$$

Otherwise, if the switching layer is considered as part of the “low-level” MM region, the energy expression is

$$E^{ONIOM}(n_1; N) = E^{QM}(n_1) - E^{MM}(n_1) + E^{MM}(N). \quad (2)$$

With regard to equations (1) and (2), the E^{QM} and E^{MM} terms represent the interactions derived by the QM calculations and by the classical MM potentials, respectively. Note that the interactions between the QM and MM regions are also described by means of MM potentials, and thus, these contributions are already included in the $E^{MM}(N)$. In the course of the ONIOM-XS MD simulation, when a particle moves into the switching layer (either from the QM or MM region), both equations (1) and (2) must be evaluated. Then, the potential energy of the entire system can be expressed as a hybrid between both energy terms (1) and (2),

$$E^{ONIOM-XS}(\{r_i\}) = (1 - \bar{s}(\{r_i\})) \cdot E^{ONIOM}(n_1 + l; N) + \bar{s}(\{r_i\}) \cdot E^{ONIOM}(n_1; N), \quad (3)$$

where $\bar{s}(\{r_i\})$ is an average over a set of switching functions for individual exchanging particles in the switching layer $s_i(x_i)$.

employed for NH_3 [23]. Note that the use of this flexible model is favorable, ensuring a smooth transition when NH_3 molecules move from the QM region with their full flexibility to the MM region, and *vice versa*. The pair potential functions for describing Na^+-NH_3 interactions were newly constructed. The 1819 HF interaction energy points for various Na^+-NH_3 configurations, obtained from Gaussian03 [22] calculations using the same basis sets as employed in the ONIOM-XS MD simulation, were fitted to an analytical form of

$$\Delta E_{\text{Na}^+-\text{NH}_3} = \sum_{i=1}^4 \left(\frac{A_{ic}}{r_{ic}^6} + \frac{B_{ic}}{r_{ic}^7} + C_{ic} \exp(-D_{ic} r_{ic}) + \frac{q_i q_c}{r_{ic}} \right), \quad (7)$$

where A , B , C and D are the fitting parameters (see Table 1), r_{ij} denotes the distances between the Na^+ ion and the i -th atoms of the NH_3 molecule and q are the atomic net charges. In this work, the charge for Na^+ was set to 1.0, and the charges for N and H atoms of NH_3 were adopted from the flexible NH_3 model [23], namely -0.8022 and 0.2674, respectively.

The ONIOM-XS MD simulation was performed in a canonical ensemble at 235 K with a time step size of 0.2 fs. The system's temperature was kept constant using the Berendsen algorithm [24]. The starting configuration of this particular system was obtained from our previous QM/MM MD studies of liquid NH_3 [25], *i.e.*, in which one NH_3 molecule was replaced by Na^+ . The periodic cubic box, with a box length of 21.80 Å, employed in the simulation contains one Na^+ and 255 ammonia molecules, assuming the experimental density of liquid NH_3 of 0.699 g cm^{-3} . The Newtonian equations of motions were treated by a general predictor-corrector algorithm. Long-range interactions were treated using the reaction-field procedure [26]. The ONIOM-XS MD simulation was performed with the system's re-equilibration for 15 ps, followed by another 40 ps to collect configurations every 10^{th} step.

3. Results and discussion

The structural details of the Na^+ solvation can be illustrated through the Na-N and Na-H radial distribution functions (RDFs) and their corresponding integration numbers, as depicted in Fig. 1. By means of the ONIOM-XS MD simulation, a pronounced first Na-N RDF is exhibited at 2.58 Å, together with a recognizable second Na-N peak centered at around 4.22 Å. As can be seen in Fig. 1a, the smooth

6

$$\bar{s}(\{r_i\}) = \frac{1}{7} \sum_{i=1}^7 s_i(x_i), \quad (4)$$

In general, the switching function applied in equation (4) can be of any form.

In this study, a polynomial expression is employed,

$$s_i(x_i) = 6 \left(x_i - \frac{1}{2} \right)^5 - 5 \left(x_i - \frac{1}{2} \right)^3 + \frac{15}{18} \left(x_i - \frac{1}{2} \right) + \frac{1}{2}, \quad (5)$$

where $x_i = ((r_i - r_0)/(r_1 - r_0))$, and r_0 and r_1 are the radius of the inner and outer surfaces of the switching shell, respectively, and r_i is the distance between the center of mass of the exchanging particle and the center of the QM sphere. Note that the above polynomial form and parameter sets were derived to have an S-shape that converges to 0 and 1 at r_0 and r_1 , respectively [10]. Finally, the gradient of the energy can be written as

$$\begin{aligned} \nabla_{\mathbf{r}} E^{\text{ONIOM-XS}}(\{r_i\}) &= \left(-\bar{s}(\{r_i\}) \right) \cdot \nabla_{\mathbf{r}} E^{\text{ONIOM}}(n_i + l; N) + \bar{s}(\{r_i\}) \\ &\cdot \nabla_{\mathbf{r}} E^{\text{ONIOM}}(n_i; N) + \frac{1}{(r_1 - r_0)} \nabla_{\mathbf{r}} \bar{s}(\{r_i\}) \\ &\cdot \left(E^{\text{ONIOM}}(n_i; N) - E^{\text{ONIOM}}(n_i + l; N) \right) \end{aligned} \quad (6)$$

In this work, a QM radius of 4.4 Å and a switching width of 0.2 Å were chosen, which correspond to the ONIOM-XS parameters r_0 and r_1 of 4.2 and 4.4 Å, respectively. Inside the QM region, all interactions were treated at the Hartree-Fock (HF) level of accuracy using LANL2DZ [19,20] and DZP [21] basis sets for Na^+ and NH_3 , respectively. All the QM calculations were carried out using the Gaussian03 program [22]. Note that the HF method and the basis sets employed in this study were selected according to a compromise between the quality of the simulation results and the requirement of the CPU time. In this respect, it should be concerned that the instantaneous electron correlation and the charge transfer effects are not typically well-described by the HF theory, and that the use of LANL2DZ and DZP basis sets could result in high basis set superposition error and an exaggeration of ligand-to-metal charge transfer. For interactions within the MM and between the QM and MM regions, a flexible model, which describes inter- and intramolecular interactions, was

5

well as with the shorter simulation period of 12 ps. According to the data in Table 2, it is obvious that most MC and MD simulations using pair potentials or pair plus three-body correction functions fail to predict the solvation structure of Na^+ in liquid NH_3 , *i.e.*, most of which predict sharper, narrower and better separated first Na-N peaks with relative higher coordination numbers.

The probability distributions of the coordination numbers, calculated within the first and second solvation shells of Na^+ , are displayed in Fig. 2. Within the first solvation shell of Na^+ , it is apparent that this ion prefers the coordination number of 5, followed by 6 and 4 in smaller amounts. In the second solvation layer, a number of NH_3 molecules, ranging from 7 to 14 with the most prevalent number of 11, are observed. The arrangement of NH_3 molecules in the first solvation shell of Na^+ can be analyzed from the distributions of N-Na-N angle, as depicted in Fig. 3. With regard to the coordination number of 5, one could assume two possible geometrical arrangements, namely a trigonal bipyramidal and a square pyramidal structure. In general, the trigonal bipyramidal structure is characterized by the N-Na-N angles of 90, 120 and 180°, with the probability ratio of 6:3:1, while the square pyramidal structure corresponds to the N-Na-N angles of 90 and 180°, with the probability ratio of 8:2. According to the plot in Fig. 3, it is apparent that NH_3 molecules in the first solvation shell of Na^+ are somewhat flexible, forming the preferred 5-fold coordinated complexes with respect to the distorted square pyramidal geometry. Additional information regarding the orientation of NH_3 molecules in the vicinity of Na^+ is also given in Fig. 4. In this context, the angle θ is defined by the Na---N axis and the dipole vector of the surrounding NH_3 molecules. As can be seen in Fig. 4, the shape of the distribution peaks clearly indicates that NH_3 molecules in the first solvation shell of Na^+ stick quite rigidly to their dipole-oriented configurations, and that NH_3 molecules in the second solvation layer are also arranged with respect to a remarkable influence of Na^+ .

The dynamics properties of the ion-ligand complexes can be visualized from plots of time dependence of the Na-N distance and number of first-shell ligands, as shown in Fig. 5. Within the 40 ps of the ONIOM-XS MD simulation, it is observed that the first solvation shell of Na^+ is arranged with respect to the preferred $\text{Na}^+(\text{NH}_3)_5$ configuration, *i.e.*, this penta-coordinated ion-ligand complex is found to dominate over the 6- and 4-fold coordinated complexes with the probability distributions of

8

shape of the Na-N RDF between 4.2 and 4.4 Å (which correspond to the ONIOM-XS parameters r_0 and r_1) clearly confirms that the transition of NH_3 molecules between the QM and MM regions occurs smoothly, and that the ion-ligand and ligand-ligand interactions beyond the QM region could be well accounted for by the MM potentials. The shape and height of the first and second Na-N RDFs reveal a clear “structure-making” ability of Na^+ in liquid NH_3 , *i.e.*, a significant influence of the Na^+ ion in ordering its surrounding NH_3 ligands to form specific ion-ligand complexes. Note that, according to the recent ONIOM-XS MD simulation of Na^+ in aqueous solution [13], the Na^+ ion has been classified as a weak “structure-maker”. In liquid NH_3 , the observed higher intensity of the Na-N RDF, *i.e.*, when compared to the Na-O RDF for the case of Na^+ in aqueous solution [13], clearly implies a stronger “structure-making” ability of Na^+ in this media. In addition, the pronounced second peak of the Na-N RDF clearly indicates the influence of Na^+ beyond the first solvation layer. With regard to the Na-N RDF in Fig. 1a, the first solvation shell of Na^+ is rather well separated from the second one, suggesting that NH_3 molecules in the first solvation shell are strongly attached to the ion, and that ligand exchange processes between the first and the second solvation shells may not frequently occur during the ONIOM-XS MD simulation. Integrations up to first and second minimum of the Na-N RDF yield about 5.1 and 16.3 NH_3 molecules, respectively. Note that, since the second minimum of the Na-N RDF is broad, the structural parameters with respect to the second solvation shell are considered as rough estimates, *i.e.*, the position of the second Na-N minimum is assumed to be 5.25 Å throughout this work.

Some structural parameters for the first solvation shell of Na^+ , as obtained from various MC and MD simulations, are summarized in Table 2. As compared to the recent QM/MM MD study [8], the ONIOM-XS MD simulation, although predicts a similar coordination number of about 5, reveals significant difference regarding the characteristics of the Na-N RDF. In particular, the ONIOM-XS MD results clearly show relatively higher, sharper and more pronounced first and second peaks of the Na-N RDF, leading to better defined first and second solvation shells. This observed difference clearly confirms the important treatment of the ONIOM-XS MD technique for the study of such condensed-phase system. Regarding the observed discrepancies between the ONIOM-XS and QM/MM [8] MD simulations, it should be noticed that the latter one was performed with the use of different basis set, namely the ECP, as

7

corresponds to the strength of the Na^+ -ligand interactions, *i.e.*, when compared to the interactions among NH_3 molecules in the bulk. Fourier transforms of the translational motions of NH_3 molecules in the first and second solvation shells of Na^+ and in the bulk are shown in Fig. 7. In the liquid NH_3 (bulk), the Fourier transformation exhibits a broad maximum between 15–45 cm^{-1} . In the first and second solvation shells of Na^+ , the power spectra of NH_3 molecules in these two shells are shifted to higher frequencies of about 127 and 52 cm^{-1} , respectively, *i.e.*, due to the strong interactions between the ion and NH_3 molecules. In addition to the translational motions, the Fourier transforms of the librational motions of NH_3 molecules in the first and second solvation shells of Na^+ and in the bulk are also plotted in Fig. 8. Note that, according to the normal-coordinate analyses [29], the power spectra of the librational motions are calculated from the three components of the hydrogen's velocities of all NH_3 molecules found within the defined solvation layer. In the liquid NH_3 (bulk), the rotation about the dipole axis (z axis) exhibits a maximum at zero frequency, implying a rather free rotational motion around this axis, while the rotation around the x axis shows a maximum peak at 160 cm^{-1} . As compared to liquid water [30,31], it is apparent that the rotational motions of NH_3 molecules in the liquid phase are rather fast processes, which reflect in short-time dynamics of the hydrogen bonds in liquid NH_3 . With regard to the power spectra in Fig. 8, the rotations of NH_3 molecules in the solvation shells of Na^+ are subject to the effects of the ion. In this respect, the effects of the ion cause the spectral densities shift to higher frequencies. Regarding the rotations about the x axis, as compared to the peak for bulk NH_3 , the power spectra of NH_3 molecules in the first and second solvation shells of Na^+ increase to 490 and 235 cm^{-1} , respectively. For the rotations about the z axis, the frequency for the first-shell NH_3 molecules is shifted from zero frequency (in the bulk) to 135 cm^{-1} , while that of the second-shell NH_3 molecules shows spectrum at 0 cm^{-1} , but with a tailing peak shifted to higher frequency.

The rates of ligand exchange processes at Na^+ were evaluated through mean residence times (MRTs) of NH_3 molecules in the first and second solvation shells of the ion. In this work, the MRT data were calculated using the “direct” method [32], as the product of the average number of NH_3 molecules in the solvation shell of ion with the duration of the ONIOM-XS MD simulation, divided by the observed number of exchange events lasting a given time interval t^* . In general, a t^* value of 0.0 ps is

10

about 67%, 18% and 15%, respectively (cf. Fig. 2). In this respect, it is observed that the most favorable $\text{Na}^+(\text{NH}_3)_3$ species can convert back and forth to the lower probability $\text{Na}^+(\text{NH}_3)_6$ and $\text{Na}^+(\text{NH}_3)_4$ structures. For example, at the simulation time of 2.5 ps, an arrangement of $\text{Na}^+(\text{NH}_3)_4$ complex is formed, in which one NH_3 molecule in the favorable $\text{Na}^+(\text{NH}_3)_3$ complex is repelled. At the simulation time of 21 ps, one NH_3 molecule from the outer (second-shell) region come into the favorable $\text{Na}^+(\text{NH}_3)_3$ complex, forming an $\text{Na}^+(\text{NH}_3)_6$ intermediate.

According to Fig. 1a, the non-zero first minimum of the Na-N RDF suggests that NH_3 molecules in the first solvation shell of Na^+ can possibly exchange with those in the outer region, in particular the second solvation layer. The lability of NH_3 molecules in the first and second solvation shells of Na^+ can be interpreted from the self-diffusion coefficient (D). In this study, the D values for NH_3 molecules surrounding the ion were calculated from their center-of-mass velocity autocorrelation functions (VACFs) using the Green-Kubo relation [28],

$$D = \frac{1}{3} \lim_{t \rightarrow \infty} \int_0^t C_v(t) dt. \quad (8)$$

Based on the ONIOM-XS MD simulation, the D values for NH_3 molecules in the first and second solvation shells of Na^+ are estimated to be 1.98×10^{-5} and $3.82 \times 10^{-5} \text{ cm}^2 \text{ s}^{-1}$, respectively, which are significantly less than the value of $11.99 \times 10^{-5} \text{ cm}^2 \text{ s}^{-1}$ of liquid NH_3 derived by a compatible ONIOM-XS MD simulation (*i.e.*, an additional ONIOM-XS MD simulation in which the Na^+ ion was replaced by a reference NH_3 molecule using the ONIOM-XS parameters r_0 and r_1 of 5.0 and 5.2 Å, respectively). With regard to the ONIOM-XS MD results, it is obvious that Na^+ can order its surrounding NH_3 molecules to form both the first and second solvation structures. In this context, it is worth noting that the correct degree of lability of NH_3 molecules in the solvation shells of Na^+ is crucial in accurately determining the reactivity of Na^+ in liquid NH_3 .

More details regarding the particle motions can be gained by computing the center-of-mass VACFs for NH_3 molecules in the first and second solvation shells of Na^+ and in the bulk, as shown in Fig. 6. Obviously, the VACFs of NH_3 molecules surrounding the ion decay to zero faster than that of NH_3 molecules in the bulk, which

9

T.K. acknowledges financial support from Mahidol University. High-performance computer facilities provided by the National e-Science Infrastructure Consortium are gratefully acknowledged.

recommended for the estimation of hydrogen bond lifetimes, while a τ value of 0.5 ps is chosen as a good measure for ligand exchange processes [32]. The calculated MRT data with respect to τ values of 0.0 and 0.5 ps are summarized in Table 3. To provide useful discussion with respect to the “structure-making” ability of Na^+ , the MRT data for liquid NH_3 , as well as for the cases of Na^+ in aqueous solution [13] and pure water [14], obtained by the compatible ONIOM-XS MD simulations are also given for comparison. As compared to the MRT value of bulk NH_3 , Na^+ clearly acts as a “structure-maker”, *i.e.*, the MRT values for NH_3 molecules in the first and second solvation shells of Na^+ are higher than the corresponding value observed in the liquid NH_3 . As can be seen in Table 3, the “structure-making” ability of Na^+ in liquid NH_3 is significantly stronger than in aqueous solution. In particular, it is obvious that the ability of Na^+ in ordering its surrounding NH_3 molecules to form specific ion-ligand complexes exists beyond its first solvation layer.

4. Conclusion

The high-level ONIOM-XS MD technique has been applied for studying the solvation structure and dynamics of Na^+ in liquid NH_3 . With regard to the detailed analyzes on the ONIOM-XS MD’s trajectories, Na^+ clearly acts as a “structure-maker”, *i.e.*, this ion can order its surrounding NH_3 molecules to form specific first and second solvation shells with the average coordination numbers of 5.1 and 11.2, respectively. In this respect, the first solvation shell of Na^+ is rather well-defined, forming a preferred 5-fold coordinated complex with a distorted square pyramidal geometry, in which the most preferential $\text{Na}^+(\text{NH}_3)_5$ species could convert back and forth to the lower probability $\text{Na}^+(\text{NH}_3)_6$ and $\text{Na}^+(\text{NH}_3)_4$ configurations. The second solvation shell of Na^+ is loosely formed, indicating a recognizable influence of Na^+ in ordering NH_3 molecules in this shell.

5. Acknowledgment

This work was financially supported by grant fund under the program Strategic Scholarships for Frontier Research Network for the Ph.D. Program Thai Doctoral degree from the Commission on Higher Education, Thailand. A.T. also acknowledges support by Suranaree University of Technology (SUT) and the National Research University (NRU) Project of Thailand, Office of the Higher Education Commission.

Hratchian, J.B. Cross, V. Bakken, C. Adamo, J. Jaramillo, R. Gomperts, R.E. Stratmann, O. Yazyev, A.J. Austin, R. Cammi, C. Pomelli, J.W. Ochterski, P.Y. Ayala, K. Morokuma, G.A. Voth, P. Salvador, J.J. Dannenberg, V.G. Zakrzewski, S. Dapprich, A.D. Daniels, M.C. Strain, O. Farkas, D.K. Malick, A.D. Rabuck, K. Raghavachari, J.B. Foresman, J.V. Ortiz, Q. Cui, A.G. Baboul, S. Clifford, J. Cioslowski, B.B. Stefanov, G. Liu, A. Liashenko, P. Piskorz, I. Komaromi, R.L. Martin, D.J. Fox, T. Keith, M.A. Al-Laham, C.Y. Peng, A. Nanayakkara, M. Challacombe, P.M.W. Gill, B. Johnson, W. Chen, M.W. Wong, C. Gonzalez, J.A. Pople, *GAUSSIAN 03*, Revision D.1; Gaussian, Inc.: Wallingford, CT, 2005.

[23] S. Hannongbua, T. Ishida, E. Spohr, K. Heinzinger, Z. Naturforsch. 43a (1988) 572.

[24] H.J.C. Berendsen, J.P.M. Postma, W.F. van Gunsteren, A. DiNola, J.R. Haak, J. Phys. Chem. 81 (1984) 3684.

[25] A. Tongraar, T. Kerdraroen, S. Hannongbua, J. Phys. Chem. A 110 (2006) 4924.

[26] D.J. Adams, E.H. Adams, G.J. Hills, Mol. Phys. 38 (1979) 387.

[27] S.S. Azam, T.S. Hofer, B.R. Randolf, B.M. Rode, J. Phys. Chem. A 113 (2009) 1827.

[28] D.A. McQuarrie, in *Statistical Mechanics*; Harper & Row, New York, 1976.

[29] P. Bopp, Chem. Phys. 196 (1986) 205.

[30] A. Tongraar, K.R. Liedl, B.M. Rode, J. Phys. Chem. A 101 (1997) 6299.

[31] D. Xenides, B.R. Randolf, B.M. Rode, J. Chem. Phys. 122 (2005) 174506.

[32] T.S. Hofer, H.T. Tran, C.F. Schwenk, B.M. Rode, J. Comput. Chem. 25 (2004) 211.

References

- [1] S. Hannongbua, Aust. J. Chem. 44 (1991) 447.
- [2] S. Hannongbua, J. Chem. Phys. 106 (1997) 6076.
- [3] M. Marchi, M. Sprik, M.L. Klein, J. Phys.: Condens. Matter 2 (1990) 5833.
- [4] U.C. Singh, P.A. Kollman, J. Comput. Chem. 7 (1986) 718.
- [5] M.J. Field, P.A. Bash, M. Karplus, J. Comput. Chem. 11 (1990) 700.
- [6] J. Gao, Rev. Comput. Chem. 7 (1996) 119.
- [7] J.L. Gao, D.G. Truhlar, Annu. Rev. Phys. Chem. 53 (2002) 467.
- [8] T. Kerdraroen, B.M. Rode, J. Phys. Chem. A 104 (2000) 7073.
- [9] B.R. Brooks, R.E. Bruccoleri, B.D. Olafson, D.J. States, S. Swaminathan, M. Karplus, J. Comput. Chem. 4 (1983) 187.
- [10] T. Kerdraroen, K. Morokuma, Chem. Phys. Lett. 355 (2002) 257.
- [11] T. Kerdraroen, K. Morokuma, J. Chem. Phys. 118 (2003) 8856.
- [12] S. Wanprakhon, A. Tongraar, T. Kerdraroen, Chem. Phys. Lett. 517 (2011) 171.
- [13] P. Sripa, A. Tongraar, T. Kerdraroen, J. Phys. Chem. A 117 (2013) 1826.
- [14] S. Thaomola, A. Tongraar, T. Kerdraroen, J. Mol. Liq. 174 (2012) 26.
- [15] P. Sripa, A. Tongraar, T. Kerdraroen, J. Mol. Liq. 208 (2015) 280.
- [16] P. Kabbalee, A. Tongraar, T. Kerdraroen, Chem. Phys. 446 (2015) 70.
- [17] P. Kabbalee, P. Sripa, A. Tongraar, T. Kerdraroen, Chem. Phys. Lett. 633 (2015) 152.
- [18] M. Svensson, S. Humbel, R.D.J. Froese, T. Mutsubara, S. Sieber, K. Morokuma, J. Phys. Chem. 100 (1996) 19357.
- [19] P.J. Hay, W.R. Wadt, J. Chem. Phys. 82 (1985) 284.
- [20] C.E. Cheek, T.O. Faust, J.M. Bailey, B.J. Wright, T.M. Gilbert, L.S. Sunderlin, J. Phys. Chem. A 105 (2001) 8111.
- [21] T. H. Jr. Dunning, P. J. Hay, Modern Theoretical Chemistry, III, Plenum, New York, 1976.
- [22] M.J. Frisch, G.W. Trucks, H.B. Schlegel, G.E. Scuseria, M.A. Robb, J.R. Cheeseman, J.A. Montgomery, T. Vreven, K.N. Kudin, J.C. Burant, J.M. Millam, S.S. Iyengar, J. Tomasi, V. Barone, B. Mennucci, M. Cossi, G. Scalmani, N. Rega, G.A. Peterson, H. Nakatsuji, M. Hada, M. Ehara, K. Toyota, R. Fukuda, J. Hasegawa, M. Ishida, T. Nakajima, Y. Honda, O. Kitao, H. Nakai, M. Klene, X. Li, J.E. Knox, H.P.

TABLE CAPTIONS

Table 1 Optimized parameters of the analytical pair potentials for the interactions of ammonia with Na^+ (interaction energies in kcal.mol^{-1} and distances in \AA).

Table 2 Comparison of some structural parameters for the first solvation shell of Na^+ .

Table 3 Number of ligand exchange events (N_{ex}) and mean residence times (MRTs) of ligand molecules in the bulk and in the vicinity of Na^+ , as obtained by the ONIOM-XS MD simulations.

FIGURE CAPTIONS

Figure 1 a) Na-N and b) Na-H radial distribution functions and their corresponding integration numbers.

Figure 2 Distributions of the coordination numbers, calculated within the first and second solvation shells of Na^+ .

Figure 3 Distributions of the N--Na--N angle, calculated within the first minimum of the Na-N RDF.

Figure 4 Probability distributions of θ angle in the first solvation shell of Na^+ , calculated within the first minimum of the Na-N RDF.

Figure 5 Time dependence of a) $\text{Na}^{\text{+}}\text{--}\text{N}$ distance and b) number of first-shell ammonia molecules, as obtained by the ONIOM-XS MD simulation. In Figure 5a), the dash line parallel to the x-axis indicates the first minimum of the Na-N RDF.

Figure 6 Center-of-mass VACFs for NH_3 molecules in the first and second solvation shells of Na^+ and in the bulk.

Figure 7 Fourier transforms of the translational motions of NH_3 in the first and second solvation shells of Na^+ and in the bulk.

Figure 8 Fourier transforms of the librational motions of NH_3 in the first and second solvation shells of Na^+ and in the bulk.



Figure 1

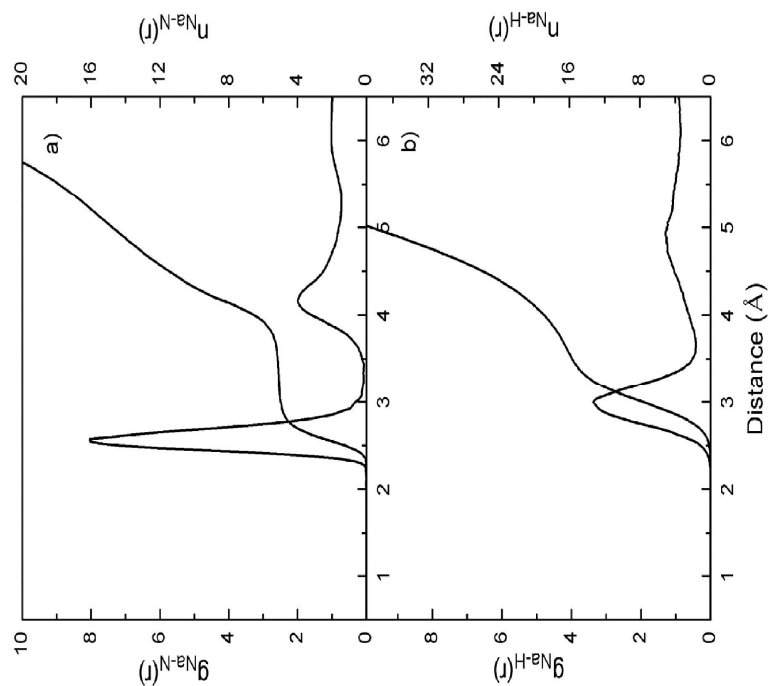


Table 1

Pair	A (kcal mol ⁻¹ Å ⁴)	B (kcal mol ⁻¹ Å ⁶)	C (kcal mol ⁻¹)	D (Å ⁻¹)
Na-N	-32461.57236	37734.03948	47752.17357	2.711467277
Na-H	-901.0111121	1323.287312	151.4842753	1.237012174

Table 2

Method	ion/solvent	Temp (K)	$r_{\text{MAX}}(\text{Å})$	RDF(r_{MAX})	CN	Ref.
ONIOM-XS MD	1/255	235	2.58	8.0	5.1	This work
QM/MM MD	1/215	235	2.55	4.4	5.0	[8]
MM MD (2-body)	1/215	235	2.55	14.8	8.0	[8]
MM MD (2-body)	1/215	235	2.49	16.6	8.0	[1]
MM MD (2-body)	1/215	266	2.42	14.6	7.0	[1]
MM MC (2-body)	1/201	277	2.68	11.6	9.0	[2]
MM MC (3-body)	1/201	277	2.68	10.0	8.0	[2]
MC (empirical)	1/250	260	2.25	9.5	5.0	[3]

Table 3

Ion/solute	CN	t_{sim}	$t^* = 0.0$ ps		$t^* = 0.5$ ps	
			$N_{\text{cc}}^{\text{0.0}}$	$\tau_{\text{NH}_3}^{\text{0.0}}$	$N_{\text{cc}}^{\text{0.5}}$	$\tau_{\text{NH}_3}^{\text{0.5}}$
Na⁺ in liquid NH₃						
Na ⁺ (first-shell)	5.1	40.0	42	4.86	16	12.75
(second-shell)	11.2	40.0	734	0.61	157	2.85
Na⁺ in water						
Na ⁺ (first-shell) [13]	5.4	41.0	164	1.35	36	6.18
Pure solvents						
Liq. NH ₃	11.8	30.0	885	0.40	270	1.31
Pure H ₂ O [30]	4.7	30.0	607	0.23	65	2.17

Figure 4

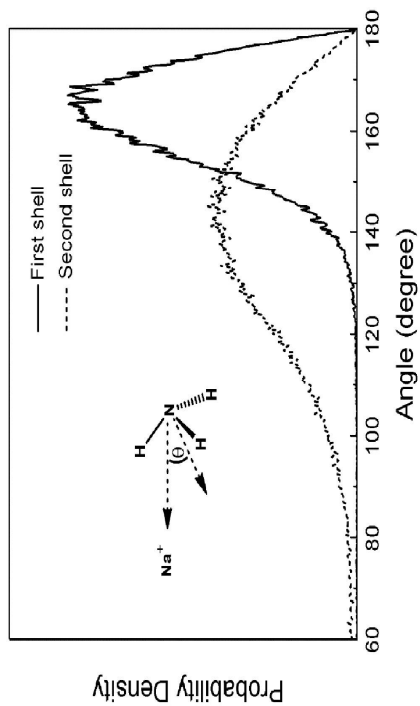


Figure 2

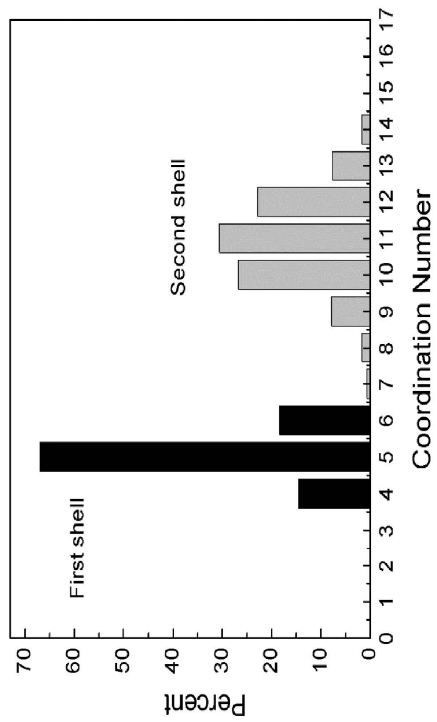


Figure 5

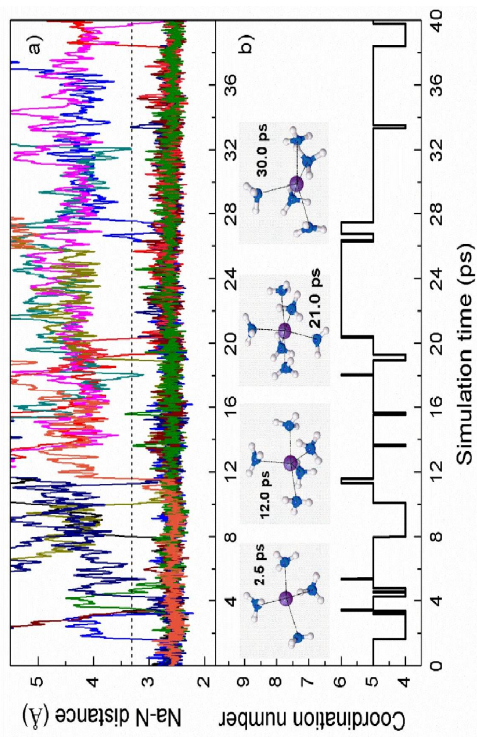


Figure 3

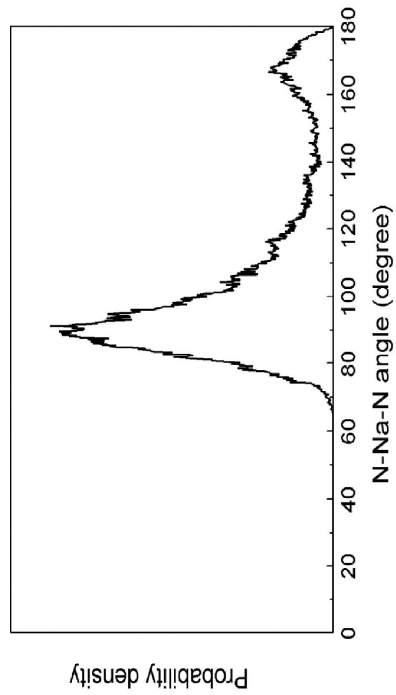


Figure 6

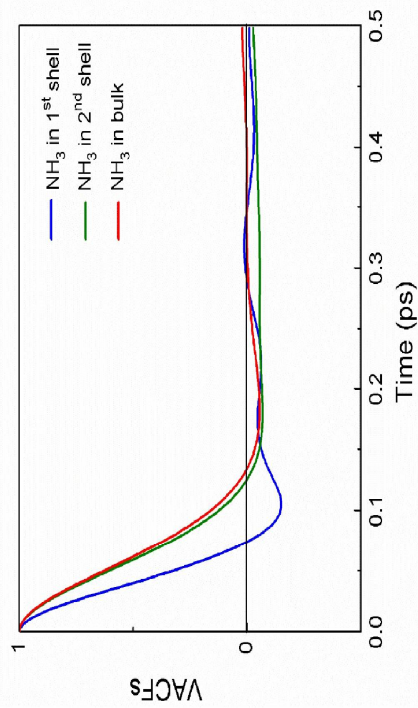


Figure 7

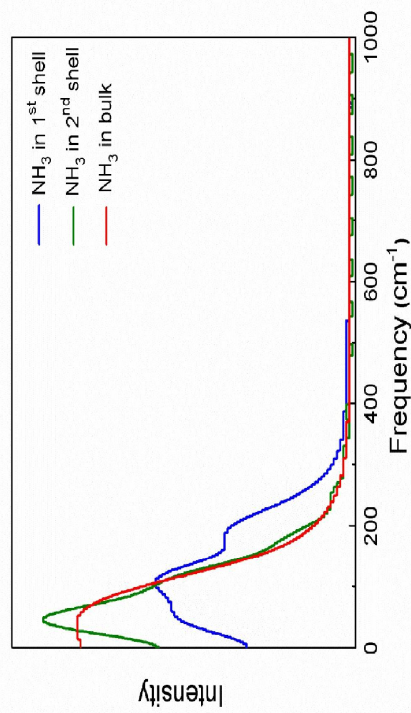
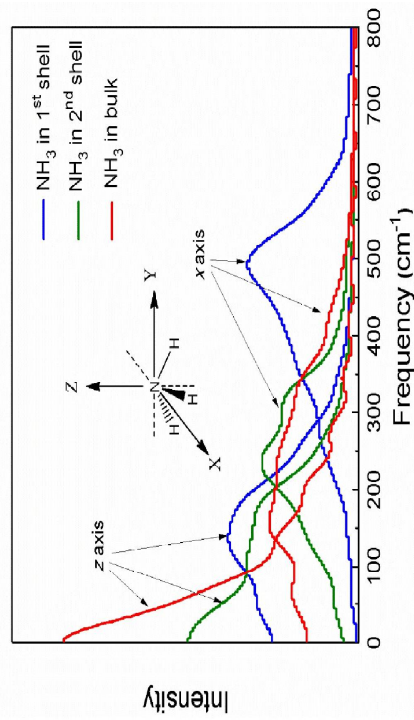


Figure 8



CURRICULUM VITAE

MISS JARUKORN SRIPRADITE

Education Background:

2009-Present Ph.D. Candidate (Chemistry), Suranaree University of Technology,
Nakhon Ratchasima, Thailand

2008 B.Sc. Second Class Honor (Chemistry), Ubon Ratchathani University,
Ubonratchathani, Thailand

Experiences:

2014-2015 Research Coop, The Crans group, Colorado State University (CSU),
Denver, USA

2010-2014 Teaching Assistant, School of Chemistry, Institute of Science, Suranaree
University of Technology, Nakhon Ratchasima, Thailand

Grant and Fellowships:

2009-2014 CHE-PHD-THA scholarships, under the Office of the Higher
Education Commission, Thailand

2006-2009 Science Achievement Scholarship of Thailand